UNITED NATIONS EDUCATIONAL, SCIENTIFIC AND CULTURAL ORGANIZATION
INTERNATIONAL CENTRE FOR THEORETICAL PHYSICS
I.C.T.P., P.O. BOX 586, 34100 TRIESTE, ITALY, CABLE: CENTRATOM TRIESTE

H4.SMR/782-6

Second Workshop on
Three-Dimensional Modelling of Seismic Waves
Generation, Propagation and their Inversion

7 - 18 November 1994

Ground Motion Modelling and Local Soil Effects

G. F. Panza

Università di Trieste
Istituto di Geodesia e Geofisica
Trieste, Italy

MAIN BUILDING STRADA COSTIERA, 11 TEL. 22401 TELEFAX 224163 TELEX 460392 ADRIATICO GUEST HOUSE VIA GRIGNANO, 9 TEL. 224241 TELEFAX 224531 TELEX 460449
MICROPROCESSOR LAB. VIA BEIRUT, 31 TEL. 224471 TELEFAX 224600 TELEX 460392 GALILEO GUEST HOUSE VIA BEIRUT, 7 TEL. 22401 TELEFAX 2240310 TELEX 460392

1.

A New Method for the Realistic Estimation of Seismic Ground Motion in Megacities: the Case of Rome

Donat Fäh, Claudio Iodice, Peter Suhadolc, and Guilano F. Panza

A hybrid technique, based on mode summation and finite differences, is used to simulate the ground motion induced in the city of Rome by the January 13, 1915, Fucino (Italy) earthquake (M_L=6.8). The technique allows us to take into consideration source, path, and local soil effects. The results of the numerical simulations are used for a comparison between the observed distribution of damage in Rome, and the computed peak ground acceleration, the maximum response of simple oscillators, and the so-called "total energy of ground motion". The total energy of ground motion is in good agreement with the observed distribution of damage. From the computation of spectral ratios, it has been recognized that the presence of a near-surface layer of rigid material is not sufficient to classify a location as a "hard-rock site" when the rigid material has a sedimentary complex below it. This is because the underlying sedimentary complex causes amplifications due to resonances. Within sedimentary basins, incident energy in certain frequency bands can also be shifted from the vertical, into the radial component of motion. This phenomenon is very localized, both in frequency and space, and closely neighboring sites can be characterized by large differences in the seismic response.

INTRODUCTION

Over the past few decades there has been a rapid growth in the world's population, and a tendency for this growth to be concentrated in urban areas. This growth of the cities, in general, is accompanied by the concentration of population in sedimentary valleys where it is easy to build. Such valleys are the zones most vulnerable to earthquakes, due to the presence of soft sediments. The 1985 Michoacan, Mexico event, the 1988 Spitak earthquake, and the 1989 Loma Prieta earthquakes are recent reminders that local ground conditions can have a strong influence on the damage in urban areas. It is therefore of crucial interest to estimate seismic ground motion in such areas, before an earthquake occurs. This requires knowledge of both

(DF, CI, PS, GFP) Istituto di Geodesia e Geofisica, Via dell' Università 7, Università degli Studi, I-34100 Trieste.
(GFP) International Center for Theoretical Physics, Strada Costiera 11, I-34100 Trieste.
(DF) Institut für Geophysik, ETH Hönggerberg, CH-8093 Zürich.

the sub-soil structures and the possible causative seismic sources, along with the availability of computational techniques that permit us to map the expected ground motion and the seismic hazard. Special developments will be necessary to improve current-day seismic programs, which in general do not include two-, and three-dimensional effects in sedimentary basins, and which underestimate the hazard on soft soils.

Several methods for estimating the seismic shaking potential are currently in use, but their reliability and accuracy are not well known and have not been rigorously tested. Moreover, the costs of their application are not well determined. For this reason, in the last few years, several working groups have instituted international programs to pursue these questions. One of these projects is the IASPEI/IAEE (International Association of Seismology and Physics of the Earth's Interior/ International Association of Earthquake Engineering) Joint Working Group. The purpose of this group is to coordinate the establishment of an international series of test areas (for example the Turkey Flat test area and the SMART-1 array in Taiwan) to provide a database for comparing, testing and improving the available methods. Also, in 1990 the United Nations began a ten-year project: the International Decade for Natural Disaster Reduction, to reduce the vulnerability of high-risk areas.

Numerical simulations play an important role in the estimation of strong ground motion. They can provide synthetic signals for areas where recordings are absent and are therefore very useful for engineering design of earthquake-resistant structures. In recent years many computational techniques have been proposed to estimate ground motion at a specific site. The methods commonly used are one-, and two-dimensional techniques; three-dimensional studies are too expensive to be applied routinely. The standard one-dimensional methods that are generally applied in zonation studies, are those developed by Thomson (1950) and Haskell (1953), and by Seed (Program Shake). These techniques are very cheap and they provide the first few resonance frequencies (fundamental and harmonics) of soft, soil layers, and the results show that the strongest effects usually occur at the fundamental frequency. Relative to the response of a reference, bedrock model, one-dimensional techniques yield estimates of the wave amplification caused by unconsolidated surficial sediments overlying the bedrock. However, such techniques fail to predict the ground motion close to lateral heterogeneities or when the soil layers have a non-planar geometry. The lateral heterogeneities and sloping layers, commonly present in nature, can cause effects that dominate the ground motion: the excitation of local surface-waves, focusing and defocusing, and resonances. In such circumstances, the treatment of realistic structures requires at least two-dimensional techniques to estimate the ground motion.

For ease of reference we divide the methods for handling wave propagation in two-dimensional media into a *numerical class* of methods, where the computational algorithm is based on an approximate mathematical method for solving the formal representation of the problem; and into an *analytical class* of methods, where the computational algorithm is based on an exact formal solution. The *numerical class* includes the finite-difference method (Alterman and Karal, 1968; Boore, 1972), the pseudo-spectral method (Gazdag, 1981; Kosloff and Baysal, 1982), and the finite-element method (Lysmer and Drake, 1972); while the *analytical class* includes the integral equation methods (Sánchez-Sesma and Esquivel, 1979), the 2D mode-summation technique (Levshin, 1985; Vaccari et al., 1989), the Rayleigh-Ansatz method (Aki and Larner, 1970; Bard and Bouchon, 1980a, 1980b), and the discrete-wavenumber, boundary-element method (Kawase, 1988). The finite-difference method, the pseudo-spectral method, and the finite-element method are capable of treating very complex structures; however, they are restricted in the size of the models, which they can handle by computer memory limitations. Often, the source cannot be included in the structural model, because its distance from the site of interest is too large; and the incoming wavefield is approximated by a plane polarized body-wave. The advantage of the *analytical class* of methods, such as 2D mode summation or the Rayleigh-Ansatz method, is the possibility of treating realistic source models and extended structural models. These methods can be applied effectively to simple two-dimensional geometries of sedimentary basins.

To include both a realistic source model and a complex structural model of the sedimentary basin, a hybrid method has been developed that combines modal summation and the finite difference technique (Fäh et al., 1990; Fäh, 1992). The propagation of the waves from the source up to the sedimentary basin is computed with the mode-summation method for a plane layered structure. The mode-summation method allows the simulation of the complete incident wavefield in a given frequency-phase velocity band, and in this band, it can automatically account for all surface waves and shear waves. Explicit finite-difference schemes are then used to simulate the propagation of seismic waves in the sedimentary basin. The hybrid method is particularly suitable to estimate ground motion in sedimentary basins of any complexity and allows us to take into account the source, path and local site effects, also when dealing with paths of a few hundreds kilometers. This innovation is the main advantage of the hybrid method with respect to other techniques.

The area of Rome, considered in our study, is characterized by several sedimentary basins of considerable thickness, which in some parts are covered by volcanic rocks. The area is very vulnerable to earthquakes, as indicated, for example, by the well documented damage distribution caused by the January 13, 1915, Fucino (Italy) earthquake (M_L=6.8). Using the hybrid technique, a series of different numerical simulations of ground motion are performed, and the results are used for a comparison between the observed damage distribution and the peak ground acceleration, the maximum response of simple oscillators and the so-called "total energy of ground motion" which is related to the Arias Intensity. If one is interested only in the local response of a sedimentary basin, the source and path effects can be removed computing ratios between representative values of the ground motion, such as peak ground acceleration (PGA) and the "total energy of ground motion", determined for the two-dimensional model and for a one-dimensional model, which is used as a reference. In the frequency domain, a good representation of two-dimensional effects is given by the computation of spectral ratios between the signals obtained for the two-dimensional model of the sedimentary basin, and the one-dimensional reference model. Both signals have in common the source and the path, so that from the spectral ratios the effects of the sedimentary basin are clearly exhibited. The spectral ratios allow us the identification of the sites and the frequency bands in which amplification effects are predicted to occur.

THE HYBRID TECHNIQUE

The hybrid technique combines modal summation and the finite-difference method, and it can be used to study wave propagation in sedimentary basins. Each of the two techniques is applied in that part of the structural model where it works most efficiently: the finite-difference method in the laterally heterogeneous part of the structural model which contains the sedimentary basin (see Figure 1), and modal summation is applied to simulate wave propagation from source position to the sedimentary basin of interest. This hybrid approach allows us to calculate the local wavefield from a seismic event, both for small (a few kilometers) and large (a few hundreds of kilometers) epicentral distances. The technique combines the advantages of both modal summation and finite-difference technique. The use of the mode-summation method allows us to include an extended source, which can be modelled by a sum of point sources appropriately distributed in space and time. This allows the simulation of a realistic rupture process on the fault. The path from source position to the sedimentary basin can be approximated by a structure composed of flat, homogeneous layers. Modal summation then allows the treatment of many layers which can take into consideration low-velocity zones and fine details of the crustal section under consideration. The finite-difference method, applied to treat wave propagation in the sedimentary basin, permits the modelling of wave propagation in complicated and rapidly varying velocity structures, as is required when dealing with sedimentary basins. The coupling of the two methods is carried out by introducing the resulting time series obtained with modal summation into the finite-difference computations. In the SH computations the displacements are used as input to the finite-difference calculations, whereas in the P-SV case the input consists of the velocity time series, in relation to the specific finite-difference techniques used for SH and P-SV waves.

In the mode-summation method, the treatment of P-SV waves is based on Schwab's (1970) optimization of Knopoff's (1964) method (Panza, 1985), and the handling of SH waves is based on Haskell's (1953) formulation (Florsch et al., 1991); these computations include the "mode-follower" procedure and structure minimization described by Panza and Suhadolc (1987). The introduction of anelasticity into the computations is based on variational methods (Takeuchi and Saito, 1972; Schwab and Knopoff, 1972), and includes Futterman's (1962) results concerning the dispersion of body-waves in a linearly anelastic medium. By comparison with the results obtained from the exact treatment of anelasticity (Schwab, 1988; Schwab and Knopoff, 1971; 1972; 1973), the attenuation effects obtained from the variational technique turn out to be in error by about 20 percent, a value certainly acceptable for our purposes.

The seismic source is introduced by using the Ben-Menahem and Harkrider (1964) formalism. These far-field expressions are valid, if the distance from the source, Δ, is larger than the dominant wavelength, λ, of the computed signal; if $\Delta > \lambda$, the first term of the asymptotic expansion of the cylindrical Hankel functions, appearing in the far-field expressions, is exact with at least three significant figures (Panza et al., 1973). The seismograms computed with modal summation contain all the body waves and surface waves, whose phase velocities are smaller than the shear-wave velocity of the half-space that terminates the structural model at depth. These computations therefore supply a realistic incoming wave-field, to be used as input in the finite-difference computations.

2

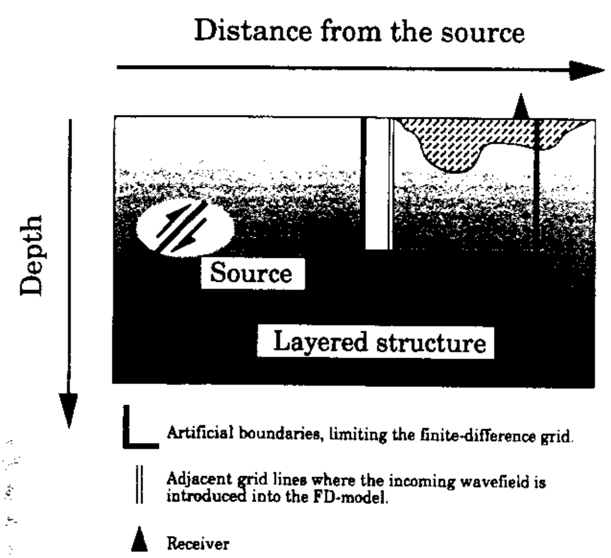

Figure 1 Geometry of the problem.

Explicit finite-difference schemes are used to simulate the propagation of seismic waves in the sedimentary basin. These schemes are based on the formulation of Korn and Stöckl (1982) for SH waves, and on the velocity-stress, finite-difference method for P-SV waves (Virieux, 1986). The algorithms can handle structural models containing a solid-liquid interface, and are numerically stable for materials with normal, as well as high values of Poisson's ratio. Intrinsic attenuation in soft sediments is an important process and should always be taken into account to prevent serious errors in seismic hazard estimations. In the finite-difference computations, anelasticity is included using the rheological model of the generalized Maxwell body (Emmerich and Korn, 1987; Emmerich, 1992; Fäh, 1992). This method can account for a constant quality factor over a certain frequency band.

Once the numerical algorithms and related computer codes are developed, one of the major problem to obtain realistic numerical simulations is represented by the necessity to know as accurately as possible the source and structural parameters. In fact, the numerical simulation can satisfactorily predict the ground motion at a specific site, only if the source parameters, the layered structure describing the path from the source up to the sedimentary basin, and the mechanical parameters (density, velocities, damping, etc.) and geometrical parameters (e.g. thickness) of the sedimentary basin are reasonably well-known. The choice of these parameters is based on all available seismological, geological and geotechnical information, and it is discussed in the following for the specific case of the Fucino earthquake and the area of Rome.

3

THE JANUARY 13, 1915, FUCINO EARTHQUAKE

One benefit of the important historical role of Rome during the last two thousand years is the large quantity of descriptions of earthquakes that have been felt in the city (Molin et al., 1986; Basili et al., 1987). The most important seismogenetic zones (Figure 2) which can cause structural damage in Rome are the Colli Albani (observed maximum intensity in Rome MCS VI-VII (Mercalli-Cancani-Sieberg intensity scale)), the Central Apennines (observed maximum intensity in Rome MCS VII-VIII) and the Tyrrhenian Sea (observed maximum intensity in Rome MCS V-VI). There is also local seismic activity in the area of Rome (observed maximum intensity in Rome MCS VII). The modification of local geotechnical properties in the last 50 years, due to digging, water pumping, and man-made fill, may also increase current intensities beyond those observed earlier even if the earthquake magnitudes do not exceed historical ones.

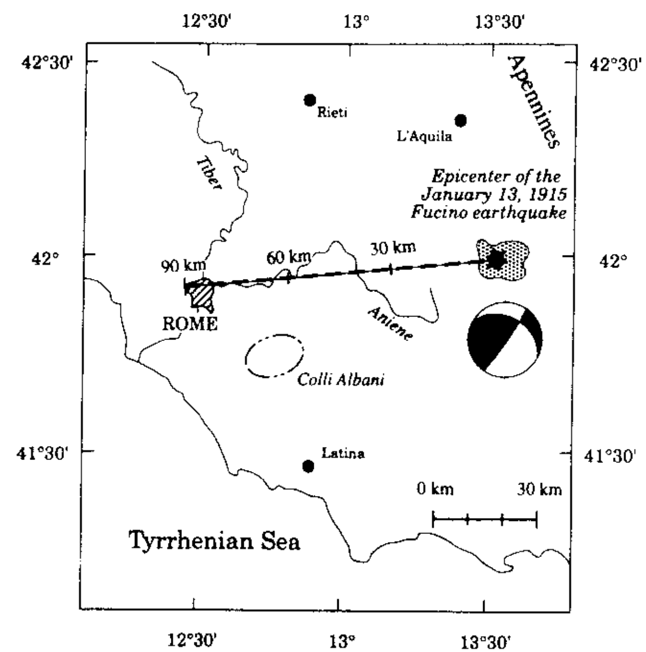

Figure 2 Approximate epicenter location of the January 13, 1915 earthquake in the Fucino valley (dotted area). The dashed line indicates the cross section with which the numerical modelling has been performed.

The January 13, 1915 Fucino earthquake (Figure 2) is one of the strongest events that occurred in Italy during this century. This event, with maximum Intensity XI on the MCS scale (M_L=6.8), caused damage in the city of Rome (Ambrosini et al., 1986). The damage distribution is shown in Figure 3. The epicenter is localized about 85 km east of Rome (Figure 2). The source parameters of this event are given by Gasparini et al. (1985). The strike of the fault (N62W) coincides well with the geological lineaments of the area and with the observed direction of the main fault (Serva et al., 1986). The source depth is 8 km, the angle between the strike of the fault and the epicenter-station line is 38°, the fault dip 39°, and the rake with respect to the strike 172°. In the numerical simulation, we use a simple point source.

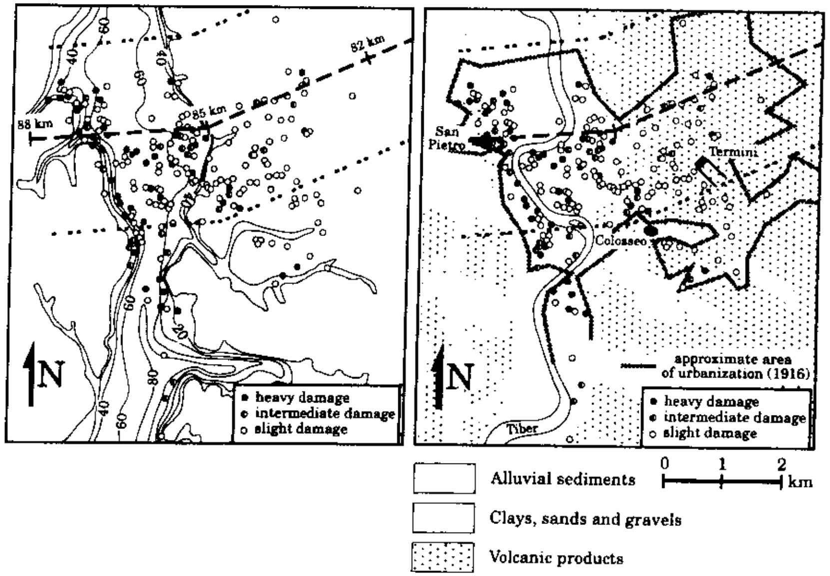

Figure 3. Damage distribution in Rome caused by the January 13, 1915 Fucino earthquake (after Ambrosini et al., 1986), thickness of the alluvial sediments (given in meters), and lithology (Ventriglia, 1971; Funiciello et al., 1987; Feroci et al., 1990). Three types of damage are distinguished: slight damage (cracking of plaster, the downfall of small pieces of mouldings), intermediate damage (between slight and heavy damage), and heavy damage (deep and diffuse damage of indoor and outdoor walls, downfall of large parts of mouldings and of chimneys). The dashed line indicates the position of the cross section, for which numerical modelling has been performed. The distribution of damage within the area limited by the two dotted lines has been projected on the cross section to construct the histograms, shown in Figures 9, and 10.

The synthetic seismograms are originally computed for a seismic source of 1 dyne c
The amplitudes are then scaled according to the seismic moment (M_0) of 10^{26} dyne c
proposed by Ward and Valensise (1989) for the Fucino earthquake. This scaling requires t
use of the wide-band spectrum scaling law proposed by Gusev (1983), because the domina
frequency of our synthetic signals is above the corner frequency of an event with seism
moment of 10^{26} dyne cm. For an average frequency of 2 Hz, the resulting amplificatio
factor applied to the original seismograms is 10^{24}. With this amplification factor and at
distance of about 85 km from the seismic source, the maximum horizontal acceleration reach
values of the order of 40-60 cm s^{-2}. This is in good agreement with the values estimated fro
an empirical relation between maximum, horizontal peak ground acceleration, epicentr
distance, and seismic moment, proposed by Sabetta and Pugliese (1987) for Italia
earthquakes.

NUMERICAL MODELLING FOR A TWO-DIMENSIONAL STRUCTURAL MODEL

The one-dimensional model describing the path from the source to Rome is shown i
Figure 4 (Iodice et al., 1992). The P-wave velocities in the crust are based on seismi
refraction measurements made along the profile Latina-Pescara (Nicolich, 1981). The shear
wave velocities are chosen by assuming that $v_S^2=v_P^2/3$. The Moho depth (28km) is in goo
agreement with other published results (Nicolich, 1989; Suhadolc and Panza, 1989). The par
of the upper mantle corresponds to the model proposed by Vaccari et al. (1990) for the Irpinia,
Italy, area, and is in agreement with surface waves dispersion measurements (Panza et al.,
1980). This one-dimensional model is used to compute the input time series for the finite-difference computations.

The two-dimensional structural model for Rome was proposed by Iodice et al. (1992), and is shown in Figure 5. It is based on all the available geological and geotechnical information (Ventriglia, 1971; Funiciello et al., 1987; Boschi et al., 1989; Feroci et al., 1990; Carboni et al., 1991). Alluvial sediments can be found in two areas, the river beds of the Aniene and Tiber. The ancient river bed of the Tiber (referred as Paleotiber) is composed by Sicilian clays, sands and gravels. This sedimentary complex is covered by volcanic rocks which have their origin in the Pleistocene volcanic activity (Ventriglia, 1971). The volcanic rocks have greater wave velocities than the underlying sediments (Sicilian), which therefore defines a buried low-velocity zone. The surficial layer, 10 m thick, consists of compacted fill, and of the foundations of man-made structures. The transition from the alluvial sediments in the Tiber river bed to the compacted clay in the west is characterized by a very high impedance contrast. In Figure 5, the compacted clay is referred as bedrock.

The high-frequency limit for our numerical simulation has been chosen to be 4 Hz, which is in agreement with the experience derived from strong motions generated by magnitude 5-to-6 earthquakes recorded in Italy (e.g. CNEN-ENEL, 1977; Vaccari et al., 1990). With a maximum frequency of 4 Hz and with a minimum shear-wave velocity of 0.4 km/s, in the finite-difference computations, it is necessary to use a minimum grid spacing of 10 m. Since the characteristics of the hardware available to us limit the number of grid points in the finite-difference computations to 800x300 points, the structural model is too large to be treated in a single computer run. For this reason, the model had to be divided into two overlapping parts (cross section "Paleotiber", and cross section "Tiber" in Figure 5). This procedure is justified since the main features of the seismograms are determined by the local soil conditions, and control of continuity from one section to the other has been made on the overlapping portions.

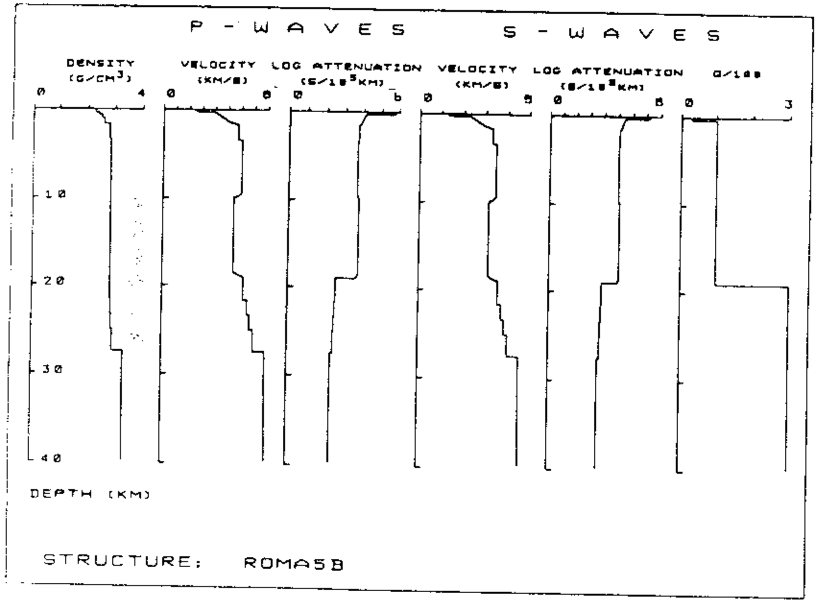

Figure 4 Structural model ROMA5B, representative of the path from the epicenter of the January 13, 1915 Fucino earthquake to the city of Rome (Iodice et al., 1992). $Q_\alpha=2.2\ Q_\beta$.

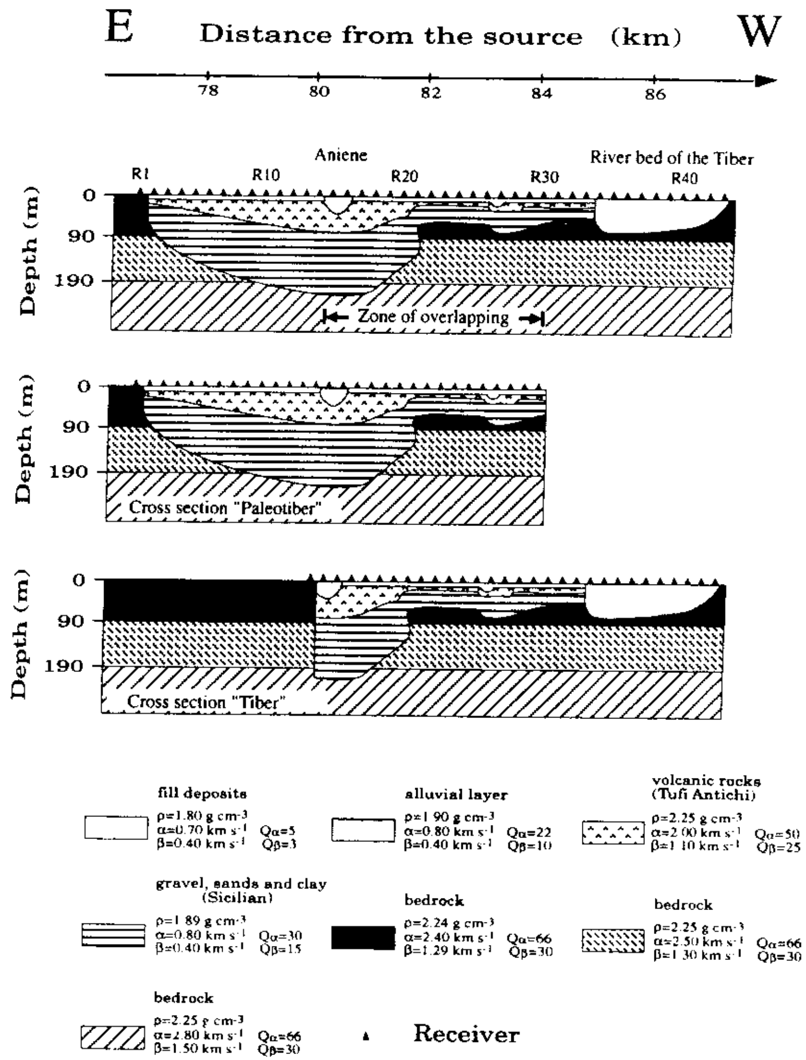

Figure 5 Two-dimensional model (uppermost cross section) corresponding to the dashed line shown in Figure 3. Only the part near the surface is shown, where the 2D model deviates from the horizontally-layered structural model in Figure 4. For practical reasons, the numerical modelling has been carried out for two parts separately: the cross section "Paleotiber" (middle cross section), and the cross section "Tiber" (lowest cross section).

PROPERTIES OF GROUND MOTION AND COMPARISON WITH THE OBSERVED DAMAGE DISTRIBUTION

The acceleration time series obtained with the hybrid technique for cross sections "Paleotiber" and "Tiber" are shown in Figures 6 and 7. The main features of the time series are two peaks which can be related to the Sg and the Lg phases. In general, due to the presence of low-velocity material near to the surface, the radial component is two-to-three times larger than the vertical component, while, due to the SH and P-SV radiation patterns of the source, the transverse component is half the size of the radial component. Several characteristics of the ground accelerations can be related successfully to local features of the structure. The strongest effects are caused by the presence of alluvial sediments in the river beds of the Tiber and Aniene. There the signals have the largest amplitudes and durations due to the low impedance of the alluvial sediments, the excitation of local surface waves, and resonance effects.

Minimum accelerations can be observed for receivers placed above the volcanic layer, which acts as a shield, and reflects part of the incoming energy: the thicker the layer, the smaller the observed surface accelerations. The underlying layer (Sicilian) can function as a low-velocity waveguide, inside which a relevant part of energy is trapped. At places where this waveguide and the overlying volcanic layer thin, focusing effects occur and the trapped energy reaches the surface. This can be seen for the receivers R21, R22 and R23, where the amplitudes of the ground motion are much larger than the ones observed in the area with a thick volcanic layer.

The synthetic accelerograms can be used to compute some ground motion related quantities, reasonably correlated with the structural damage. These quantities are those commonly used for engineering purposes, e.g. (1) the peak ground acceleration (PGA), (2) the peak acceleration of the response of simple undamped oscillators with different resonance frequencies (peak oscillator response, POR), which corresponds to the maximum acceleration of the response spectrum for zero damping, and (3) the total energy of acceleration (W), defined in Equations 1 and 2. The Husid plot is defined as

$$w(t) = \int_0^t [\ddot{x}(\tau)]^2 \, d\tau \ , \qquad (1)$$

where x is the ground displacement. The function w(t) is monotonically increasing. The so-called "total energy of ground motion" or "total energy of acceleration" W (Jennings, 1983), which is proportional to the Arias Intensity (Arias, 1970), is defined as

$$W = \lim_{t \to \infty} w(t) \ . \qquad (2)$$

In the two sections, the signals at the same distance from the source differ due to the different propagation paths. The abrupt change from the one-dimensional model, to the model "Tiber", can lead to local surface waves and diffractions. In fact, at the beginning of the zone of overlap, the acceleration time series obtained for the two cross sections differ strongly (Figures 6 and 7).

6

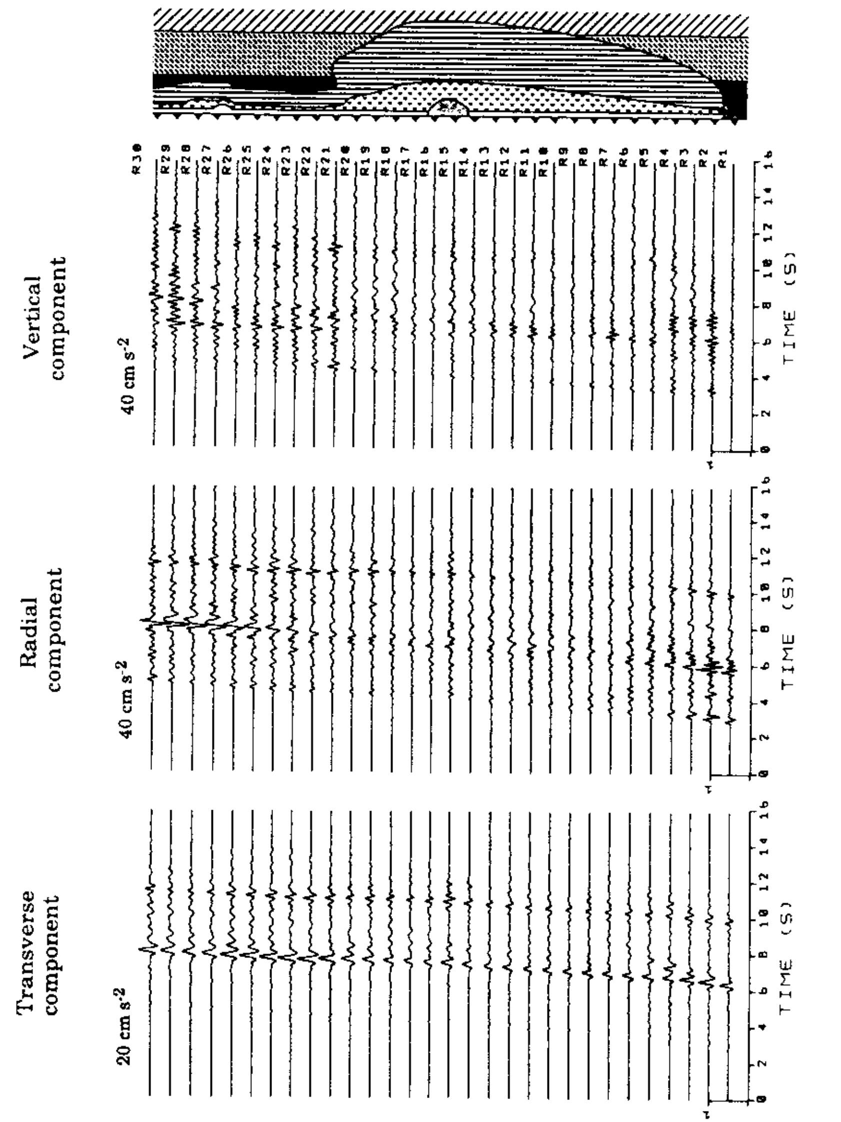

Figure 6 Acceleration time series for SH waves and P-SV waves at an array of receivers over cross section "Paleotiber", shown in Figure 5. In each column, the signals are normalized. The peak acceleration is indicated in units of cm s^{-2}. The time scale is shifted by +20 seconds from the origin time (0 s in the figure corresponds to 20 s in absolute travel time from the earthquake source).

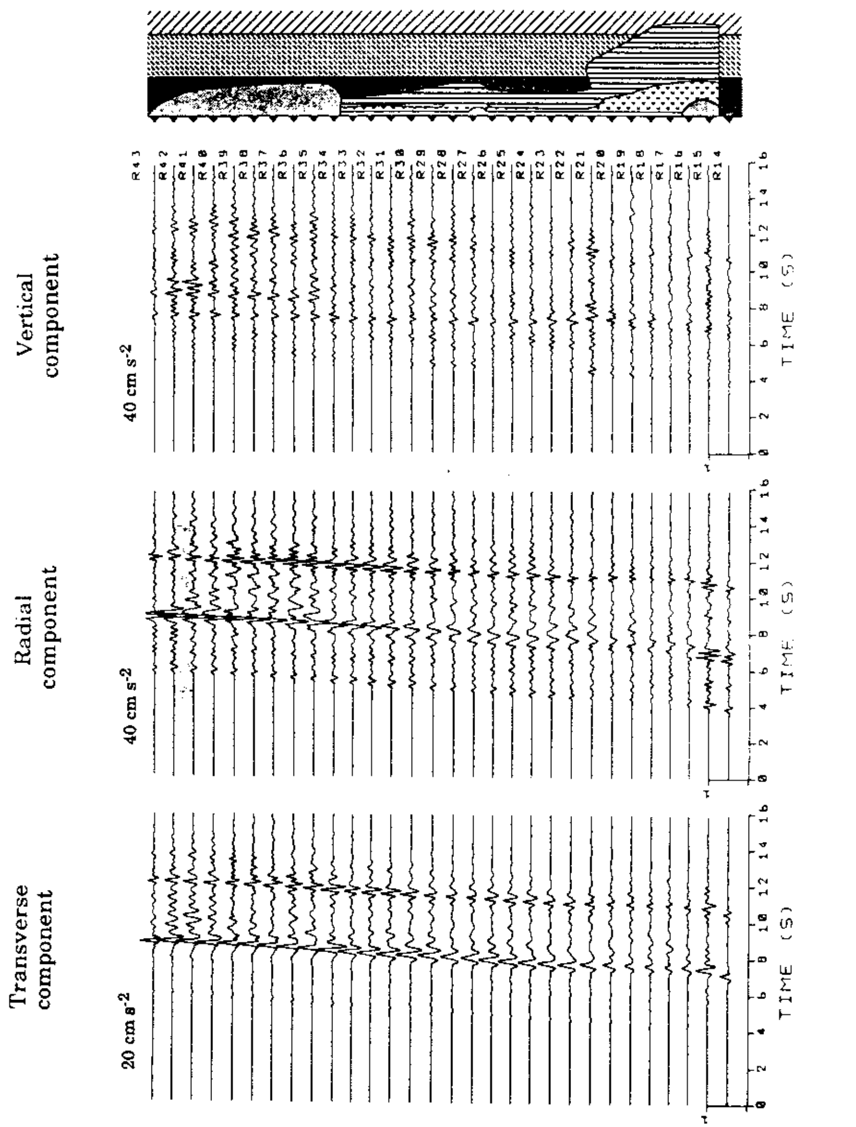

Figure 7 The same as in Figure 6 for an array of receivers over cross section "Tiber", shown in Figure 5.

Inside the zone of overlap, the signals become more and more similar, as the distance from the abrupt discontinuity in the cross section "Tiber" increases. In the central part of the zone of overlap, the signals are similar, as is shown for the receiver R25 in Figure 8. The small differences are due to dispersion effects in the ancient, Tiber river bed, and to diffractions at the vertical interface in cross section "Tiber".

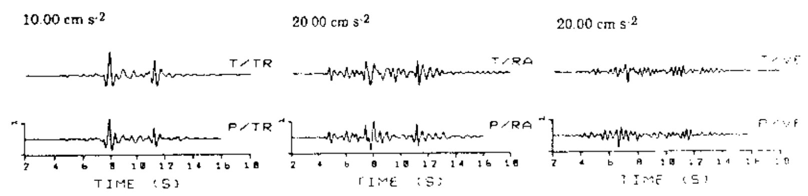

Figure 8 Comparison between the signals obtained at the same distance from the source for the two cross sections "Paleotiber" and "Tiber" (Figure 5). The transverse (left), radial (middle), and vertical (right) accelerations are shown. The lower traces are related to the cross section "Paleotiber", the upper traces, to the cross section "Tiber". The epicentral distance is 82.8 km. The signals are normalized. The peak acceleration is in units of cm s^{-2}.

The critical point is to combine the information obtained from the two cross sections. Therefore, PGA, POR, and W have been computed for the signals obtained for the two cross sections "Paleotiber" and "Tiber". In the central part of the zone of overlap (81.5-83.0 km from the source), the values obtained for the two cross sections differ only by 4 to 8 percent, whereas the maximum difference in PGA along the overlapping zone can be as high as 30 percent (35 percent for POR, and 30 percent for the quantity W). If the transition from one cross section to the other is performed, when the difference between the seismograms is minimum, the errors introduced by the use of two distinct cross sections are minimized. In fact, the errors are only a small fraction of the variations in PGA, POR, and W over the entire array. Following this procedure, we can extract from our signals a set of values of PGA, POR, and W, which can be compared with the distribution of damage from the Fucino earthquake, shown in Figure 3. A quick glance at the spatial distribution of damage allows us to identify, in the alluvial basin of Tiber, a concentration of intermediate and heavy damage, more severe near to the edges of the basin. To quantify this observation, the damage distribution has been projected on the cross section used in the numerical modelling. Only those points of the distribution have been used which are situated in an area where the geometry of the structure does not differ too much from the geometry of the two-dimensional cross section. The limits of this area are indicated in Figure 3. The type of damage to each building has been projected on the closest point of the cross section with similar lithology and depth-of-the-sedimentary-cover characteristics. The resulting histogram is shown in Figures 9 and 10. These damage statistics should be interpreted only in a qualitative manner, as neither the type of buildings nor the density of urbanization has been taken into account. However, it seems that the observed damage does not depend on the type of building (Ambrosini et al., 1986).

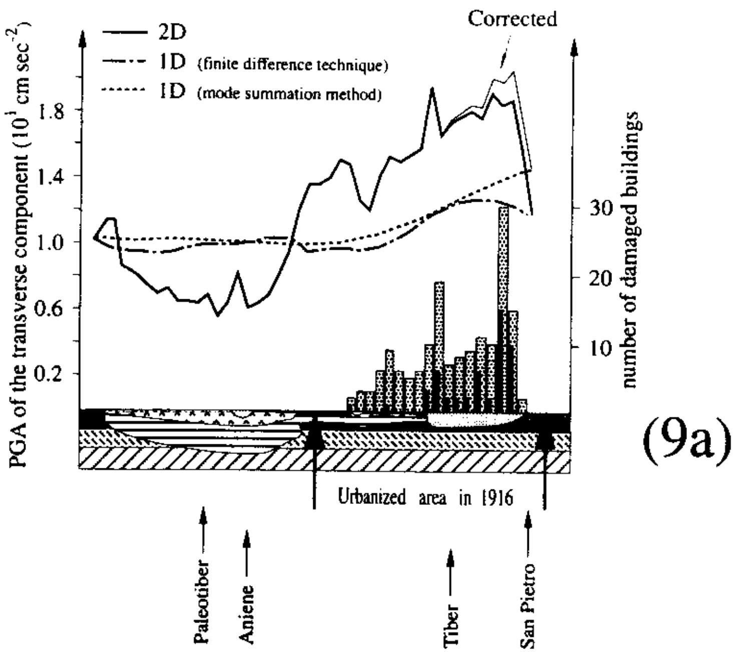

Figure 9 a) Peak ground acceleration (PGA), and b) total energy (W) of the transverse acceleration, obtained for the one-dimensional model (dotted and dash-dotted lines) given in Figure 4, and the two-dimensional model of Rome (thick solid line) shown in Figure 5. They are compared with the damage distribution caused by the January 13, 1915 Fucino earthquake. The thin solid line indicates the two-dimensional results corrected for the loss of signal due to the vertical limitation of the used finite-difference grid.

8

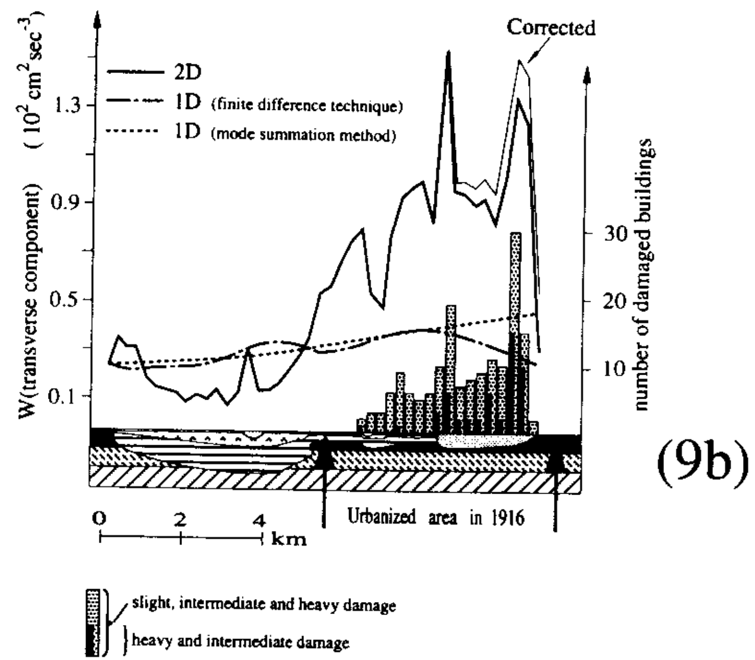

The comparison between the observed damage in the city of Rome, with the spatial distribution of PGA and W for the transverse component of motion is shown in Figure 9. Also shown are the results obtained with the one-dimensional layered structure (Figure 4). For this 1D model, the waveform does not change significantly along the array of receivers. Peak ground acceleration (PGA) increases with increasing distance from the source (Figure 9a), and this fact can be defined as the regional trend of PGA. This behaviour of the PGA is due to the incoming of postcritically reflected shear waves from the Moho for epicentral distances larger than 80 km (Suhadolc and Chiaruttini, 1985).

The structural model described by the finite-difference grid does not include structural features extending to large depths (see Figure 1). This causes incompleteness of the signals at large distances from the vertical grid lines, where the incoming wavefield is introduced into the finite-difference computations. As a consequence, for the last few receivers, the PGA value obtained with the hybrid method is systematically smaller than that from the mode-summation method (Figure 9a). The curves obtained for a 2D structural model also contain this loss of energy at the end of the model. The difference between the results obtained with 1D modal summation, and the 1D finite-difference method, provides us with an easy way to correct the

2D results. The amount of this first-order correction, which can be applied to the continuous line in Figure 9a, can be deduced from the distances between the dotted and the dash-dotted lines shown in the same figure.

High PGA are observed for locations with surficial sediments (Figure 9a), while PGA values are low where the volcanic layer is thick. Relative peaks can be seen at the beginning of the alluvial valley of the Tiber and within the alluvial valley of the Aniene. The POR curve, which is not shown here, has about the same shape as the curve for the PGA. The peaks and troughs are more evident in the curve representing the total energy W (Figure 9b). There are four peaks: two at the edges of the Tiber basin, one within the alluvial valley of the Aniene, and a broad peak when the Sicilian low-velocity zone gets close to the surface. The agreement between the W curve and the observed damage distribution is very good.

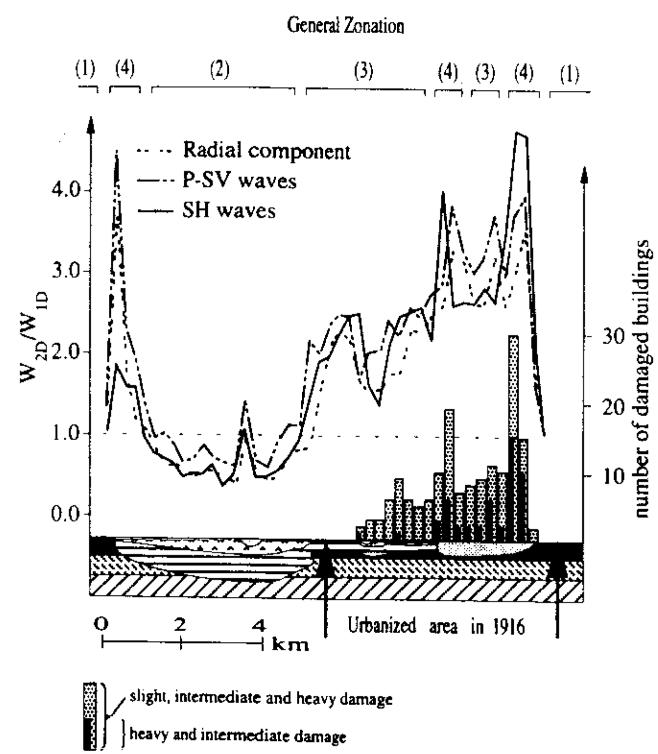

Figure 10 Ratios of the total energy of acceleration, W_{2D}/W_{1D}, between the results obtained for the two-dimensional, and one-dimensional models. They are compared with the damage distribution caused by the January 13, 1915 Fucino earthquake. The general zonation is explained in the text.

The source effect and regional trend can be removed by calculating the ratios between the values obtained for the two-dimensional model and those obtained for the one-dimensional model. The ratios of the total energy W computed for the transverse component of motion (SH waves), the radial component of motion, and the total P-SV wavefield are shown in Figure 10. Similar conclusions can be drawn for the radial and the transverse component of acceleration. The new feature in the case of the radial component is the strong peak at the edge of the ancient Tiber bed which can be attributed to the different frequency content of SH and P-SV components of motion, and to different physical processes, e.g. the S- to P-wave conversion for P-SV waves at strong impedance contrasts. The representation of the results given in Figure 10 can be used directly for general zonation purposes. With respect to the Apennines seismogenetic area, four zones can be distinguished: (1) the bedrock, which is chosen as the reference for the zonation; (2) the region above the volcanic layer; the thicker this layer, the smaller the W values at the surface; (3) the zones inside the sedimentary basin of the Tiber, at the end of the low-velocity waveguide, and the zones with a thick layer of low-velocity sediments close to the surface where large values of W are obtained; (4) the edges of the sedimentary basins characterized by the biggest values of W.

The very good correlation between the damage statistic and the computed ground motion makes it reasonable to extend the zonation to the entire town (Figure 10). This zonation includes also the area of Rome which was not urbanized in 1915, thus providing a basis for the prediction of the expected damage distribution from a future event in the Apennines region, which has to be expected from the study of pattern recognition (Caputo et al., 1980), to occur at a distance even smaller than the one considered in this study.

RESULTS IN THE FREQUENCY DOMAIN

A good representation of the two-dimensional effects is given by the spectral ratios between the signals obtained for the two-dimensional and the one-dimensional model. This procedure removes the source effect and the regional trend from the ground motion, and it allows us to identify, for a given seismogenetic area, the frequency bands and sites at which amplification and deamplification effects occur. The result for the transverse component is illustrated in Figure 11, where these ratios are shown as a function of frequency and spatial location along the section. The darker an area, the stronger the amplifications due to the two-dimensional effects. The greatest amplification is observed at the western edge of the sedimentary basin of the Tiber river (87 km from the source), for frequencies around 2 Hz. The maximum amplification with respect to the one-dimensional model is of the order of 5-6, and it is due to the combination of resonance effects and the excitation of local surface waves.

The general distribution of the shaded areas can be related to the geometry of the structural model. An amplification over almost the entire frequency band is observed outside the Paleotiber basin (82-87 km from the source). Some amplification occurs in the Aniene basin, for frequencies above 2 Hz. For frequencies above 0.8 Hz, in the Paleotiber basin, the volcanic layer acts as a shield reflecting part of the incoming energy, and the values of the spectral ratios are smaller than 1. The underlying sedimentary complex (Sicilian) causes spectral ratios between 4 and 5, due to resonances. These are most pronounced at frequencies

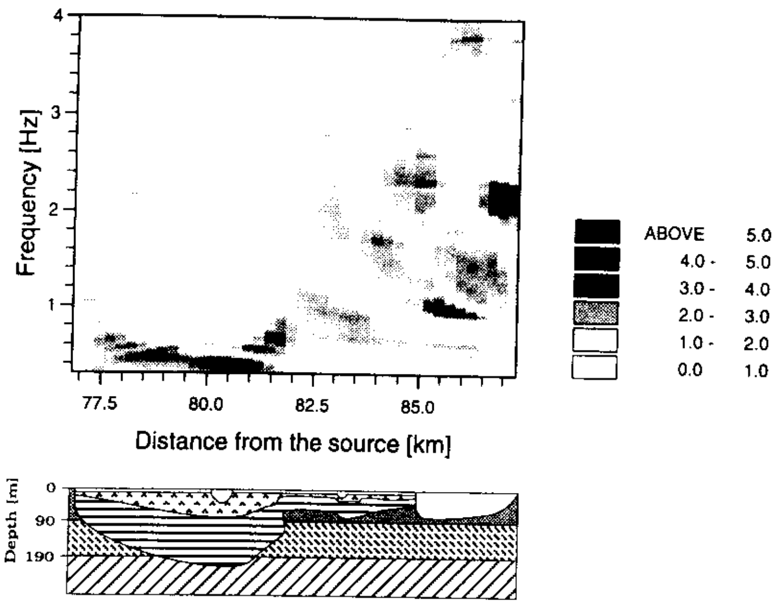

Figure 11 Spectral ratios for transverse accelerations over the entire cross section. The reference signal is the one obtained for the one-dimensional layered model ROMA5B.

around 0.4 Hz, where the fundamental resonance of this low-velocity zone is excited. In this part of the Paleotiber, in the frequency band 1.5-2.0 Hz, there is also evidence for the excitation of some higher modes of resonance. At distances of the order of 82-83 km from the source, between the Paleotiber and the Tiber basins, where the waveguide and overlying volcanic cover are thinning, focusing effects occur and the trapped energy reaches the surface. This leads to amplifications over almost the entire frequency band being considered, and values of the spectral ratios are of the order of 2. Therefore, the presence of a near-surface layer of rigid material is not sufficient to classify a site as a "hard-rock site". A correct zonation, in addition to the knowledge of the frequency content of the incoming signal, requires knowledge of both the thickness of the surficial layer and of the deeper parts of the structure, down to real bedrock. This is especially important in volcanic areas, where pyroclastic material often covers alluvial basins.

When considering the radial component of motion, the situation is more complicated (Figure 12). The sedimentary cover causes polarization of P-SV waves into the radial component. This polarization then gives rise to a series of scattered dark zones--high amplifications--for frequencies higher than 1 Hz; in the frequency band 0.8-1.0 Hz, the

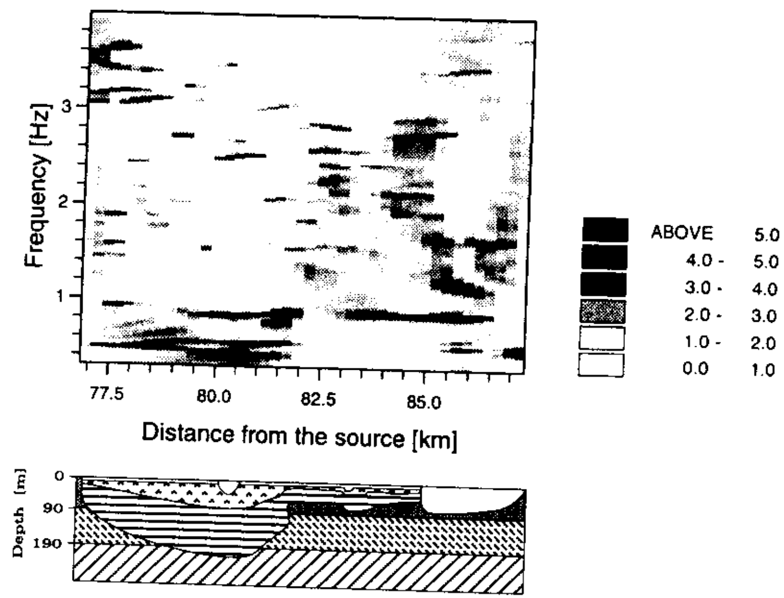

Figure 12 The same as Figure 11, for the radial component of motion.

polarization and amplification effect is present along almost the entire section. The amplification at 0.8-1.0 Hz leads to a maximum value of the spectral ratio of 25.0 at 80.0-80.5 km from the source. For frequencies above 1 Hz, the polarization effects are highly localized, both in frequency and distance from the source, so that at neighboring sites we can have large differences in the seismic response.

Spectral ratios can also be computed for the total P-SV wavefield, considering a complex time-series formed by the radial component (real part) and the vertical component (imaginary part). The result of this combination is shown in Figure 13. Since the amplitudes of the radial component are double those of the vertical component, the pattern in Figure 13 is similar to the one in Figure 12. A shift of energy from the vertical into the radial component of motion disappears in this representation, as long as there is no amplification of the incident waves. This occurs in the frequency band 0.8-1.0 Hz, at which a polarization was present for the spectral ratios of the radial component almost along the entire section (Figure 12). Amplification phenomena, which were not visible in Figure 12, can be observed in and around the river bed of the Aniene at frequencies of the order of 0.9 Hz. Therefore, they are mostly associated with the vertical component of motion.

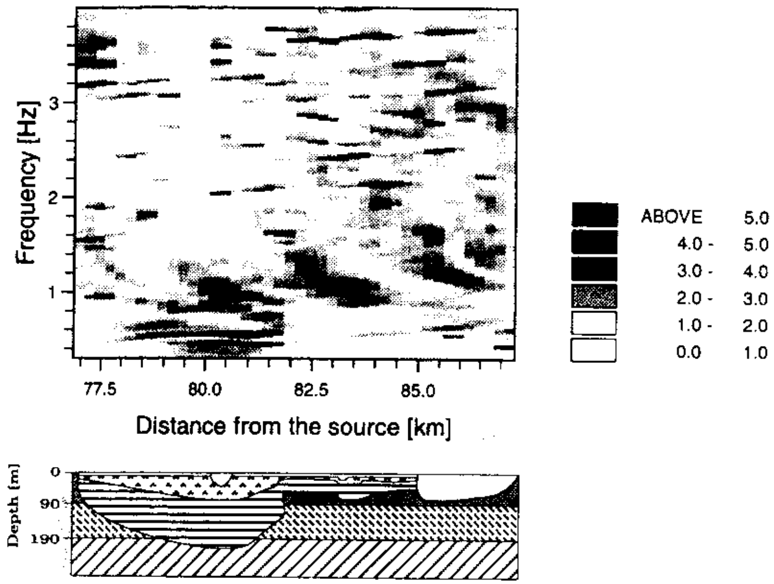

Figure 13 The same as Figure 12, for the total P-SV wavefield.

SUMMARY AND CONCLUSIONS

In absence of instrumental data, a numerical simulation of the ground motion in the city of Rome due to the January 13, 1915 Fucino (Italy) earthquake has been compared with the observed distribution of damage. This distribution has been compared with certain quantities related to the computed ground motion; these are quantities commonly used for engineering purposes: the peak ground acceleration (PGA), the maximum response of simple oscillators (POR), and the so-called "total energy of ground motion" (W) which is related to the Arias Intensity. The damage distribution in Rome shows essentially that the damage is concentrated at the edges of the alluvial basin of the Tiber river; the heavy and intermediate damage are located in that basin. The same distribution of damage can be expected on the basis of our numerical simulations of this event. The highest values of PGA, POR and W are observed at the edges of this alluvial basin. Strong amplification effects can be observed in the river beds of the Tiber and Aniene. The signals are characterized by large amplitudes and long durations due to (1) the low impedance of the alluvial sediments, (2) resonance effects, and (3) the excitation of local surface waves. Minimum values of PGA, POR and W can be observed for receivers placed above the volcanic layer which is present in the ancient river bed of the Tiber. This layer

11

acts as a shield, reflecting part of the incoming energy. The thicker the layer, the smaller the observed surface amplitudes of the signals. A good agreement with the observed distribution of damage is obtained for the "total energy of ground motion". This quantity and the related Arias Intensity turn out to be good representations of ground motion for hazard assessment. The very good correlation between the damage statistic and the ground motion makes it reasonable to use the total energy of ground motion for an immediate zonation of the entire town, including the part constructed after the Fucino event.

From the computation of spectral ratios, it has been recognized that the presence of a near-surface volcanic layer of rigid material is not sufficient to classify a location as a "hard-rock site", since the existence of an underlying sedimentary complex can cause amplifications due to resonances. A correct zonation requires knowledge of both the thickness of the surficial layer and of the deeper parts of the structure, down to real bedrock. This is especially important in volcanic areas, where lava flows often cover alluvial basins. In certain frequency bands, the presence of sediments causes the shift of energy from the vertical, into the radial component of motion. This phenomenon is very localized, both in frequency and space, and closely neighboring sites can be characterized by very large differences in the seismic response, even if the lateral variations of the local soil conditions are relatively smooth.

The hybrid technique we have developed makes it possible (1) to study local effects even at large distances (hundreds of kilometers) from the source, (2) to include highly realistic modelling of the source, and (3) to take into account the effects of the propagation path. This technique can assist in the interpretation and prediction of ground motion at a given site. This new approach can be applied routinely in zonation studies, and it provides realistic estimates of ground motion for two-dimensional, anelastic models. The resulting synthetic seismograms can be used to complete existing databases of recorded ground motion. Such databases would then serve to establish estimates of the maximum accelerations and total energies of ground motion to be expected at given sites. The results of this paper give the possibility for a fast seismic zonation, with no need to wait for a strong earthquake to occur, and allow prediction of the variation of seismic hazard due to possible temporal changes in geotechnical parameters, e.g. due to digging or changes in the ground water level. Since geotechnical data are available for several areas, especially in urban environments, the proposed technique can provide a valid seismic zonation with a small cost relative to the funds routinely invested in geotechnical analysis.

ACKNOWLEDGEMENTS

This study has been made possible by the CNR contracts 90.02382.CT15, 90.01026.PF54. We would like to thank ENEA for allowing us the use of the IBM3090E computer at the ENEA INFO BOL Computer Center. This research has been carried out in the framework of the activities of the ILP Task Group II.4.

REFERENCES

Aki, K., and K. L. Larner. 1970. Surface motion of a layered medium having an irregular interface due to incident plane SH waves. *J. Geophys. Res.* 75:933-954.

Alterman, Z. S., and F. C. Karal. 1968. Propagation of elastic waves in layered media by finite difference methods. *Bull. Seism. Soc. Am.* 58:367-398.

Ambrosini, S., Castenetto, S., Cevolani, F., Di Loreto, E., Funiciello, R., Liperi, L., and D. Molin. 1986. Risposta sismica dell'area urbana di Roma in occasione del terremoto del Fucino del 13 gennaio 1915. Risultati preliminari. *Mem. Soc. Geol. It.* 35:445-452.

Arias, A. 1970. A measure of earthquake intensity. *Seismic design for nuclear power plants*, R. Hansen (Ed.), Cambridge, Mass., 438-483.

Bard, P.-Y., and M. Bouchon. 1980a. The seismic response of sediment-filled valleys. Part 1: The case of incident SH waves. *Bull. Seism. Soc. Am.* 70:1263-1286.

Bard, P.-Y., and M. Bouchon. 1980b. The seismic response of sediment-filled valleys. Part 2: The case of incident P and SV waves. *Bull. Seism. Soc. Am.* 70:1921-1941.

Basili, A., Favali, P., Scalera, G., and G. Smriglio. 1987. Valutazione della pericolosità sismica in Italia centrale con particolare riguardo alla città di Roma. *Atti del 6° Convegno del Gruppo Nazionale di Geofisica della Terra Solida*, CNR, Roma, 379-393.

Ben-Menahem, A., and D. G. Harkrider. 1964. Radiation patterns of seismic surface waves from buried dipolar point sources in a flat stratified Earth. *J. Geophys. Res.* 69:2605-2620.

Boore, D. M. 1972. Finite difference methods for seismic wave propagation in heterogeneous materials. *Methods in Computational Physics*, Vol. 11, B. A. Bolt (Ed.), New York, Academic Press, 1-37.

Boschi, E., Feroci, M., Funiciello, R., Malagnini, L., Rovelli, A., and S. Salvi. 1989. Valutazione della risposta sismica in ambiente urbano: risultati per la città di Roma. *Atti del 8° Convegno Gruppo Nazionale Geofisica della Terra Solida*, CNR, Roma, 317-326.

Caputo, M., Keilis-Borok, V., Oficerova, E.,Ranzman, E., Rotwain, I., and A Solovjeff. 1980. Pattern recognition of earthquake-prone areas in Italy. *Phys. Earth. Planet. Int.* 21:305-320.

Carboni, G., Funiciello, R., Parotto, M., Marra, F., Salvi, S., Corazza, A., Lombardi, L., and M. Feroci. 1991. Geologia e idrogeologia del centro storico di Roma. Roma, in preparation.

CNEN-ENEL. 1977. Uncorrected accelerograms. Accelerograms from the Friuli, Italy, earthquake of May 6, 1976 and aftershocks: part 3, Rome, Italy, November 1977.

Emmerich, H., and M. Korn. 1987. Incorporation of attenuation into time-domain computations of seismic wave fields. *Geophysics* 52:1252-1264.

Emmerich, H. 1992. P-SV-wave propagation in a medium with local heterogeneities: a hybrid formulation and its application. *Geophys. J. Int.* 109:54-64.

Fäh, D., Suhadolc, P., and G. F. Panza. 1990. Estimation of strong ground motion in laterally heterogenenous media: modal summation - finite differences. *Proc. 9-th European Conference of Earthquake Engineering*, Sept. 11-16, 1990, Moscow, USSR, Vol.4A, 100-109.

Fäh, D. 1992. *A hybrid technique for the estimation of strong ground motion in sedimentary basins*. Ph.D. thesis Nr. 9767, Swiss Federal Institute of Technology, Zurich.

12

Feroci, M., Funiciello, R., Marra, F., and S. Salvi. 1990. Evoluzione tettonica e paleogeografica plio-pleistocenica dell'area di Roma. *Il Quaternario* 3 (2):141-158.

Florsch, N., Fäh, D., Suhadolc, P., and G. F. Panza. 1991. Complete synthetic seismograms for high-frequency multimode SH-waves. *Pure and Applied Geophys.* 136:529-560.

Funiciello, R., Loria, G., and S. Salvi. 1987. Ricostruzione delle superfici strutturali del sottosuolo della città di Roma. *Atti del 6° Convegno Gruppo Nazionale Geofisica della Terra Solida*, CNR, Roma, 395-415.

Futterman, W.I. 1962. Dispersive body waves. *J. Geophys. Res.* 67:5279-5291.

Gasparini, C., Iannaccone, G., and R. Scarpa. 1985. Fault-plane solutions and seismicity of the Italian peninsula. *Tectonophysics* 117:59-78.

Gazdag, J. 1981. Modeling of the acoustic wave equation with transform methods. *Geophysics* 46:854-859.

Gusev, A. A. 1983. Descriptive statistical model of earthquake source radiation and its application to an estimation of short period strong motion. *Geophys. J. R. astr. Soc.* 74:787-800.

Haskell, N. A. 1953. The dispersion of surface waves in multilayered media. *Bull. Seism. Soc. Am.* 43:17-34.

Iodice, C., Fäh, D., Suhadolc, P., and G. F. Panza. 1992. Un metodo generale per la zonazione sismica immediata ed accurata di grandi metropoli: applicazione alla città di Roma. *Rend. Fis. Acc. Lincei* 9 (3):195-217.

Jennings, P. C. 1983. Engineering seismology. *Terremoti: osservazione, teoria e interpretazione*. Rendiconti della Scuola Internazionale di Fisica 'Enrico Fermi'. LXXXV Corso. Società Italiana di Fisica (ed.), 138-173.

Kawase, H. 1988. Time-domain response of a semi-circular canyon for incident SV, P, and Rayleigh waves calculated by the discrete wavenumber boundary element method. *Bull. Seism. Soc. Am.* 78:1415-1437.

Knopoff, L. 1964. A matrix method for elastic wave problems. *Bull. Seism. Soc. Am.* 54:431-438.

Korn, M., and H. Stöckl. 1982. Reflection and transmission of Love channel waves at coal seam discontinuities computed with a finite difference method. *J. Geophys.* 50:171-176.

Kosloff, D., and E. Baysal. 1982. Forward modeling by a Fourier method. *Geophysics* 47:1402-1412.

Levshin, A. L. 1985. Effects of lateral inhomogeneities on surface waves amplitude measurements. *Ann. Geophys.* 3:511-518.

Lysmer, J., and L. A. Drake. 1972. A finite element method for seismology. *Seismology; surface waves and Earth oscillations, Methods in Computational Physics*. Vol. 11, B. A. Bolt, (Ed.), Academic Press, New York, 181-216.

Molin, D., Ambrosini, S., Castenetto, S., Di Loreto, E., Liperi, L., and A. Paciello. 1986. Aspetti della sismicità storica di Roma. *Mem. Soc. Geol. It.* 35:439-444.

Nicolich, R. 1981. Il profilo Latina-Pescara e le registrazioni mediante OBS nel Mar Tirreno. *Atti del 1° Convegno Gruppo Nazionale Geofisica della Terra Solida*, CNR, Roma, 621-637.

Nicolich, R. 1989. Crustal structures from seismic studies in the frame of the European Geotraverse (Southern Segment) and CROP projects. *The Lithosphere in Italy:*

Advances in Earth Sciences Research. A. Boriani, M. Bonafede, G.B. Piccardo and G.B. Vai (Eds.), *Atti dei Convegni Lincei* 80:41-61.

Panza, G. F., Schwab, F. A., and L. Knopoff. 1973. Multimode surface waves for selected focal mechanisms. I. Dip-slip sources on a vertical fault plane. *Geophys. J. R. astr. Soc.* 34:265-278.

Panza, G. F., Mueller, St., and G. Calcagnile. 1980. The gross features of the lithosphere-asthenosphere system in Europe from seismic surface waves and body waves. *Pure and Applied Geophys.* 118:1209-1213.

Panza, G. F. 1985. Synthetic seismograms: The Rayleigh waves modal summation. *J. Geophysics* 58:125-145.

Panza, G. F., and P. Suhadolc. 1987. Complete strong motion synthetics. *Seismic Strong Motion Synthetics.* B. A. Bolt (ed.), Academic Press, Orlando, *Computational Techniques* 4:153-204.

Sabetta, F., and A. Pugliese. 1987. Attenuation of peak horizontal acceleration and velocity from Italian strong-motion records. *Bull. Seism. Soc. Am.* 77:1491-1513.

Sánchez-Sesma, F. J., and J. A. Esquivel. 1979. Ground motion on alluvial valleys under incident plane SH waves. *Bull. Seism. Soc. Am.* 69:1107-1120.

Schwab, F. 1970. Surface-wave dispersion computations: Knopoff's method. *Bull. Seism. Soc. Am.* 60:1491-1520.

Schwab, F., and L. Knopoff. 1971. Surface waves on multilayered anelastic media. *Bull. Seism. Soc. Am.* 61:893-912.

Schwab, F., and L. Knopoff. 1972. Fast surface wave and free mode computations. *Seismology; surface waves and Earth oscillations. Methods in Computational Physics.* Vol. 11, B. A. Bolt (Ed.), New York, Academic Press, 87-180.

Schwab, F., and L. Knopoff. 1973. Love waves and torsional free modes of a multilayered anelastic sphere. *Bull. Seism. Soc. Am.* 63:1103-1117.

Schwab, F. 1988. Mechanism of anelasticity. *Geophys. J. Int.* 95:261-284.

Serva, L., Blumetti, A. M., and A. M. Michetti. 1986. Gli effetti sul terreno del terremoto del Fucino (13 gennaio 1915); tentativo di interpretazione della evoluzione tettonica recente di alcune strutture. *Mem. Soc. Geol. It.* 35:893-907.

Suhadolc, P., and C. Chiaruttini. 1985. A theoretical study of the dependence of peak ground acceleration on source and structure parameters. *Strong ground motion seismology. Proceedings of the NATO ASI on Strong Ground Motion Seismology.* Ankara, Turkey, 1985, 143-183.

Suhadolc, P., and G. F. Panza. 1989. Physical properties of the lithosphere-asthenosphere system in Europe from Geophysical Data. *The lithosphere in Italy: Advances in Earth Science Research.* A. Boriani, Bonafede, G.B. Piccardo and G.B. Vai (Eds.). *Atti dei Convegni Lincei* 80:15-40.

Takeuchi, H., and M. Saito. 1972. Seismic surface waves. *Seismology; surface waves and Earth oscillations. Methods in computational physics.* B. A. Bolt (Ed.), Vol. 11, Academic Press, 217-295.

Thomson, W. T. 1950. Transmission of elastic waves through a stratified solid medium. *J. Appl. Phys.* 21:89-93.

13

Vaccari, F., Gregersen, S., Furlan, M., and G. F. Panza. 1989. Synthetic seismograms in laterally heterogeneous, anelastic media by modal summation of P-SV waves. *Geophys. J. Int.* 99:285-295.

Vaccari, F., Suhadolc, P., and G. F. Panza. 1990. Irpinia, Italy, 1980 earthquake; waveform modelling of strong motion data. *Geophys. J. Int.* 101:631-647.

Ventriglia, U. 1971. *La geologia della città di Roma.* Amm. Prov. di Roma, Roma.

Virieux, J. 1986. P-SV wave propagation in heterogeneous media: velocity-stress finite-difference method. *Geophysics* 51 (4):889-901.

Ward, S. N., and G. R. Valensise. 1989. Fault parameters and slip distribution of the 1915 Avezzano , Italy, earthquake derived from geodetic observations. *Bull. Seism. Soc. Am.* 79:690-710.

Bulletin of the Seismological Society of America, Vol. 84, No. 2, pp. 383–399, April 1994

A Hybrid Method for the Estimation of Ground Motion in Sedimentary Basins: Quantitative Modeling for Mexico City

by D. Fäh, P. Suhadolc, St. Mueller, and G. F. Panza

Abstract To estimate the ground motion in two-dimensional (2D), laterally heterogeneous, anelastic media, a hybrid technique has been developed that combines modal summation and the finite-difference method. In the calculation of the local wave field owing to a seismic event, both for small and large epicentral distances, it is possible to take into account the source, path, and local soil effects.

As a practical application, we have simulated the ground motion in Mexico City caused by the Michoacan earthquake of September 19, 1985. By studying the one-dimensional (1D) response of the two sedimentary layers present in Mexico City, it is possible to explain the difference in amplitudes observed between records for receivers inside and outside the lake-bed zone. These simple models show that the sedimentary cover produces the concentration of high-frequency waves (0.2 to 0.5 Hz) on the horizontal components of motion. The large amplitude coda of ground motion observed inside the lake-bed zone and the spectral ratios between signals observed inside and outside the lake-bed zone can only be explained by 2D models of the sedimentary basin. In such models, the ground motion is mainly controlled by the response of the uppermost clay layer. The synthetic signals explain the major characteristics (relative amplitudes, spectral ratios, and frequency content) of the observed ground motion. The large amplitude coda of the ground motion observed in the lake-bed zone can be explained as resonance effects and the excitation of local surface waves in the laterally heterogeneous clay layer. Also, for the 1985 Michoacan event, the energy contributions of the three subevents are important to explain the observed durations.

Introduction

Numerical simulations play an important role in the estimation of strong ground motion in sedimentary basins. They can provide synthetic signals for areas where recordings are absent and are, therefore, very useful for engineering design of earthquake-resistant structures. In recent years, many computational techniques have been proposed to estimate ground motion at a specific site. The methods commonly used are one- and two-dimensional (1D and 2D) techniques; three-dimensional (3D) studies are too expensive to be applied routinely. The standard 1D methods, such as the Thomson–Haskell method (Thomson, 1950; Haskell, 1953), are very cheap, and they easily provide the first few resonance frequencies (fundamental and harmonics) of unconsolidated sedimentary layers. The results show that the strongest effects usually occur at the fundamental frequency. Relative to the response of a reference, bedrock model, 1D techniques yield estimates of the wave amplification caused by unconsolidated surficial sediments overlying the bedrock. However, such techniques fail to predict the ground motion close to lateral heterogeneities or when the sedimentary layers have a nonplanar geometry. For realistic structures where lateral heterogeneities and sloping layers are common, these departures from lateral homogeneity can cause effects that dominate the ground motion: the excitation of local surface waves, focusing and defocusing, and spatially variable resonances. Thus, the treatment of realistic structures requires at least 2D techniques to estimate ground motion. In many of these techniques, such as in the finite-difference (e.g., Alterman and Karal, 1968) or finite-element methods (e.g., Lysmer and Drake, 1972), the source cannot be included in the structural model, because its distance from the site of interest is too large. The incoming wave field is then approximated by a plane-polarized body wave. Other techniques, such as the 2D mode summation method

(Levshin, 1985; Vaccari *et al.*, 1989), are capable of treating realistic source models but can be practically applied only to simple 2D geometries of sedimentary basins.

To include both a realistic source model and a complex structural model of the sedimentary basin, a hybrid method has been developed that combines modal summation and the finite-difference technique (Fäh *et al.*, 1990; Fäh, 1992). The propagation of waves from the source position to the sedimentary basin is treated with the mode summation method for a plane-layered structure. Explicit finite-difference schemes are then used to simulate the propagation of seismic waves in the sedimentary basin. This hybrid method is particularly suitable to estimate ground motion in sedimentary basins of any complexity, and it allows us to take into account the source, path, and local site effects, even when dealing with path lengths of a few hundred kilometers. A similar method that combines modal summation and the finite-element technique has been used by Regan and Harkrider (1989) to study the propagation of *SH Lg* waves in and near continental margins.

Numerical simulations should always be compared with observed ground motion for the same simulated event to establish validity of the numerical results. This will be done for the case of Mexico City that has experienced extensive damage in the recent past owing to strong earthquakes with hypocenters in the Mexican subduction zone. The Michoacan earthquake of September 19, 1985 (M_S = 8.1), together with its aftershocks, produced the worst earthquake damage in the history of Mexico. Although the epicenter of the earthquake was close to the Pacific coastline, damage at coastal sites was relatively small. The reason for this is that most of the populated areas near the coast are situated on hard bedrock. In contrast, Mexico City, which is about 400 km away from the epicenter, suffered extensive damage. This can be attributed to the geotechnical and geometrical characteristics of the sediments in the valley of Mexico City. They were responsible for a very long duration of ground motion with large amplitude coda and large relative spectral amplifications that reached values of up to 50.

Using data from a recently installed VBB (Very Broad Band) seismograph at CU (a hill-zone site of Mexico City), Singh and Ordaz (1992) proposed a simple explanation of the long duration of recorded coda in the lake-bed zone. They state that the long-duration coda has always been present in the excitation, but the accelerations did not reach the necessary threshold for the standard instruments at hill-zone sites to remain triggered. The clay layers present in the lake-bed zone are natural narrow-band amplifiers that explain the recorded coda. They reach the conclusion that 2D or 3D models are not needed to account for the duration observed in the lake-bed zone. Their conclusion is based on only indirect and qualitative comparisons: they compare observed signals and synthetics (obtained with 1D modeling) for different events. Therefore, they could not give quantitative estimates of the amplification in the lake-bed zone with respect to a hill-zone site, since the hill-zone-site duration and waveform of the two earthquakes could be completely different. However, they fail to provide an explanation for the records (e.g., station CDAO) that exhibit a large amplitude coda well within the time windows for which stations on firm sites (e.g., station TACY) were recording. As was already shown by Kawase and Aki (1989), 1D modeling fails to explain this effect; and spectral ratios obtained with theoretical 1D models cannot explain the observations. Moreover, the variability and polarization of ground motion in the lake-bed zone also cannot be interpreted with 1D models (F. J. Sánchez-Sesma, personal comm.). These facts motivate the present-day research toward 2D and 3D modeling of wave propagation in sedimentary basins.

The 2D numerical modeling of the Michoacan earthquake and the effects of this earthquake in Mexico City exhibit some interesting numerical problems that arise from the large distance of Mexico City from the seismic source. This distance causes a long duration of the incident seismic signals in Mexico City, and the presence there of sediments with very low shear-wave velocities requires the use of a small grid spacing in the finite-difference computations. This small grid spacing, on the other hand, requires very efficient absorbing boundaries in the finite-difference part of the hybrid approach.

The Hybrid Method

The hybrid technique combines modal summation and the finite-difference method, and it can be used to study wave propagation in sedimentary basins. Each of the two techniques is applied in that part of the structural model where it works most efficiently: the finite-difference method in the laterally heterogeneous part of the structural model that contains the sedimentary basin (see Fig. 1), and modal summation is applied to simulate wave propagation from the source position to the sedimentary basin of interest. The use of the mode summation method allows us to include an extended source, which can be modeled by a sum of point sources appropriately distributed in space and time. The path from the source position to the sedimentary basin can be approximated by a structure composed of flat, homogeneous layers. Modal summation then allows the treatment of many layers that can take into consideration low-velocity zones and fine details of the crustal section under consideration. The finite-difference method, applied to wave propagation in the sedimentary basin, permits the mod-

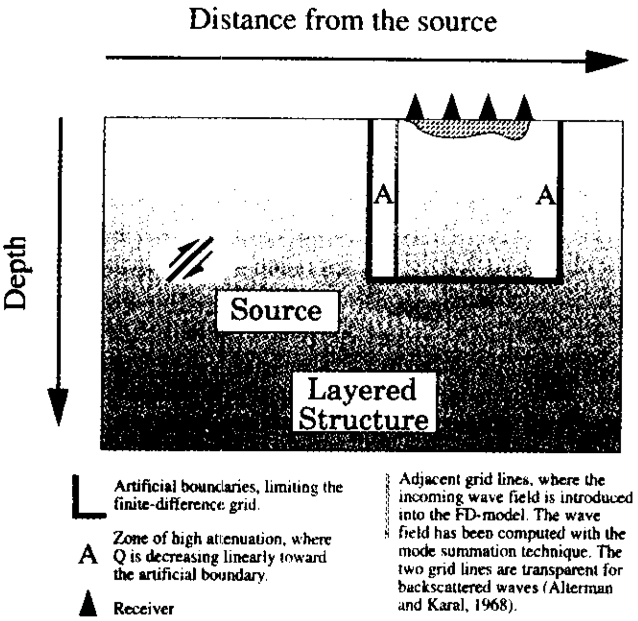

Figure 1. Schematic geometry used in the hybrid method (see text).

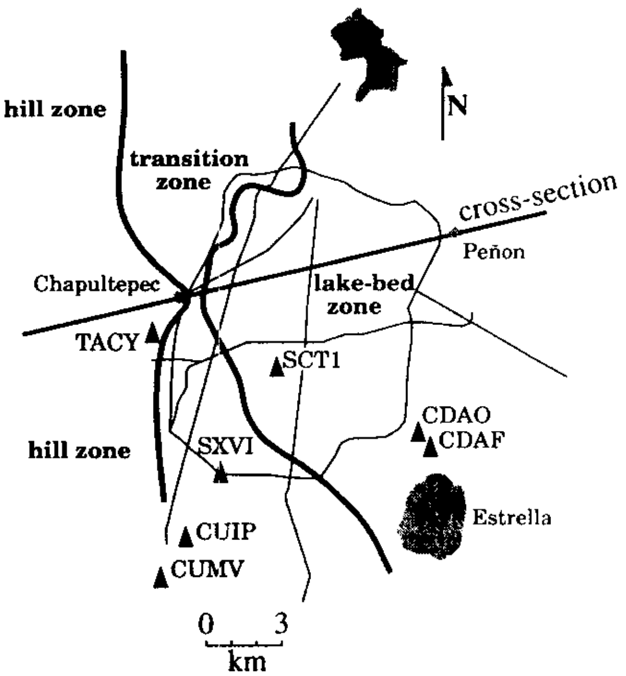

Figure 2. Map of the area of Mexico City. On the map, the locations of the strong-motion accelerometer stations are shown; these stations were operating during the 1985 Michoacan event. The locations of stations CU01 and CUIP are the same. The solid line indicates the cross section, for which 2D modeling has been performed.

eling of wave propagation in complicated and rapidly varying velocity structures, as is required when dealing with sedimentary basins. The coupling of the two methods is carried out by introducing the time series obtained with modal summation into the finite-difference computations.

In the modal summation method, the treatment of *P-SV* waves is based on Schwab's (1970) optimization of Knopoff's (1964) method (Panza, 1985), and the handling of *SH* waves is based on Haskell's (1953) formulation (Florsch *et al.*, 1991); these computations include the "mode-follower" procedure and structure minimization described by Panza and Suhadolc (1987). The introduction of anelasticity into the computations is based on variational methods (Takeuchi and Saito, 1972; Schwab and Knopoff, 1972) and includes Futterman's (1962) results concerning the dispersion of body waves in a linearly anelastic medium.

The seismic source is introduced by using the Ben-Menahem and Harkrider (1964) formalism. In these expressions, the first-term approximation to cylindrical Hankel functions is used that gives the displacements in the far-field. Calculation of synthetic seismograms is then accurate to at least three significant figures, as long as the distance to the source is greater than the wavelength (Panza *et al.*, 1973). The seismograms computed with modal summation contain all the body waves and surface waves, whose phase velocities are smaller than the *S*-wave velocity of the half-space that terminates the structural model at depth. These computations therefore supply a realistic incoming *S*-wave and surface-wave wave field that is used as input in the finite-difference computations.

Explicit finite-difference schemes are used to simulate the propagation of seismic waves in the sedimentary basin. These schemes are based on the formulation of Korn and Stöckl (1982) for *SH* waves and on the velocity-stress, finite-difference method for *P-SV* waves (Virieux, 1986). The algorithms can handle structural models containing a solid-liquid interface and are numerically stable for materials with normal as well as high values of Poisson's ratio. However, the numerical error

Table 1
Numerical Data for the Schematic Crustal Model Describing the Path from the Source in the Michoacan Subduction Zone, to Mexico City*

Layer	Thickness (km)	ρ (g/cm^3)	α (km/sec)	β (km/sec)	Q_α	Q_β
1	5.0	2.67	4.30	2.53	800	500
2	10.0	2.77	5.70	3.30	800	500
3	15.0	3.09	6.80	4.03	800	500
4	15.0	3.09	7.00	4.10	800	500
5	∞	3.30	8.20	4.82	800	500

*Campillo *et al.* (1989).

increases with decreasing velocities, so it is usually bigger near the surface of the models. Therefore, in the *P-SV* case, a fourth-order approximation to the spatial differential operators is used for the upperpart of the structural model (Levander, 1988). This offers the possibility to reduce the spatial sampling required to accurately model wave propagation. The finite-difference operator in time is always of second order, since a fourth-order approximation would require too much computer memory.

A cause of error in the results of the hybrid technique can be the insufficient depth of the structural model described by the finite-difference grid. When this insufficiency occurs, the signals are incomplete for receivers at large distances from the vertical grid lines where the incident wave field is introduced into the finite-difference computations. To deal with this problem, the lower artificial boundary of the finite-difference grid is simply placed at greater depth. Moreover, to reduce the number of grid points in the vertical direction, the grid spacing is increased at depth. The number of grid points per wavelength in this deeper region of the structure is chosen large enough to prevent numerical errors.

Energy loss in unconsolidated sediments is an important process and should always be taken into account to prevent serious errors in seismic hazard estimations. In the finite-difference computations, anelasticity is included by using the rheological model of the generalized Maxwell body (Emmerich and Korn, 1987; Emmerich, 1992; Fäh, 1992). This approach allows us to approximate the viscoelastic modulus by a low-order, rational function of frequency. This approximation of the viscoelastic modulus can account for a constant quality factor over a certain frequency band. Replacement of all elastic moduli by viscoelastic ones, and transformation of the stress-strain relation into the time domain, yields a formulation that can be handled with a finite-difference algorithm (Emmerich and Korn, 1987).

The finite-difference method has the disadvantage that limitations of computer memory require the introduction of artificial boundaries, which form the border

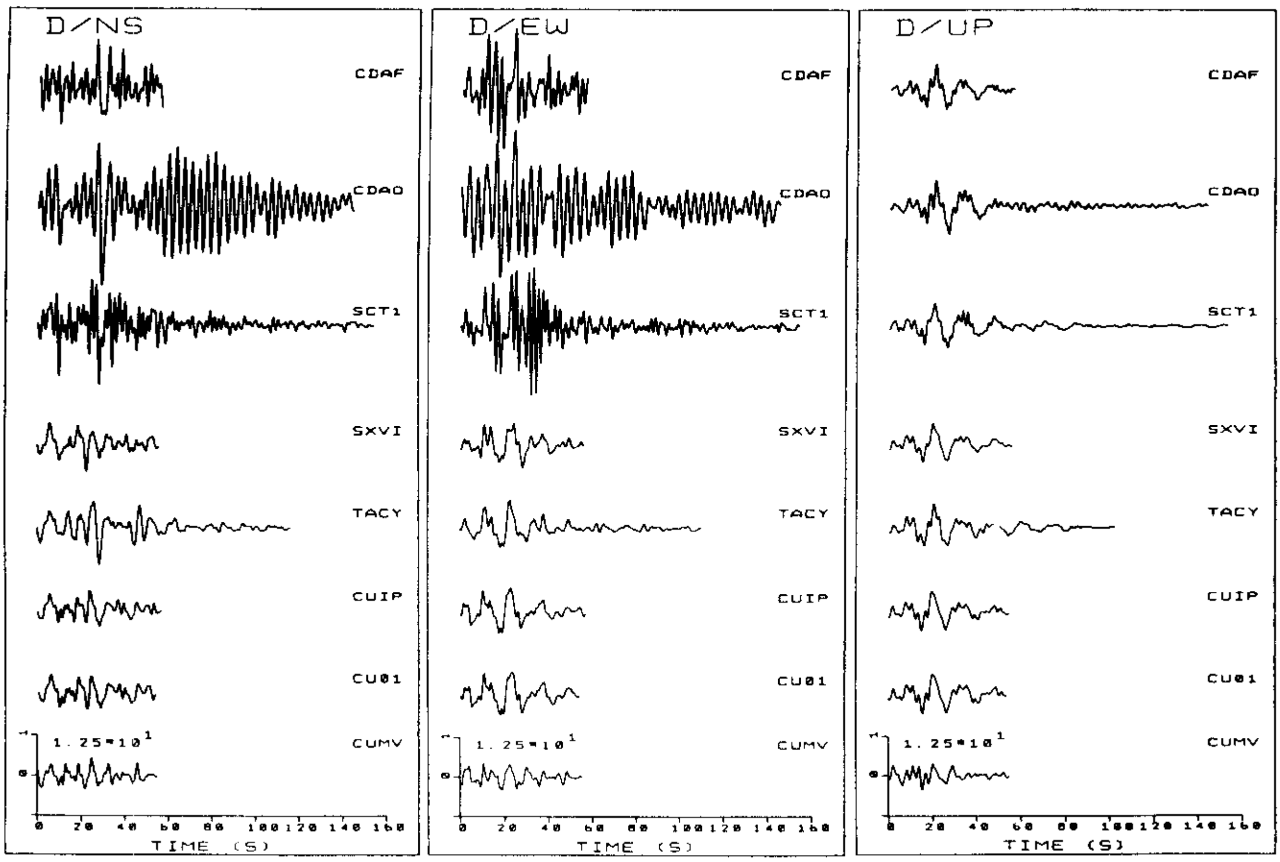

Figure 3. Horizontal and vertical components of displacement recorded in the valley of Mexico City (Mena *et al.*, 1986). The N–S component of motion is denoted by D/NS, the E–W component by D/EW, and the vertical component by D/UP. In each column, the signals are normalized to the same peak displacement. The peak displacement is indicated in units of centimeters.

of the finite-difference grid in space. These boundaries are a severe problem in finite-difference methods, since they can generate reflections of the waves impinging upon them from the interior of the grid. In this study, several methods for the prevention of these reflections are combined. Paraxial approximation of the wave equation (Clayton and Engquist, 1977) works well at the boundary limiting the structural model at depth. The two vertical boundaries at each side of the grid are chosen in relation to the grid spacing in the finite-difference computations. In the case of a large grid spacing (50 m in the *P-SV* case; 25 m in the *SH* case), the method proposed by Smith (1974) reduces this contamination almost perfectly. Smith's method is only applied at the right boundary, whereas at the left boundary, the paraxial approximation is chosen. With this technique, the contamination first appears at the right boundary having passed through the model two times. The disadvantage of Smith's boundary conditions is an increase in computer time by a factor of 2. In the case of a small grid spacing (20 m in the *P-SV* case; 10 m in the *SH* case), Smith's boundary condition is too time-consuming. Then, the paraxial wave equation is also applied at the right artificial boundary. To improve the absorption at the ar-

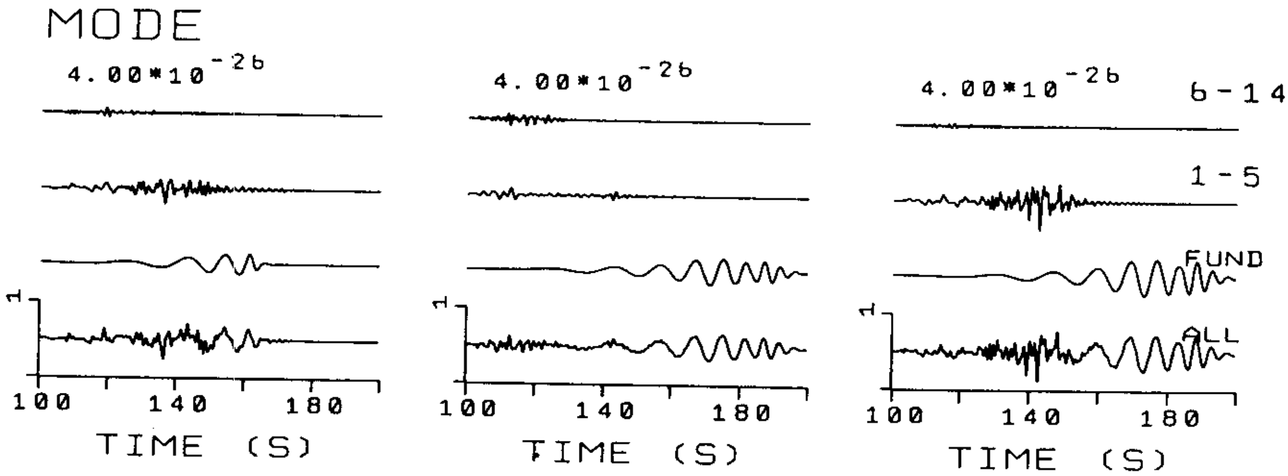

Figure 4. Transverse (left column), radial (middle column), and vertical displacements (right column) obtained for a point source (see text) in a 1D structural model (Table 1) at a distance of 400 km. All amplitudes are related to a source with seismic moment of 10^{-7} N-m. The signals are normalized to the same peak displacement. The peak displacement is in units of centimeters. Each component is decomposed into different sets of modes (upper three traces for each component: modes 6 to 14, modes 1 to 5, fundamental mode FUND).

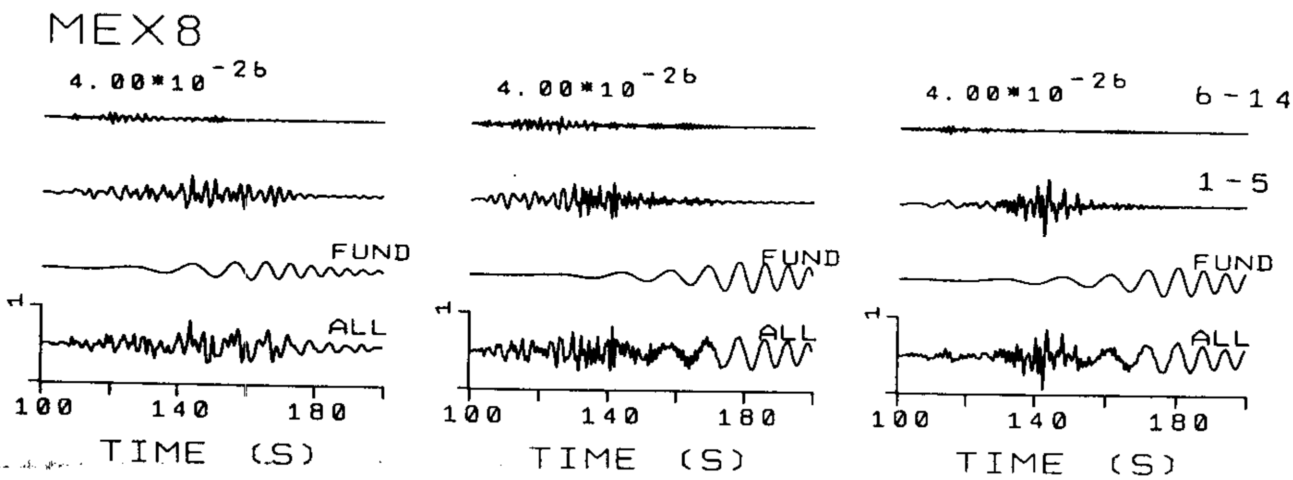

Figure 5. The same as in Figure 4, but replacing the first 400 m of the layered model (Table 1) with a surficial sedimentary layer, which represents the deep sediments (400-m thickness, $\rho = 2.0$ g/cm^3, $\alpha = 2.0$ km/sec, $\beta = 0.6$ km/sec, $Q_\alpha = 100$, and $Q_\beta = 50$).

tificial boundaries, regions of high absorption are introduced close to the boundaries. Since anelastic absorption is included in our numerical finite-difference scheme, this approach requires no additional computer time. The quality factor Q has to be space dependent so that Q is decreasing linearly toward the artificial boundary. The gradient should not be too steep, to avoid reflections. With this method, the amplitude of the incoming wave field is sufficiently well-attenuated as long as the zone including damping is larger than the dominant wavelength. In the low-frequency part of the wave field, the gradient of the quality factor close to the artificial boundary can produce reflections of the outgoing waves. Since the region of high absorption is characterized by the absence of low-velocity sediments, the grid spacing in the horizontal direction can be increased still having enough grid points per wavelength. This new grid spacing enlarges the geometrical extension of the region of high absorption and, therefore, reduces the steepness of the gradient of the quality factor.

Observations in Mexico City

From the geotechnical point of view, the valley of Mexico City can be divided into three zones (Fig. 2): the hill zone, the transition zone, and the lake-bed zone. The hill zone is formed by alluvial and glacial deposits and by lava flows. The transition zone is mainly composed of sandy and silty layers of alluvial origin. The surficial layers in the lake-bed zone consist mainly of clays. These deposits are poorly consolidated, with high water content and very low rigidity. The geometrical characteristics and mechanical properties are quite well-known from different borehole and laboratory tests. The mechanical properties exhibit a great variability. This surficial layer varies between 10 and 70 m in thickness, where this thickness increases regularly toward the east (Suarez *et al.*, 1987). The topmost layer is composed of compacted fill and of the foundations for man-made structures (Chávez-Garcia and Bard, 1990). It is more resistant than the clay, and its thickness can be up to 10 m.

The clay layer is overlying the so-called "deep sediments" found below 10 to 70 m. These deeper deposits reach depths down to 700 m, where the uncertainty of the thickness of the deep sediments may be as large as a few hundred meters (e.g., Bard *et al.*, 1988). The mechanical characteristics of the deep sediments are very poorly known; the topography of the bedrock interface has been estimated from boreholes and gravimetric data (Suarez *et al.*, 1987). There are three outcrops of the basement: at Chapultepec, Peñon, and Cerro de la Estrella (Fig. 2).

During the Michoacan earthquake, a strong motion network was operating in the valley of Mexico City (Mena *et al.*, 1986). The positions of the stations are shown in Figure 2. Some of these were located in the lake-bed zone (SCT1, CDAO, CDAF), some in the hill zone (TACY, CUIP, CU01, CUMV), and one in the transition zone (SXVI). The observed displacements are shown in Figure 3. The records are corrected for the instrumental response and have been convolved with a high-pass Ormsby filter whose largest low-frequency cutoff is 0.10 Hz for the stations outside the lake-bed zone and 0.07 Hz for those inside the lake-bed zone (Mena *et al.*, 1986). These frequency limits do not influence our conclusions, since the dominant energy in the synthetic signals is above these frequency limits.

Absolute time references are absent in the recorded signals. To estimate the relative times to an arbitrarily

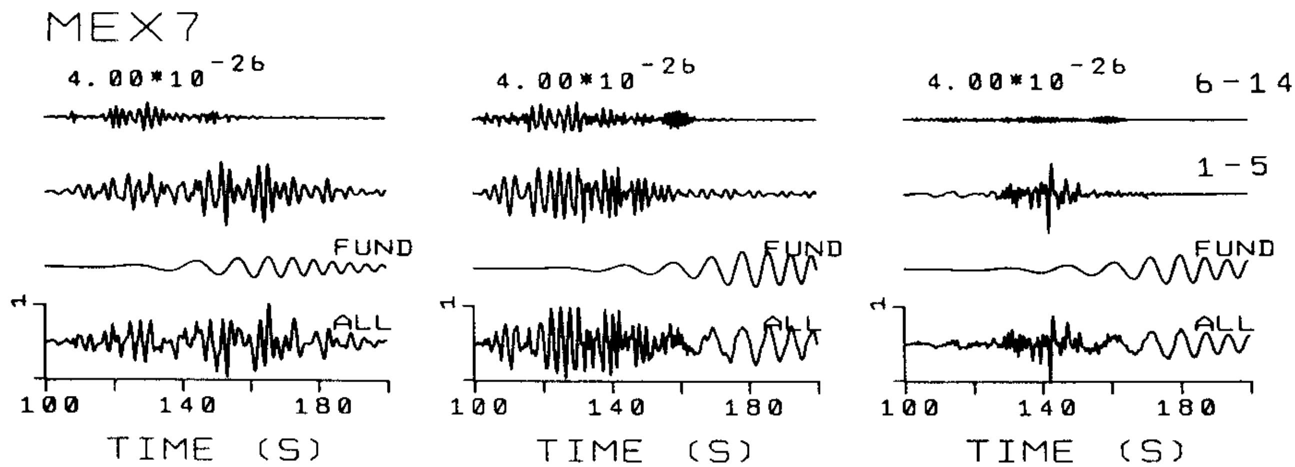

Figure 6. The same as in Figure 5, but now the model also contains a surficial clay layer (55-m thickness, $\rho = 1.3$ g/cm^3, $\alpha = 1.5$ km/sec, $\beta = 0.08$ km/sec, $Q_\alpha = 50$, and $Q_\beta = 25$), which replaces the first 55 m of the sedimentary layer described in the caption of Figure 5.

chosen zero-time, the signals have been shifted so that the long-period part of the vertical displacements are in phase (Campillo *et al.*, 1988). This is justified since the long-period vertical displacements (Fig. 3, label D/UP) have nearly identical waveforms and amplitudes at all stations. The time shifts have been given by Bard *et al.* (1988): CDAF (2.00 sec), CDAO (35.75 sec), SCT1 (26.00 sec), TACY (40.00 sec), CUIP (3.00 sec), and CUO1 (6.50 sec). The time shifts for the stations SXVI and CUMV are not given in the literature and are here determined to be 4.50 and 5.00 sec, respectively.

The differences between the records in the lake-bed zone and the records in the hill zone reflect the differences at the sites. In the lake-bed zone (stations SCT1, CDAO, and CDAF), the horizontal components of motion are the dominant ones. They have a larger high-frequency content than the corresponding vertical or horizontal components recorded outside the lake-bed zone. The spectral peaks are in the interval between 0.2 and 0.5 Hz.

Choice of the Source and Path Models for the Numerical Modeling

The flat-layered structure, describing the path from the seismic source to the valley of Mexico City, is shown in Table 1. This model has been proposed by Campillo *et al.* (1989) and was deduced directly from refraction measurements in the Oaxaca, Southern Mexico, region (Valdes *et al.*, 1986). The structural model is rather simple and in agreement with the resolving power of the available data. The depth of the Moho is about 45 km, and the upper 5 km are composed of relative low-velocity material.

The epicenter of the Michoacan earthquake is close to the Pacific coastline. It is a typical intraplate subduc-

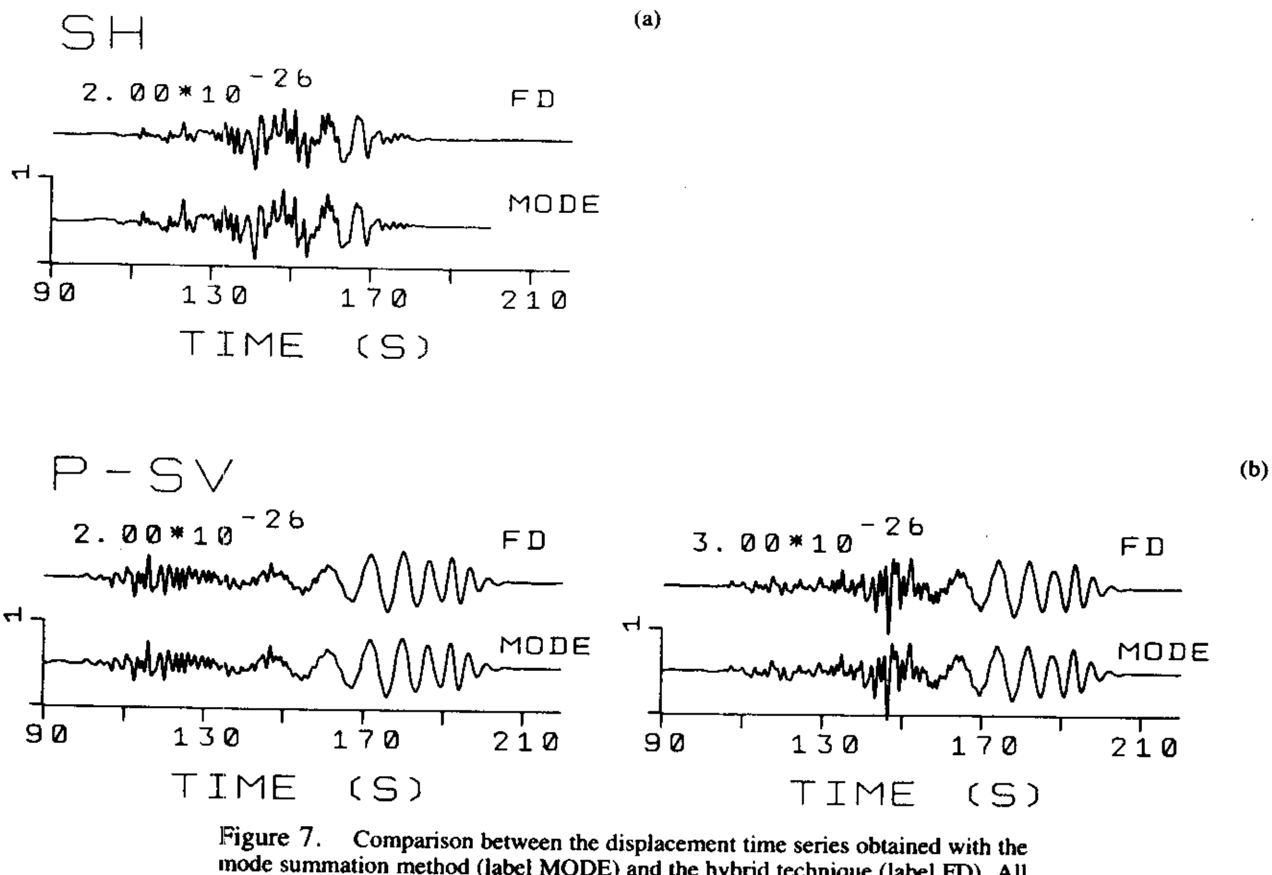

Figure 7. Comparison between the displacement time series obtained with the mode summation method (label MODE) and the hybrid technique (label FD). All amplitudes are related to a source (see text) with seismic moment of 10^{-7} N-m. In each column, the signals are normalized to the same peak displacement. The peak displacement is given in units of centimeters. (a) *SH* case: The distance between the source and the vertical grid lines, where the incident wave field is introduced into the finite-difference computations, is 400 km; the source-receiver distance is 412 km; the grid spacing is 25 m. (b) *P-SV* case (with the radial displacements on the left and the vertical ones on the right): The distance between the source and the vertical grid lines is 396.5 km; the source-receiver distance is 408.5 km; the grid spacing is 50 m.

tion event, with a small dip angle and striking parallel to the Central America trench. The rupture started in the north and propagated through the zone of the 1981 Playa Azul earthquake with a low-moment release (Eissler *et al.*, 1986; Houston and Kanamori, 1986). It then ruptured an asperity in the south. Least-squares inversion of the Michoacan earthquake records, for the source time function, yielded three source pulses (Houston and Kanamori, 1986). The first two subevents have similar seismic moments and durations (about 15 sec); the moment of the third is about 20% that of the first subevent and has a duration of about 10 sec (Eissler *et al.*, 1986). The arrival time of the second event is shifted by 26 sec with respect to the first, and the location is about 80 km to the southeast of the first event. The third event occurred 21 sec after the second one, and its position is about 40 km seaward of the second event. The Michoacan earthquake is characterized by high spectral amplitudes for periods between 2 and 5 sec. Campillo *et al.* (1989) attribute the enhanced energy in the 2-to-5 sec period range to the irregularity of the rupture propagation. They suggest that the rupture developed as a smooth crack toward the ocean.

For the computations presented here, an average source model for the 1985 Michoacan earthquake has been chosen. To keep the source model as simple as possible, we restrict the model first to a simple point source with a duration of 0 sec. This allows us to study the behavior of the waves in the entire frequency band from 0.01 to 1 Hz, with no *a priori* assumptions about the frequency content of the source. This choice of a delta function will enhance high-frequency energy in parts of the computed ground motion. Therefore, for an easy qualitative comparison with the observed ground motion, we will only consider the displacement time series.

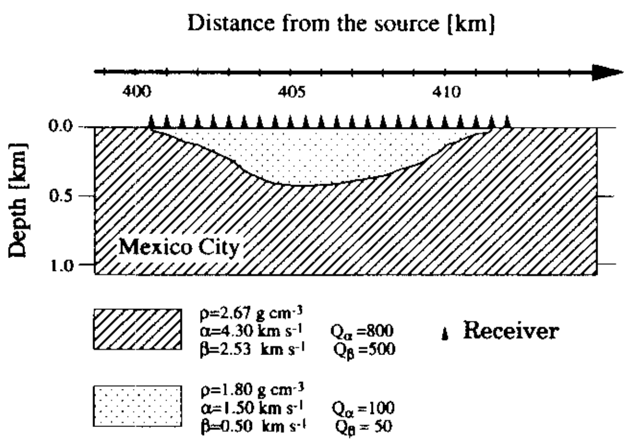

Figure 8. A 2D model related to the Chapultepec–Peñon cross section. Only the part of the structure near the surface is shown, where the 2D model deviates from the plane-layered structural model.

The focal mechanism is the one proposed by Campillo *et al.* (1989), based on the results of Houston and Kanamori (1986) and Riedesel *et al.* (1986). The distance from the source to the valley of Mexico City is 400 km, the angle between the strike of the fault and the epicenter-station line is 220° (further on, referred to as the strike-receiver angle), the source depth is 10 km, the dip 15°, and the rake is 76°.

Due to uncertainties in the available models, only estimates of the strong ground motion in Mexico City can be given. Nevertheless, this modeling allows us to understand the main features of seismic wave propagation in the Mexico City valley as a consequence of strong earthquakes. One-dimensional structural models for the Mexico City valley will be considered first, with the purpose of studying the 1D response of the sedimentary cover with modal summation. The 2D models that will then be considered describe the cross section from Chapultepec to Peñon across the sedimentary basin (for position, see Fig. 2). This cross section is of particular interest since it intersects the area where extensive damage occurred in the strong earthquakes of 1957, 1979, and 1985. This area has been the subject of several theoretical studies (e.g., Sánchez-Sesma *et al.*, 1988; Bard *et al.*, 1988; Kawase and Aki, 1989). The final part is dedicated to the comparison between observed and synthetic seismograms.

One-Dimensional Structural Models

The 1D structural model used to describe the path from the source position to the sedimentary basin in Mexico City is given in Table 1. Because of the large distance of Mexico City from the source and the relatively low velocities of seismic waves in the upper crust, the signals are strongly dispersed (Fig. 4). The simple, depth-limited structural model of Table 1 has only 15 modes in the frequency-phase velocity band being considered; the energy at frequencies below 0.2 Hz is limited to the fundamental mode, both for Love and Rayleigh waves.

In a second step of the 1D modeling, the sedimentary cover that is present in the valley of Mexico City is included in our structural model. Two models are proposed. In the first, a surficial sedimentary layer of 400-m thickness replaces the upper 400 m of the model shown in Table 1. This layer represents the deep sediments. The second model is obtained from the previous one by replacing the upper 55 m of the deep sediments with a surficial clay layer. The resulting 1D structure represents a 1D model for the lake-bed zone. The values of the densities, body-wave velocities, and quality factors of the layers are given in the captions of Figures 5 and 6, where the displacements obtained for both models are shown. The seismic source remains the same for all results shown in Figures 4, 5, and 6.

In passing from a model without a sedimentary layer (Fig. 4), to a model with sediments (Figs. 5 and 6), the arrival times and dispersion characteristics of the surface waves change. Group velocities decrease to values as low as 0.08 km/sec for the model with the surficial clay layer. The main effect of the sedimentary cover on the fundamental mode is a strong dispersion, caused by the low-velocity surficial layer(s). The amplitudes of fundamental-mode Love and Rayleigh waves remain approximately the same for all three structural models, whereas for the high-frequency part of the wave field, the amplitudes, the frequency content, and the arrival times are different. The amplitudes are larger for the models with a sedimentary cover. Because of the low shear-wave velocity of the clay layer, the high-frequency part (0.2 to 0.5 Hz) of the waves is concentrated in the horizontal components of motion (Fig. 6). The vertical components of motion obtained for the different structural models are similar.

The seismograms obtained for the 1D models of the Mexico City valley are of limited value for the interpretation of the observations in Mexico City; in fact, the surficial sedimentary layers are present only in the region surrounding Mexico City. In our results, this leads to unrealistically strong dispersion of the fundamental mode. On the other hand, these simple models show that the sedimentary cover can produce the observed concentration of the 0.2 to 0.5 Hz waves in the horizontal components. These models also explain the difference in amplitudes for receivers inside and outside the lake-bed zone and the almost unchanged form and amplitude of the vertical displacements [see Kawase and Aki (1989) for a review of the 1D results].

Before going into 2D computations, we must first compare the results of modal summation and the hybrid technique for the simple case of a 1D structural model. This comparison is necessary each time the hybrid technique is applied in a new region. The comparison allows us to establish control over the accuracy of the finite-difference part of the computations, relative to: (1) the correct discretization of the structural model in space, (2) the efficiency of the absorbing, artificial boundaries, (3) the presence of all phases in the seismograms, and (4) the treatment of anelasticity. The comparison is per-

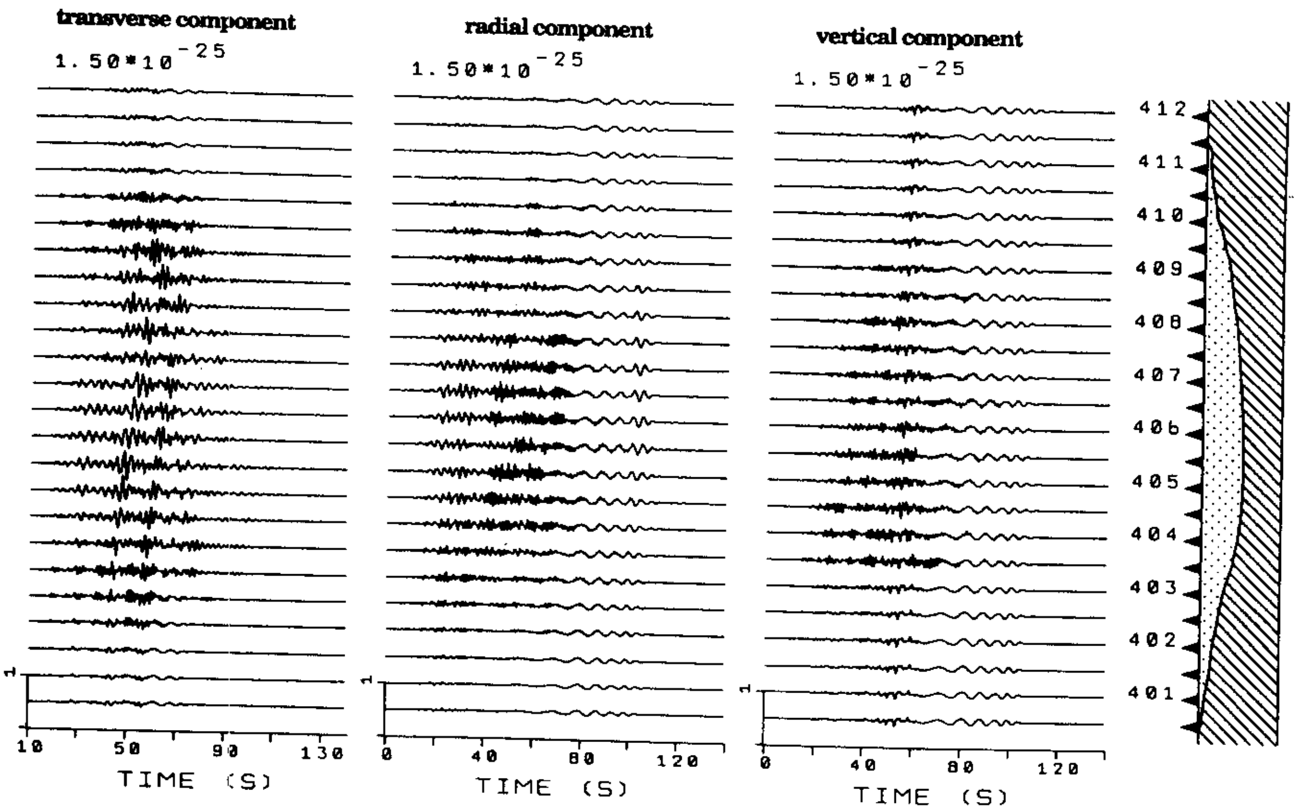

Figure 9. Displacement time series for *P-SV* and *SH* waves at an array of receivers over cross section Chapultepec–Peñon. All amplitudes are related to a source (see text) with seismic moment of 10^{-7} N-m. In each column, the signals are normalized to the same peak displacement. The peak displacement is indicated in units of centimeters. The time scale is shifted by 90 sec from the origin time (0 sec in the figure is in fact 90 sec from the origin time).

formed for the same layered structural model that describes the path from the source position to the region where the finite-difference method is applied (Table 1). It can be seen from Figure 7 that the results obtained with the hybrid technique and modal summation practically coincide. There are only small differences, which originate in the differences between the two computational techniques and in the small reflections from the artificial boundaries.

Two-Dimensional Models: The Chapultepec-Peñon Cross Section

Since the lake-bed zone is filled by the deep sediments and the clay layer, it is of interest to isolate the influence on the ground motion of these two layers. We first consider only the deep sediments. Because of uncertainties in the structural parameters, we consider different maximum thicknesses (400 and 700 m) and two extreme values of the S-wave velocity (0.5 and 1.0 km/sec) of the sediments. In a further step, a low-velocity surficial clay layer is added to the structural model; this layer replaces the first tens of meters of the deep sediments. For all computations, the source is the same impulsive point source (depth 10 km, dip 15°, rake 76°, and angle strike-receiver 220°). The 1D structural model, without the sediment and clay layer, describing the path from the source position to the valley of Mexico City is given in Table 1. This is the model used in the first portion of our hybrid computations where the modal summation method is applied.

Effects of the Deep Sediments

The 2D structure, modeling the Chapultepec–Peñon cross section, is shown in Figure 8. The distances between the observation points and the source is in the range 400 to 412 km. The mesh size used in the finite-difference grid is 25 by 25 m for SH waves and 50 by 50 m for P-SV waves.

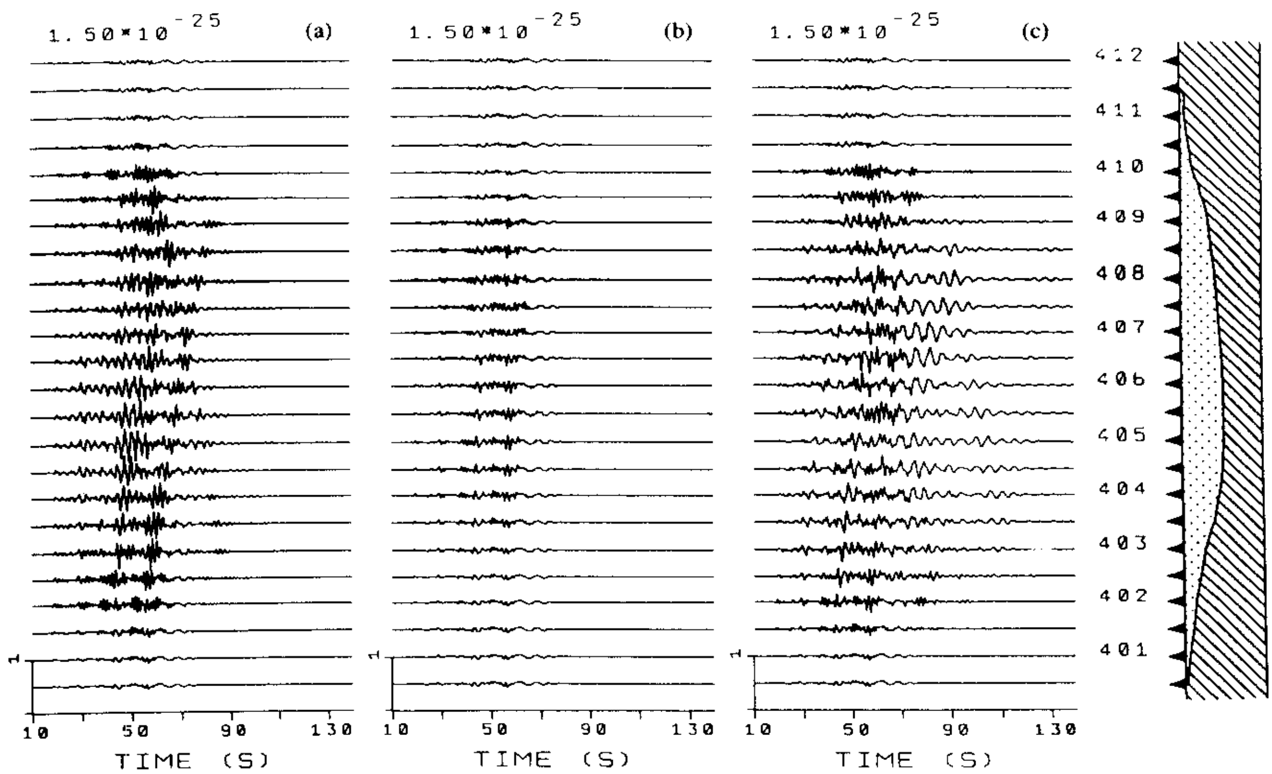

Figure 10. The same as in Figure 9 for the displacement time series for SH waves, assuming:
(a) Linear gradients in the material properties of the deep sediments: α = 1.3 to 1.5 km/sec, β = 0.25 to 0.6 km/sec, ρ = 1.8 g/cm^3, Q_α = 50 to 100, and Q_β = 25 to 50.
(b) Relatively high wave velocities for the deep sediments: α = 2.0 km/sec, β = 1.0 km/sec, ρ = 2.0 g/cm^3, Q_α = 100, and Q_β = 50.
(c) A sedimentary basin with a maximum thickness of 700 m and with material properties given in Figure 8.

The displacement time series, related to the receivers in Figure 8, are shown in Figure 9. In agreement with the observations in Mexico City during the Michoacan earthquake, our computational results show that the fundamental Rayleigh mode passes the sedimentary basin without significant change in amplitude and shape. The reason for this is the large wavelengths of the fundamental mode with respect to the spatial dimensions of the sedimentary basin. For the high-frequency part of the wave field, however, there is a great spatial variability of ground motion within the sedimentary basin. Two adjacent observation points can have very different waveforms. In the sedimentary basin, the amplitudes of the transverse displacement dominates that for *P-SV* waves.

Because of the long duration of the incident wave field, a superposition of different types of waves occurs. Therefore, it is difficult to distinguish different phases on the seismograms. In comparison with the results obtained for the 1D model (Fig. 4), the most important effect is the duration of the ground motion, which at some sites can be up to 40 sec longer than in the 1D case. This effect is mainly caused by local surface waves and their reflections at the edges of the sedimentary basin and is more pronounced for *SH* waves. This difference between the *SH* and *P-SV* case is due to the different dominant frequency content of the two wave types, which depends mainly on the source characteristics (e.g., depth, duration, rupture process). Local surface waves can only be a dominant phase in the seismograms if the incident wave field has much energy in the frequency band of the excited local surface waves.

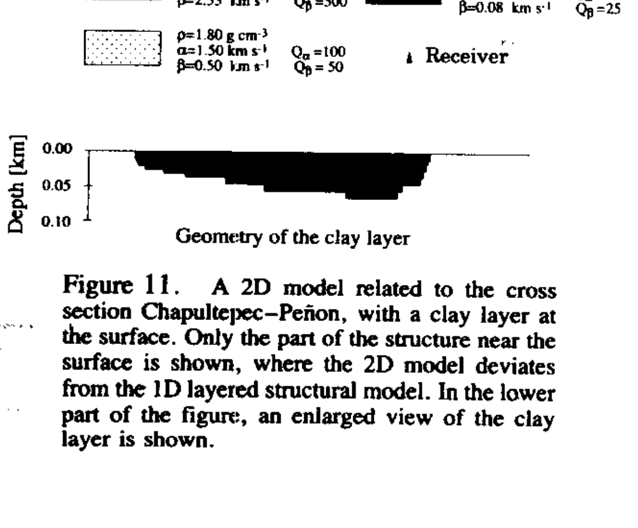

Figure 11. A 2D model related to the cross section Chapultepec–Peñon, with a clay layer at the surface. Only the part of the structure near the surface is shown, where the 2D model deviates from the 1D layered structural model. In the lower part of the figure, an enlarged view of the clay layer is shown.

The uncertainty in ground motion predicted from numerical modeling can now be quantified by a parametric study. As the deep sediments are known very poorly, three different velocity models and thicknesses are considered. The first variant is characterized by a gradient in the material properties (shear-wave velocities vary from 0.25 km/sec at the surface to 0.6 km/sec at the interface between sediments and bedrock). The second variant assumes a relatively high shear-wave velocity for the deep sediments ($\beta = 1.0$ km/sec). The displacement time series for *SH* waves relative to the first and second variant are shown in Figures 10a and b, respectively.

The model containing a gradient in the material properties is used to estimate the maximum possible effects caused by the deep sediments (Fig. 10a). The effects are a strong amplification and the lateral propagation of local surface waves excited at the edges of the sedimentary basin. The model containing sediments with high *S*-wave velocities is used to estimate the minimum effects caused by the deep sediments (Fig. 10b). Apart from a factor of about 2 in amplitude, there are no large variations between signals outside and inside the sedimentary basin. The difference in amplitudes can be explained by the impedance contrast between bedrock and sediments. There is no significant excitation of local surface waves at the edges of the basin.

The maximum thickness of the deep sediments is increased to 700 m in the third and last variant. This deep basin causes the excitation of long-period local surface waves, which dominate the waveforms and increase duration (Fig. 10c). Qualitatively, the results are the same as those discussed for the shallow sedimentary basin; however, in the deep basin, local surface waves are mainly excited by the fundamental mode, while in the shallow basin, higher modes are responsible for the generation of these local waves. This leads to very different shapes of the signals computed for the two structural models.

Effects of a Clay Layer

A surficial clay layer is now added to the structural model of the deep sediments (Fig. 11). As indicated by the information available about the soil properties in Mexico City, the clay thickness increases gradually toward the east. Due to the very low shear-wave velocity of the clay ($\beta = 0.08$ km/sec), the mesh size used in the finite-difference grid is 10 by 10 m for *SH* waves and 20 by 20 m for *P-SV* waves.

The displacement time series are shown in Figure 12. At the margin of the sedimentary basin, ground motion is determined mainly by the 1D response of the uppermost clay layer. Within the basin, both for incident Love and Rayleigh waves, there is evidence of local surface waves that propagate in the clay layer. Local resonance effects lead to long duration and large amplitude codas; this phenomenon is most pronounced on the radial component, at distances of 409 to 410 km from the source. The resonance is excited by two distinct arrivals: the *Lg* waves and the fundamental Rayleigh wave. Also for this model, the differences between the *SH* and *P-SV* case is due to the different frequency content of the two wave types. The vertical components of our synthetics, for frequencies below 0.5 Hz, are not significantly changed by the presence of the clay layer; this agrees with the recordings taken in Mexico City during the Michoacan earthquake.

A good representation of the amplification effects in sedimentary basins is given by the computation of spectral ratios between the signals obtained for the 2D model (Fig. 12) and the corresponding signals obtained for the 1D model (Table 1). The results for the transverse and the radial components are shown in Figure 13, where these ratios are illustrated as a function of frequency and location along the section. The darker an area, the stronger are the amplifications that characterize the 2D model with respect to the 1D case. The general distribution of the shaded areas can be related to the geometry of the structural model. Both the clay layer and the deeper sediments have an influence on ground motion observed at the surface. Their effects can be well-separated, as is illustrated in the lower part of Figure 13, where the different features of the spectral ratios are interpreted and schematically represented. The greatest amplifications are caused by the clay layer, for frequencies close to the fundamental mode of resonance of a corresponding infinite flat layer. The maximum amplification with respect to the 1D model is of the order of 30 to 50. This amplification factor coincides with the observed factors of up to 50 for the 1985 earthquake. At higher frequencies (above 0.8 Hz), there is also evidence for the excitation of the first higher mode of resonance for the clay layer. It must be mentioned that about the same spectral ratios are obtained if the 2D results are normalized to a specific reference ground motion observed outside the sedimentary basin.

At distances between 403 and 408 km from the source, and for frequencies above 0.5 Hz, the spectral ratios for the *SH* case are characterized by a relatively regular pattern of constructive and destructive interference. When considering the radial component of motion, more complicated features are seen (central part of Fig. 13). These features are caused by resonances and by the fact that incident energy in certain frequency bands can be shifted from the vertical into the radial component of motion. These effects give rise to a series of dark lines in the spectral ratios for the radial component. For example, around 0.5 Hz and for distances between 403 and 408 km, spectral ratios reach values of up to 35.

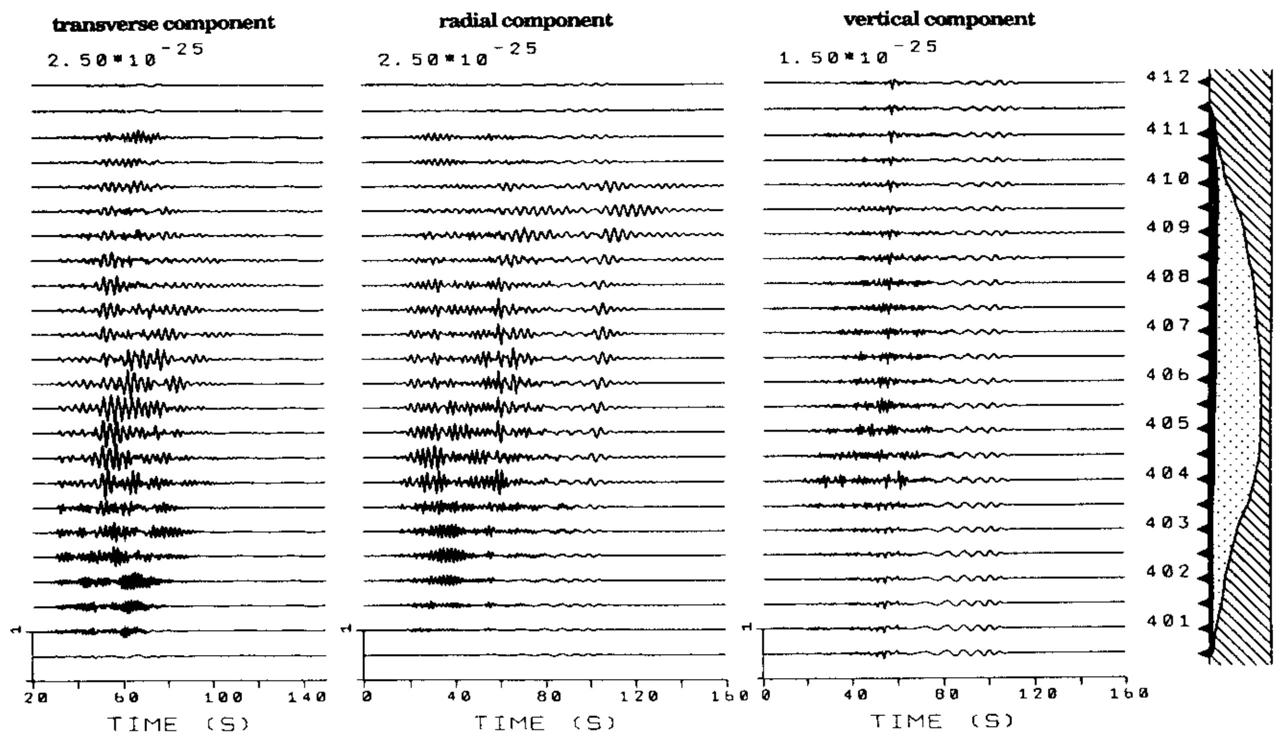

Figure 12. The same as in Figure 9 for the displacement time series, for cross section Chapultepec–Peñon shown in Figure 11. The normalization factor of the time series is different from the one used in Figure 9.

Because of the variability of strong ground motion within the sedimentary basin, the poorly known structure of the sedimentary basin in Mexico City, the simple source model, and the fact that none of the accelerometer stations are located on the cross section studied, it is difficult to compare synthetic signals directly with observed strong ground motion. On the other hand, the 2D model under study can be considered as sufficiently representative for the general geological situation in Mexico City. On observed records, an oscillation with a period of 2

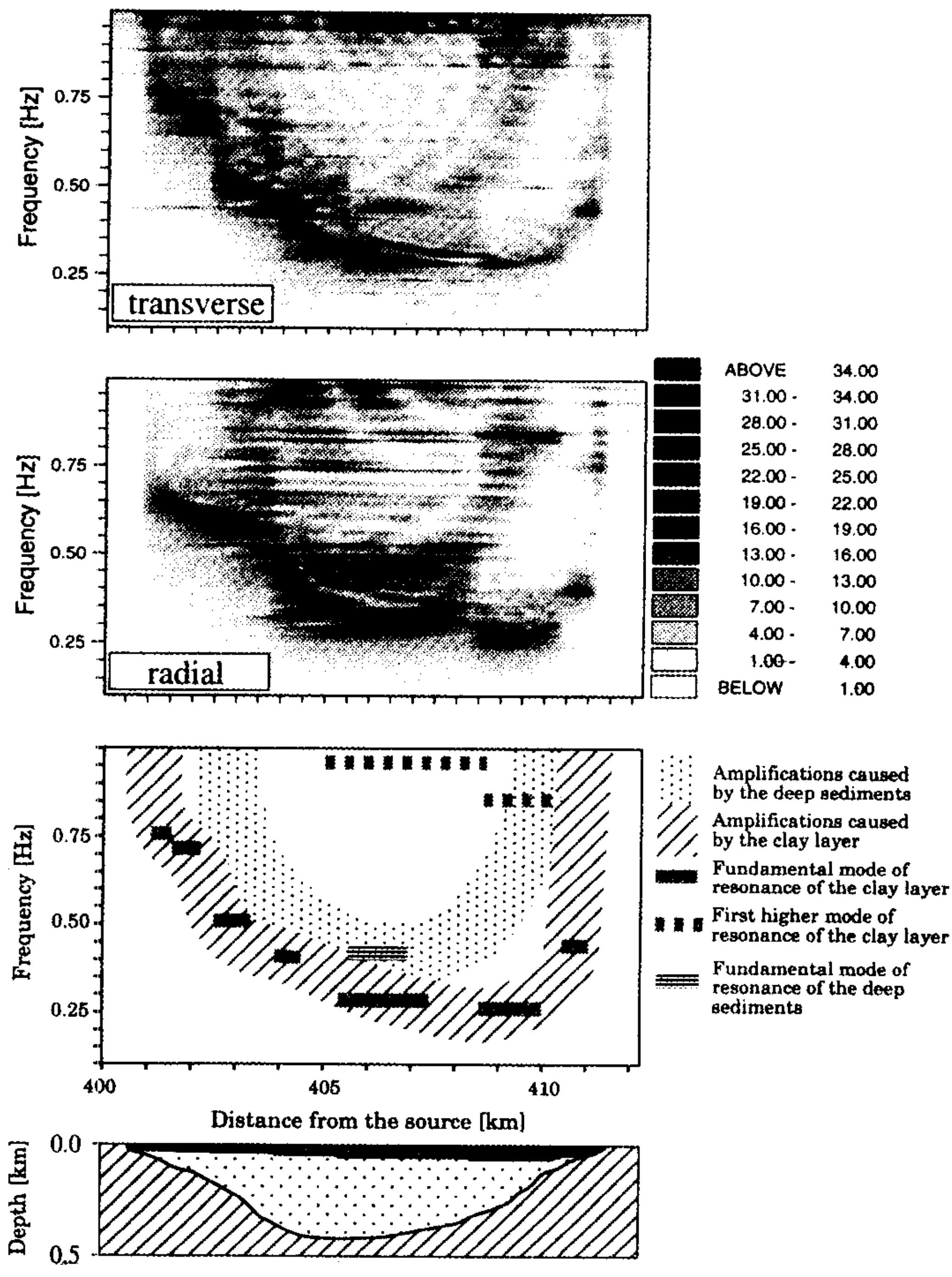

Figure 13. Spectral ratios for the transverse and radial components of motion over the entire cross section. The amplification effects are schematized and interpreted in the lower part of the figure. The step-like character of the spectral ratios clearly reflects the steps of the model in the finite-difference computations.

to 5 sec is superimposed on the fundamental modes (Fig. 3). This feature has been interpreted as a source effect (Campillo *et al.*, 1989) and is not present in our synthetic signals corresponding to a simple point source with 0-sec duration. For the synthetic signals (Fig. 12), the duration outside the sedimentary basin is about 90 sec for *P-SV* waves and 60 sec for *SH* motion, while within the sedimentary basin, the duration varies strongly and can have values of the order of 150 sec in the *P-SV* case and 120 sec for *SH* waves. If we assume a seismic source that is composed of three subevents, as proposed by Houston and Kanamori (1986), the durations increase by about 45 sec (Fig. 14b) compared to those relative to a single event (Fig. 14a). The durations and large amplitude coda are then in good agreement with observations in the lake-bed zone. Some of the computed horizontal components of motion (label L5.5 or R9.5 in Fig. 14b) are very similar to the observed signals at station CDAO.

The model that we have used for the Mexico City area can explain the difference in amplitudes for receivers located inside and outside the lake-bed zone. The ratio between the computed, horizontal peak ground displacements inside and outside the lake-bed zone reaches values of the order of five to seven; about the same ratio is obtained for the observed ground motion.

In the central part of the sedimentary basin, the frequency content of the horizontal components of the computed ground motion agrees well with the observations, while the synthetic vertical displacements have too much energy for frequencies above 0.7 Hz. This can be accounted for in several ways, e.g., by the quality factor in the layered model (Table 1) or by the choice of the source time function. Assuming lower quality factors in the layered model (about half the values given in Table 1), or a source with finite duration (for example, 3-sec duration), will reduce the high-frequency content of the synthetic signals.

The applicability of the cross section studied is confirmed by the fact that the spectral ratios obtained for the horizontal components of the synthetic seismograms can be very similar to the spectral ratios obtained from observations, as is shown in Figure 15. The maximum amplification factors, the shape of the spectral ratios, and the frequency bands at which amplification occurs, is explained by our numerical modeling. The two peaks in the spectral ratio for station CDAO can be attributed to the deep sediments (peak at about 0.8 Hz) and the surficial clay layer (peak at about 0.25 Hz). The spectral ratios for *SH* and *P-SV* waves are about the same. In the time domain, on the other hand, the local surface waves

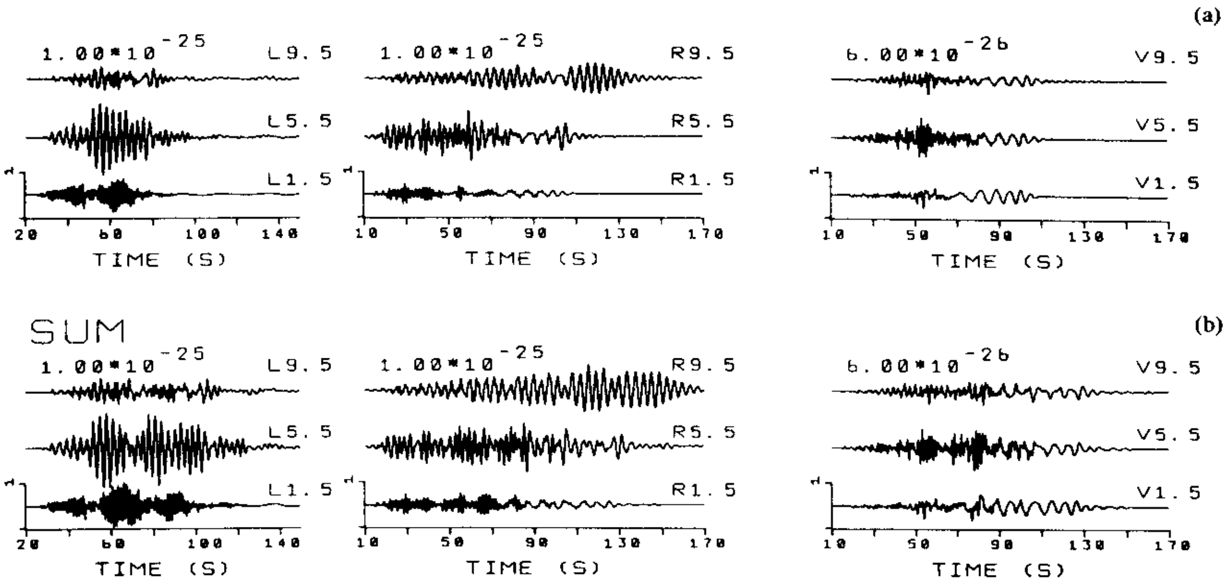

Figure 14. Transverse (left column), radial (middle column), and vertical displacements (right column) obtained at three receivers within the sedimentary basin: at the western edge of the basin, 401.5 km from the source; in the center of the basin, 405.5 km from the source; and at the eastern edge of the basin, 409.5 km from the source. The results of two computations are shown:
(a) Synthetic displacements owing to one point source.
(b) Synthetic displacements owing to three point sources, all located at a depth of 10 km and the same distance. The strike-receiver angle, dip, and rake are 220°, 15°, and 76°, respectively. The three point sources have different weights and time shifts (1.0, 1.0, and 0.2; 0, 26, and 47 sec). Weight one is given to a source with seismic moment of 10^{-7} N-m.

and resonance effects can only be a dominant phase in the seismograms, if the incident wave field has much energy in the frequency band of the excited surface waves and resonances.

Conclusions

The reasons for the damage caused by the Michoacan earthquake can be found in the special geological conditions of the valley of Mexico City. This valley consists mainly of two layers: the so-called deep sediments, and a surficial clay layer that is present in the lake-bed zone. By studying the 1D response of these two layers with the modal summation method, it was possible to explain the difference in amplitudes between records for receivers inside and outside the lake-bed zone, also shown by Kawase and Aki (1989). These simple models show that the sedimentary cover produces the concentration of high-frequency waves (0.2 to 0.5 Hz) on the horizontal components of motion. One aspect that cannot be explained with 1D models is the large amplitude coda of ground motion inside the lake-bed zone and the spectral ratios between signals observed inside and outside the lake-bed zone (Kawase and Aki, 1989). To achieve a realistic simulation of seismic ground motion in Mexico City, it is necessary to include source, path, and local soil effects; to study *SH* and *P-SV* wave propagation; and

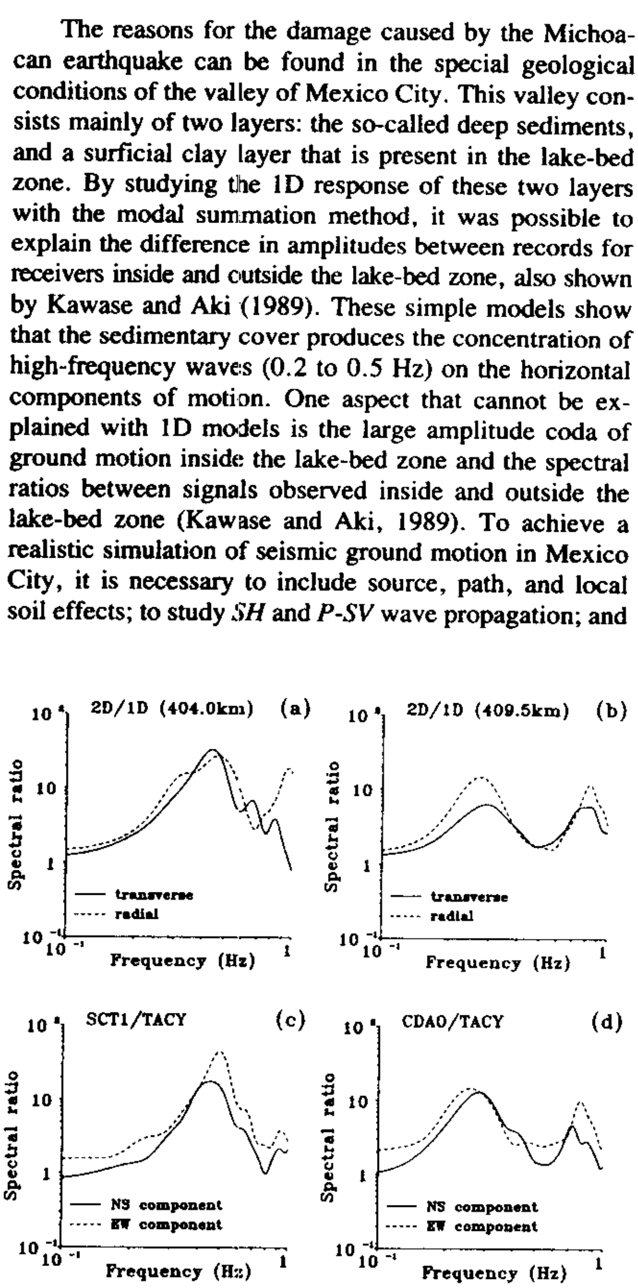

Figure 15. Smoothed spectral ratios obtained for the synthetic seismograms (a) at 404 km and (b) at 409.5 km from the source, in comparison with the spectral ratios (c) of the horizontal components recorded at station SCT1, with respect to station TACY, and (d) of the horizontal components recorded at station CDAO, with respect to station TACY.

to include also anelastic absorption. This simultaneous consideration of the different effects is the main advantage of the presented hybrid method, when compared with other techniques.

For realistic models of the sedimentary basin in Mexico City, the horizontal components of ground motion are mainly controlled by the response of the uppermost clay layer. Local surface waves and resonance effects lead to a long duration and a large amplitude coda of the signals inside the lake-bed zone. Small variations of the geometry of the uppermost clay layer lead to very different ground motion in the horizontal components. Even in close neighboring stations it is possible to observe large differences in the shape, duration, and frequency content of the signals. The vertical components of our synthetics, for frequencies below 0.5 Hz, are not significantly changed by the presence of the clay layer; this agrees with the recordings taken in Mexico City during the Michoacan earthquake.

Spectral ratios that are computed for sites inside the sedimentary basin show that the clay layer, by interaction with the deep sediments, causes amplifications of the order of 30 to 50. This amplification factor agrees with those observed in the lake-bed zone. This value is larger than the one obtained by Bard *et al.* (1988) who computed amplification factors of up to 20 for vertically incident *SH* waves. Kawase and Aki (1989) attributed the long duration of ground motion and large amplitude coda observed in Mexico City to a strong interaction between the deep sediments and the surficial clay layer. They stated that the resonance frequencies of the two layers have to be almost the same to explain the long duration. Since the observed spectral ratios show the spectral peaks of the two layers at different frequencies, we suggest that the large amplitude coda observed at station CDAO is caused by a strong resonance effect in the laterally heterogeneous clay layer. Our numerical modeling also shows that for the explanation of the signals duration in the lake-bed zone, it is necessary to consider not only a one-point source, but the energy contribution of the three subevents of the Michoacan earthquake.

The spectral properties of the seismic source control the frequency content of the incident wave field; if the dominant energy is concentrated in the frequency band close to the resonance frequency of the clay layer or the deep sediments, local surface waves and resonance effects dominate the horizontal components of motion within the sedimentary basin. For the same seismic source, *SH* and *P-SV* waves, in general, have their dominant energy in different frequency bands. In the numerical experiments, this consequently leads to differences in the ground motion: large excitation of local surface waves in the deep sediments for *SH* waves are not observed in the *P-SV* case. On the other hand, there are strong resonance effects in the clay layer for *P-SV* waves that are less pronounced for *SH* waves.

The area of severe structural damage in Mexico City is characterized by increased thickness of the deep sediments and the laterally heterogeneous clay layer. Such geometries favor the excitation of local surface waves, which could be responsible for the observed distribution of damage. The large impedance contrast between the clay at the surface and the deep sediments causes strong resonance effects in the clay layer, which result in almost monochromatic wave trains of long duration.

Acknowledgments

We would like to thank Fred Schwab, F. J. Sánchez-Sesma, and the reviewers for their contribution to this research as well as ENEA for allowing us the use of the IBM3090E computer at the ENEA INFO BOL Computer Center. This study has been made possible by the CNR Contracts 90.02382.CT15, 91.02692.CT15, 90.01026.PF54, and 91.02550.PF54. This research has been carried out in the framework of the activities of the ILP Task Group II.4.

References

Alterman, Z. S. and F. C. Karal (1968). Propagation of elastic waves in layered media by finite difference methods, *Bull. Seism. Soc. Am.* **58**, 367–398.

Bard, P.-Y., M. Campillo, F. J. Chavez-Garcia, and F. J. Sánchez-Sesma (1988). The Mexico earthquake of September 19, 1985—A theoretical investigation of large- and small-scale amplification effects in the Mexico City valley, *Earthquake Spectra* **4**, 609–633.

Ben-Menahem, A. and D. G. Harkrider (1964). Radiation patterns of seismic surface waves from buried dipolar point sources in a flat stratified Earth, *J. Geophys. Res.* **69**, 2605–2620.

Campillo, M., P.-Y. Bard, F. Nicollin, and F. J. Sánchez-Sesma (1988). The Mexico Earthquake of September 19, 1985—The incident wave field in Mexico City during the great Michoacan earthquake and its interaction with the deep basin, *Earthquake Spectra* **4**, 591–608.

Campillo, M., J.-C. Gariel, K. Aki, and F. J. Sánchez-Sesma (1989). Destructive strong ground motion in Mexico City: Source, path, and site effects during great 1985 Michaocan earthquake, *Bull. Seism. Soc. Am.* **79**, 1718–1735.

Chávez-Garcia, F. J. and P.-Y. Bard (1990). Surface ground motion modifications by the presence of a thin resistant layer. Applications to Mexico City, in *Proc. of the 9th European Conf. of Earthquake Engineering*, Moscow, USSR, 11–16 September, Vol. 4B, 37–46.

Clayton, R. and B. Engquist (1977). Absorbing boundary conditions for acoustic and elastic wave equations, *Bull. Seism. Soc. Am.* **67**, 1529–1540.

Eissler, H., L. Astiz, and H. Kanamori (1986). Tectonic setting and source parameters of the September 19, 1985 Michoacan, Mexico earthquake, *Geophys. Res. Lett.* **13**, 569–572.

Emmerich, H. and M. Korn (1987). Incorporation of attenuation into time-domain computations of seismic wave fields, *Geophysics* **52**, 1252–1264.

Emmerich, H. (1992). *P-SV*-wave propagation in a medium with local heterogeneities: A hybrid formulation and its application, *Geophys. J. Int.* **109**, 54–64.

Fäh, D., P. Suhadolc, and G. F. Panza (1990). Estimation of strong ground motion in laterally heterogeneous media: Modal summation—finite differences, in *Proc. of the 9th European Conf. of Earthquake Engineering*, Moscow, USSR, 11–16 September, Vol. 4A, 100–109.

Fäh, D. (1992). A hybrid technique for the estimation of strong ground motion in sedimentary basins, *Ph.D. Thesis*, Swiss Federal Institute of Technology, Zurich.

Florsch, N., D. Fäh, P. Suhadolc, and G. F. Panza (1991). Complete synthetic seismograms for high-frequency multimode *SH*-waves, *Pageoph.* **136**, 529–560.

Futterman, W. I. (1962). Dispersive body waves, *J. Geophys. Res.* **67**, 5279–5291.

Haskell, N. A. (1953). The dispersion of surface waves in multilayered media, *Bull. Seism. Soc. Am.* **43**, 17–34.

Houston, H. and H. Kanamori (1986). Source characteristics of the 1985 Michoacan, Mexico earthquake at periods of 1 to 30 seconds, *Geophys. Res. Lett.* **13**, 597–600.

Kawase, H. and K. Aki (1989). A study on the response of a soft basin for incident *S*, *P*, and Rayleigh waves with special reference to the long duration observed in Mexico City, *Bull. Seism. Soc. Am.* **79**, 1361–1382.

Knopoff, L. (1964). A matrix method for elastic wave problems, *Bull. Seism. Soc. Am.* **54**, 431–438.

Korn, M. and H. Stöckl (1982). Reflection and transmission of Love channel waves at coal seam discontinuities computed with a finite difference method, *J. Geophys.* **50**, 171–176.

Levander, A. R. (1988). Fourth-order finite-difference *P-SV* seismograms, *Geophysics* **53**, 1425–1436.

Levshin, A. L. (1985). Effects of lateral inhomogeneities on surface waves amplitude measurements, *Ann. Geophys.* **3**, 511–518.

Lysmer, J. and L. A. Drake (1972). A finite element method for seismology, in *Methods in Computational Physics*, B. A. Bolt (Editor) Vol. 11, Academic Press, New York, 181–216.

Mena, E., C. Carmona, R. Delgado, L. Alcántara, and O. Dominguez (1986). Catálogo de acelerogramas procesados del sismo del 19 de septiembre de 1985, Parte I: Ciudad de México, *Series del Instituto de Ingenieria No. 497*, UNAM, México, D. F. México.

Panza, G. F., F. A. Schwab, and L. Knopoff (1973). Multimode surface waves for selected focal mechanisms. Part I. Dip-slip sources on a vertical fault plane, *Geophys. J. R. Astr. Soc.* **34**, 265–278.

Panza, G. F. (1985). Synthetic seismograms: The Rayleigh waves modal summation, *J. Geophysics* **58**, 125–145.

Panza, G. F. and P. Suhadolc (1987). Complete strong motion synthetics, in *Seismic Strong Motion Synthetics*, B. A. Bolt (Editor). Academic Press, Orlando, Computational Techniques 4, 153–204.

Regan, J. and D. G. Harkrider (1989). Numerical modelling of *SH Lg* waves in and near continental margins, *Geophys. J. Int.* **98**, 107–130.

Riedesel, M. A., T. H. Jordan, A. F. Sheehan, and P. G. Silver (1986). Moment-tensor spectra of the 19 Sept. 85 and 21 Sept. 85 Michaocan, Mexico earthquakes, *Geophys. Res. Lett.* **13**, 609–612.

Sánchez-Sesma, F. J., S. Chávez-Pérez, M. Suárez, M. A. Bravo, and L. E. Pérez-Rocha (1988). The Mexico earthquake of September 19, 1985—On the seismic response of the Valley of Mexico, *Earthquake Spectra* **4**, 569–589.

Schwab, F. (1970). Surface-wave dispersion computations: Knopoff's method, *Bull. Seism. Soc. Am.* **60**, 1491–1520.

Schwab, F. and L. Knopoff (1972). Fast surface wave and free mode computations, in *Methods in Computational Physics*, B. A. Bolt (Editor). Vol. 11, Academic Press, New York, 87–180.

Singh, S. K. and M. Ordaz (1992). On the origin of long coda observed in the lake-bed strong-motion records of Mexico City. *Bull. Seism. Soc. Am.* (in press).

Smith, W. D. (1974). A non-reflecting plane boundary for wave propagation problems, *J. Comp. Physics* **15**, 492–503.

Suarez, M., F. J. Sánchez-Sesma, M. A. Bravo, and J. Lermo (1987). Caracteristicas de los depósitos superficiales del Valle de México, en *Memorias VII Congreso Nacional de Ingenieria Sismica*, Querétaro, México, 19–21 November, A61–A74.

Takeuchi, H. and M. Saito (1972). Seismic surface waves, in *Methods in Computational Physics*, B. A. Bolt (Editor). Vol. 11, Academic Press, New York, 217–295.

Thomson, W. T. (1950). Transmission of elastic waves through a stratified solid medium, *J. Appl. Phys.* **21**, 89–93.

Vaccari, F., S. Gregersen, M. Furlan, and G. F. Panza (1989). Synthetic seismograms in laterally heterogeneous, anelastic media by modal summation of *P-SV*-waves, *Geophys. J. Int.* **99**, 285–295.

Valdes, C. M., W. D. Mooney, S. K. Singh, R. P. Meyer, C. Lomnitz, J. H. Luetgert, C. E. Helsley, B. T. R. Lewis, and M. Mena (1986). Crustal structure of Oaxaca, Mexico, from seismic refraction measurements, *Bull. Seism. Soc. Am.* **76**, 547–563.

Virieux, J. (1986). *P-SV* wave propagation in heterogeneous media: Velocity-stress finite-difference method, *Geophysics* **51**, 889–901.

Istituto di Geodesia e Geofisica
Università degli Studi di Trieste
Via dell'Università 7, I-34100 Trieste, Italy
(D.F., P.S., G.P.)

Institut for Geophysik
ETH Hönggerberg, CH-8093 Zürich
(D.F., S.M.)

International Center for Theoretical Physics
Strada Costiera II, I-34100 Trieste, Italy
(G.P.)

Manuscript received 23 February 1993.

IC/94/48

INTERNATIONAL CENTRE FOR THEORETICAL PHYSICS

ESTIMATION OF STRONG GROUND MOTION AND MICRO-ZONATION FOR THE CITY OF ROME

D. Fäh

C. Iodice

P. Suhadolc

and

G.F. Panza

INTERNATIONAL ATOMIC ENERGY AGENCY

UNITED NATIONS EDUCATIONAL, SCIENTIFIC AND CULTURAL ORGANIZATION

MIRAMARE-TRIESTE

IC/94/48

International Atomic Energy Agency
and
United Nations Educational Scientific and Cultural Organization
INTERNATIONAL CENTRE FOR THEORETICAL PHYSICS

ESTIMATION OF STRONG GROUND MOTION AND MICRO-ZONATION FOR THE CITY OF ROME

D. Fäh, C. Iodice and P. Suhadolc
Istituto di Geodesia e Geofisica, Università degli Studi di Trieste,
Trieste, Italy

and

G.F. Panza
International Centre for Theoretical Physics, Trieste, Italy
and
Istituto di Geodesia e Geofisica, Università degli Studi di Trieste,
Trieste, Italy.

MIRAMARE - TRIESTE
March 1994

Abstract

A hybrid technique, based on mode summation and finite differences, is used to simulate the ground motion induced in the city of Rome by possible earthquakes occurring in the main seismogenetic areas surrounding the city: the Central Apennines and the Alban Hills. The results of the numerical simulations are used for a first order seismic micro-zonation in the city of Rome, which can be used for the retrofitting of buildings of special social and cultural value. Rome can be divided into six main zones: (1) the edges and (2) the central part of the alluvial basin of the river Tiber; (3) the edges and (4) the central part of the Paleotiber basin; the areas outside the large basins of the Tiber and Paleotiber, where we distinguish between (5) areas without, and (6) areas with a layer of volcanic rocks close to the surface. The strongest amplification effects have to be expected at the edges of the Tiber basin, with maximum spectral amplification of the order of 5 to 6, and strong amplifications occur inside the entire alluvial basin of the Tiber. The presence of a near-surface layer of rigid material is not sufficient to classify a location as a "hard-rock site", when the rigid material covers a sedimentary complex. The reason is that the underlying sedimentary complex causes amplifications at the surface due to resonance effects. This phenomenon can be observed in the Paleotiber basin, where spectral amplifications in the frequency range 0.3-1.0 Hz reach values of the order of 3 to 4.

32

Introduction

Numerical simulations play an important role in the estimation of strong ground motion. They can provide synthetic signals for areas where recordings are absent and are therefore very useful for engineering design of earthquake-resistant structures and for retrofitting of particularly important buildings. Lateral heterogeneities and sloping layers, commonly present in nature, can cause effects that dominate the ground motion: the excitation of local surface-waves, focusing and defocusing, and resonance effects. In such circumstances, at least two-dimensional techniques are necessary for a realistic estimate of the ground motion.

To include both a realistic source model and a complex structural model of the site of interest, a hybrid method has been developed that combines modal summation and the finite difference technique (Fäh, 1992; Fäh et al., 1993; Fäh et al., 1994). The propagation of the waves from the source up to the local structure at the site is computed with the mode-summation method for plane layered anelastic structures (Panza, 1985; Florsch et al. 1991). The mode-summation method allows us the simulation of the complete incident wavefield in a given phase-velocity frequency band. Explicit finite-difference schemes (Korn and Stöckl, 1982; Virieux, 1986) are then used to simulate the propagation of seismic waves in a two-dimensional model of the local structure. The hybrid method is particularly suitable to compute the ground motion in two-dimensional models of any complexity, and allows us to take into account the source and propagation effects, including local site conditions.

The area of Rome, considered here, is characterized by several sedimentary basins of considerable thickness, which in some parts are covered by volcanic rocks. The area is very vulnerable to earthquakes, as indicated, for example, by the well-documented damage distribution caused by the M_L=6.8 January 13, 1915, Fucino (Italy) earthquake (Ambrosini et al., 1986). In absence of instrumental data in the city of Rome, a numerical simulation of the ground motion due to the January 13, 1915 Fucino earthquake has been compared with

the observed damage distribution (Fäh et al., 1993). The macro-seismic data in Rome shows essentially that the damage is concentrated at the edges of the alluvial basin of the Tiber river; the heavy and intermediate damage are located in that basin. The same distribution of damage can be expected on the basis of the numerical simulations of this event (Fäh et al., 1993). The highest amplifications are observed at the edges of this alluvial basin, and large amplifications can be observed within the Tiber's river bed. The very good correlation between the damage statistic and the ground motion suggests to use the hybrid technique for a micro-zonation of the entire town, which accounts for events expected in other important seismogenetic areas. For this purpose, a series of different numerical simulations of the ground motion are performed, for different source positions and structural models of the Rome area. The results of such computations are then used for the micro-zonation, based on the spectral amplifications expected in the different zones of the city.

Parametrization of the source and of the propagation path

The most important seismogenetic zones (Figure 1) which can cause structural damage in Rome are the Central Apennines (observed maximum intensity in Rome on the Mercalli-Cancani-Sieberg intensity scale (MCS) VII-VIII) and the Alban Hills (observed maximum MCS in Rome VI-VII) (Molin et al., 1986). The source positions (Figure 1) used in this study include (1) the epicenter of the January 13, 1915 Fucino earthquake, (2) the Carseolani Mountains where, from the study of pattern recognition (Caputo et al., 1980), a strong earthquake is expected to occur, and (3) the Alban Hills. The source mechanisms assigned to these earthquakes are the mechanism of the Fucino earthquake (Gasparini et al., 1985) for event 1 and 2, and the mechanism of a recent earthquake in the Alban Hills (Amato et al., 1984) for event 3. The parameters of the focal mechanism of each event are given in Table 1.

The one-dimensional structural models for the region between the source positions and Rome are given in Table 2. These models are used as reference bedrock structures, and, for each seismic source, the ground motion computed with the hybrid method is always compared with that obtained for the related one-dimensional structure.

The position of the cross sections studied is shown in Figure 2 as dashed lines, and the related two-dimensional structural models are shown in Figure 3. They are based on all the available geological and geotechnical information (Ventriglia, 1971; Serva et al, 1986; Funiciello et al., 1987; Boschi et al., 1989; Feroci et al., 1990). Alluvial sediments can be found in two major areas, the river beds of the Aniene and Tiber. The ancient river bed of the Tiber (referred as Paleotiber) is composed by Sicilian clays, sands and gravel. This sedimentary complex is covered by volcanic rocks which have their origin in the Pleistocene volcanic activity (Ventriglia, 1971). The volcanic rocks have greater wave velocities than the underlying sediments (Sicilian), which therefore define a buried low-velocity zone. The surficial layer, consists of compacted fill, and of the foundations of man-made structures. The transition from the alluvial sediments in the Tiber river bed to the compacted clay is characterized by a very high impedance contrast. In Figure 3, the compacted clay is referred as bedrock.

Since the mechanical properties and thickness of the different soils are not well known, we have used different material properties to enhance the reliability of the micro-zonation. This includes: (1) two different models for which the seismic velocities given in Figure 3 are defined at 1Hz and at 30Hz, respectively, and (2) two different models in which the surficial layer of made ground (fill deposits) has a thickness of 5m and 10m, respectively.

Properties of ground motion for the Fucino event

Several ground motion related quantities can be extracted from the synthetic accelerograms obtained from our numerical modelling. The quantities that we consider here are: (1) the relative peak ground acceleration PGA(2D)/PGA(bedrock), (2) the so-called relative Arias intensity W(2D)/W(bedrock), where W is defined as:

$$W = \frac{\pi}{2g} \lim_{t \to \infty} \int_0^t |\ddot{x}(\tau)|^2 \, d\tau \quad ,$$

where x is the ground displacement, and (3) the relative spectral accelerations or spectral amplification Sa(2D)/Sa(bedrock). PGA(2D), W(2D), Sa(2D) indicate, respectively, PGA, W and Sa computed for the two-dimensional models shown in Figure 3, while PGA(bedrock), W(bedrock), and Sa(bedrock) indicate, respectively, PGA, W and Sa obtained for the one-dimensional reference bedrock models given in Table 2.

For each source, in order to remove the effects of the radiation pattern and of the regional propagation, PGA(2D), W(2D), and Sa(2D) are always normalized with respect to the corresponding quantities, PGA(bedrock), W(bedrock), Sa(bedrock), computed in the reference bedrock model at the given source-receiver distance .

For the Fucino event (Event 1), relative PGA and relative Arias intensity, defined by the ratios (PGA(2D)/PGA(bedrock)) and (W(2D)/W(bedrock)), computed for the transverse component of motion (SH-waves), the radial component of motion, and the total P-SV wavefield, are shown in Figure 4. High relative PGA values are observed for locations sitting on unconsolidated sediments (Figure 4a), while relative PGA values are low where the volcanic layer is thick. Relative peaks can be seen at the beginning of the alluvial valley of the Tiber and within the alluvial valley of the Aniene. The peaks and troughs are more evident in the curve representing the relative W values (Figure 4b). There are five relative peaks: two at the edges of the Tiber basin, one within the alluvial valley of the Aniene, a broad peak where the Sicilian low-velocity zone gets close to the surface, and one at the margin of the Paleotiber basin.

The macro-seismic data show essentially that, in Rome, the damage is concentrated in the basin of the Tiber with clear peaks at the edges of the alluvial basin. To quantify this observation, the damage distribution has been projected on the cross section used in the numerical modelling (Fäh et al., 1993). The resulting histogram is shown in Figure 4, which shows that a similar distribution of damage is predicted by our direct numerical simulation.

First order seismic micro-zonation

All the quantities characterizing some aspect of the strong ground motion, like the maximum amplitude, the duration and the Fourier spectrum, provide only a very limited description of the complete ground motion and certainly do not quantify its damage producing potential. A more adequate quantity, especially from the engineering point of view, is the response spectrum (or the spectral amplification) of the earthquake ground motion. Response spectra (for example Sa) are related to the maximum response of a simple oscillator, whose natural period and damping coefficient are varied, excited by a given ground motion.

The results obtained from the modelling of the Fucino event (Figure 4) can be used directly for general micro-zonation purposes. Using as reference the bedrock models given in Table 2, six zones can be distinguished (see Figures 3 and 4): (1) *zone 1* includes the edges of the Tiber river, (2) *zone 2* extends over the central part of alluvial basin of the Tiber, (3) *zone 3* includes the edges of the Paleotiber basin, and (4) *zone 4* extends over the central part of the Paleotiber basin. The *zones 5* and *6* include areas which are located outside the large basins of the Tiber and Paleotiber where we distinguish between areas (5) without and (6) with a layer of volcanic rocks close to the surface. These zones can be recognized also in the sections considered in relation with the events located in the Carseolani Mountains and the Alban Hills, as is shown in Figure 3.

For all the receivers located in each of the six zones defined above, and for all the two-dimensional models, shown in Figure 3, and the studied events, located in Figure 2, we have computed the spectral amplification Sa(2D)/Sa(bedrock). From these values we have then computed the average and the maximum spectral amplification for each given zone, which are shown in Figure 5, for zero damping and 5% damping of the oscillator.

The greatest spectral amplification is observed at the edges of the sedimentary basin of the Tiber river (zone 1), for frequencies between 2.0 and 2.5 Hz. The maximum spectral amplification with respect to the bedrock model varies between 5 and 6, and it is due to the combination of resonance effects with the excitation of local surface waves. The general shape of the maximum and

average spectral amplifications are similar for zone 1 and 2. In the frequency range from 1.0 Hz to 3.0 Hz, the maximum spectral amplification is of the order of 4 and the average spectral amplification is of the order of 2.

Similar observations can be done for the Paleotiber basin (zones 3 and 4), but in a different frequency band (0.4-1.0 Hz). The buried sedimentary complex (Sicilian) causes maximum spectral amplification between 3 and 4, due to resonance effects. These are most pronounced at frequencies around 0.6 Hz. Therefore, the presence of a near-surface layer of rigid material in the Paleotiber basin is not sufficient to classify that area as a "hard-rock site". A correct zonation requires the knowledge of both the thickness of the surficial layer and of the deeper parts of the structure, down to real bedrock. This is especially important in volcanic areas, where pyroclastic material often covers alluvial basins. The maximum spectral amplification is larger at the edges of the Paleotiber basin (zone 3). For frequencies above 1.0 Hz, in the Paleotiber basin (zone 4), the volcanic layer acts as a shield reflecting part of the incoming energy, and the values of the average spectral amplification are smaller than 1.

For the sites in the zones 5 and 6, the maximum and the average spectral amplifications are small for frequencies below 1 Hz. Since the sedimentary cover in these zones is thin, the amplification takes place at frequencies above 1.5 Hz, and changes rapidly from site to site. This rapid variation leads to average values of the order of 1.0-1.5.

Summary and Conclusions

In absence of instrumental data, a realistic numerical simulation of the ground motion, successfully tested against macro-seismic data, is used for the first order micro-zonation of Rome. The highest values of the spectral amplification are observed at the edges of the sedimentary basin of the Tiber, strong amplification are observed in the Tiber's river bed. This is caused by the large amplitudes and long duration of the ground motion due to (1) the low impedance of the alluvial sediments, (2) resonance effects, and (3) the excitation of local surface waves.

From the computation of the spectral amplification, it has been recognized that the presence of a near-surface volcanic layer of rigid material is not sufficient to classify a location as a "hard-rock site", since the existence of an underlying sedimentary complex can cause amplifications due to resonance effects. A correct zonation requires the knowledge of both the thickness of the surficial layer and of the deeper parts of the structure, down to real bedrock. This is especially important in volcanic areas, where lava flows often cover alluvial basins.

Our technique can be applied routinely in micro-zonation studies, and it provides realistic estimates of the ground motion for two-dimensional, anelastic models. Since the geotechnical data are available for several areas, especially in urban environments, the proposed technique provides a scientifically and economically valid procedure for the immediate (no need to wait for a strong earthquake to occur), first order, seismic micro-zonation of any urban area, and is therefore very useful for engineering design of earthquake-resistant structures and for retrofitting of particularly important buildings.

Acknowledgements

We would like to thank ENEA for allowing us the use of the IBM3090E computer at the ENEA INFO BO Computer Center. D.F. has been supported by the Swiss National Science Foundation under Grant Nr. 8220-037189. This study has been made possible by the contracts CNR 91.02692.CT15, CNR 92.00068.CT12, CNR 92.02422.CT15, CNR 92.02867.PF54, and EEC EPOC-CT91-0042, and by MURST (40% and 60%) funds. This research has been carried out in the framework of the ILP Task Group II.4 contributions to the IDNDR project "Physical Instability of Megacities".

References

AMATO, A., B. DE SIMONI and C. GASPARINI (1984): Considerazioni sulla sismicità dei Colli Albani, *Atti del 3° Convegno del Gruppo Nazionale di Geofisica della Terra Solida*, CNR, Roma, Vol. 2, 965-976.

AMBROSINI, S., S. CASTENETTO, F. CEVOLANI, E. DI LORETO, R. FUNICIELLO, L. LIPERI and D. MOLIN (1986): Risposta sismica dell'area urbana di Roma in occasione del terremoto del Fucino del 13 gennaio 1915, Risultati preliminari, *Mem. Soc. Geol. It.*, **35**, 445-452.

BOSCHI, E., M. FEROCI, R. FUNICIELLO, L. MALAGNINI, A. ROVELLI and S. SALVI (1989): Valutazione della risposta sismica in ambiente urbano: risultati per la città di Roma, *Atti del 8° Convegno Gruppo Nazionale Geofisica della Terra Solida*, CNR, Roma, 317-326.

CAPUTO, M., V. KEILIS-BOROK, E. OFICEROVA, E. RANZMAN, I. ROTWAIN and A. SOLOVJEFF (1980): Pattern recognition of earthquake-prone areas in Italy, *Phys. Earth. Planet. Int.*, **21**, 305-320.

FÄH, D. (1992): A hybrid technique for the estimation of strong ground motion in sedimentary basins, *Ph.D. thesis Nr. 9767, Swiss Federal Institute of Technology, Zurich.*

FÄH, D., C. IODICE, P. SUHADOLC and G.F. PANZA (1993): A new method for the realistic estimation of seismic ground motion in megacities: the case of Rome, *Earthquake Spectra*, **9**, No.4, 643-668.

FÄH, D., P. SUHADOLC, ST. MUELLER and G.F. PANZA (1994): A hybrid method for the estimation of ground motion in sedimentary basins; quantitative modelling for Mexico City, *Bull. Seism. Soc. Am.*, **84**, 000-000.

FEROCI, M., R. FUNICIELLO, F. MARRA and S. SALVI (1990): Evoluzione tettonica e paleogeografica plio-pleistocenica dell'area di Roma, *Il Quaternario*, **3**, 141-158.

FLORSCH, N., D. FÄH, P. SUHADOLC and G.F. PANZA (1991): Complete synthetic seismograms for high-frequency multimode SH-waves, *Pageoph*, **136**, 529-560.

FUNICIELLO, R., G. LORIA and S. SALVI (1987): Ricostruzione delle superfici strutturali del sottosuolo della città di Roma, *Atti del 6° Convegno Gruppo Nazionale Geofisica della Terra Solida, CNR, Roma*, 395-415.

GASPARINI, C., G. IANNACCONE and R. SCARPA (1985): Fault-plane solutions and seismicity of the Italian peninsula, *Tectonophysics*, **117**, 59-78.

KORN, M. and H. STÖCKL (1982): Reflection and transmission of Love channel waves at coal seam discontinuities computed with a finite difference method, *J. Geophys.*, **50**, 171-176.

MOLIN D., S. AMBROSINI, S. CASTENETTO, E. DI LORETO, L. LIPERI and A. PACIELLO (1986): Aspetti della sismicità storica di Roma, *Mem. Soc. Geol. It.*, **35**, 439-444.

PANZA, G.F. (1985): Synthetic seismograms: The Rayleigh waves modal summation, *J. Geophysics*, **58**, 125-145.

SERVA, L., A.M. BLUMETTI and A.M. MICHETTI (1986): Gli effetti sul terreno del terremoto del Fucino (13 gennaio 1915); tentativo di interpretazione della evoluzione tettonica recente di alcune strutture, *Mem. Soc. Geol. It.*, **35**, 893-907.

VENTRIGLIA, U. (1971): La geologia della città di Roma, *Amm. Prov. di Roma, Roma*.

VIRIEUX, J. (1986): P-SV wave propagation in heterogeneous media: Velocity-stress finite-difference method, *Geophysics*, **51**, 889-901.

Event Nr.	Location	Source depth [km]	Dip	Rake	Strike-receiver angle
1	Fucino valley	8.00	39°	172°	38°
2	Carseolani Mountains	8.00	39°	172°	38°
3	Alban Hills	3.06	74°	266°	133°

Table 1. Source mechanisms of the events shown in Figure 1.

Thickness (km)	Density (g/cm^3)	P-wave velocity (km/s)	S-wave velocity (km/s)	Q_β
0.09	2.24 (2.21)	2.40 (1.85)	1.29 (1.00)	30 (20)
0.10	2.25	2.50	1.30	30
0.10	2.25	2.80	1.50	30
0.10	2.30	4.00	2.31	100
0.10	2.40	4.10	2.37	100
0.10	2.40	4.20	2.43	100
0.10	2.50	4.30	2.48	100
0.10	2.50	4.40	2.54	100
0.10	2.50	4.50	2.60	100
0.10	2.50	4.60	2.65	100
0.10	2.60	4.70	2.70	100
0.10	2.60	4.80	2.77	100
0.10	2.60	4.90	2.83	100
0.10	2.60	5.00	2.88	100
0.10	2.60	5.20	3.00	100
0.10	2.60	5.40	3.10	100
0.10	2.60	5.60	3.20	100
1.70	2.80	5.70	3.30	100
6.10	2.85	6.00	3.46	100
0.10	2.85	5.89	3.40	100
0.10	2.85	5.80	3.35	100
0.10	2.85	5.71	3.30	100
0.10	2.85	5.54	3.20	100
8.60	2.85	5.40	3.12	100
0.10	2.85	5.49	3.17	100
0.10	2.85	5.63	3.25	100
0.10	2.85	5.71	3.30	100
0.10	2.85	5.89	3.40	100
0.10	2.85	6.06	3.50	100
2.70	2.85	6.20	3.58	300
1.70	2.88	6.50	3.75	300
1.70	2.90	6.70	3.87	300
2.40	2.95	7.00	4.04	300
4.75	3.35	7.90	4.56	300
4.75	3.35	7.92	4.57	300
4.75	3.35	7.94	4.58	300
4.75	3.35	7.96	4.59	300
4.75	3.35	7.98	4.60	300
4.75	3.35	8.00	4.62	300
4.75	3.36	8.02	4.63	300
4.75	3.37	8.04	4.64	300
4.75	3.38	8.06	4.65	300
∞	3.39	8.08	4.66	300

Table 2. Structural bedrock models representative of the path from the epicenters to the city of Rome (Q_α=2.2 Q_β). For the computations with source 3, located in the Alban Hills, the mechanical parameters of the first layer are given in parenthesis.

FIGURE CAPTIONS

Figure 1. Epicenter locations of the events used for the different numerical simulations. The source positions are (1) the epicenter of the January 13, 1915 Fucino earthquake, (2) the Carseolani Mountains, and (3) the Alban Hills.

Figure 2. Lithology and thickness of alluvial sediments in Rome (Ventriglia, 1971; Funiciello et al., 1987; Feroci et al., 1990). The dashed lines indicate the positions of the cross sections, for which numerical modelling is performed.

Figure 3. Two-dimensional models corresponding to the dashed lines shown in Figure 2. Only the part near to the surface is shown, where the 2D model deviates from the horizontally-layered structural models shown in Table 2. The general micro-zonation is explained in the text.

Figure 4. Ratios of the peak ground acceleration, PGA(2D)/PGA(bedrock), and of the Arias Intensity, W(2D)/W(bedrock), obtained for the numerical simulation of the Fucino earthquake (event 1 in Figure 1). They are compared with the damage distribution caused by the January 13, 1915 Fucino earthquake (Fäh et al., 1993). The general micro-zonation is explained in the text.

Figure 5. Maximum and average relative spectral accelerations for the zones defined in Figures 3 and 4, for zero damping and 5% damping.

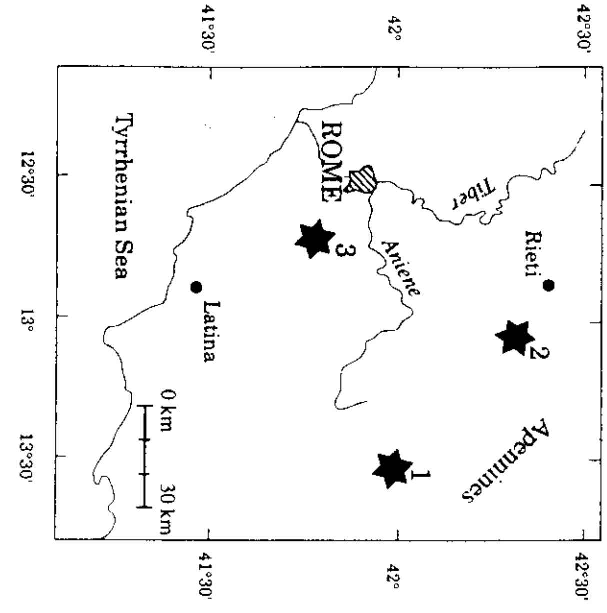

42°30'
42°
41°30'
12°30'
13°
13°30'
Tiber
Rieti
ROME
Aniene
Apennines
Latina
Tyrrhenian Sea
1
2
3
0 km
30 km

Fig.1

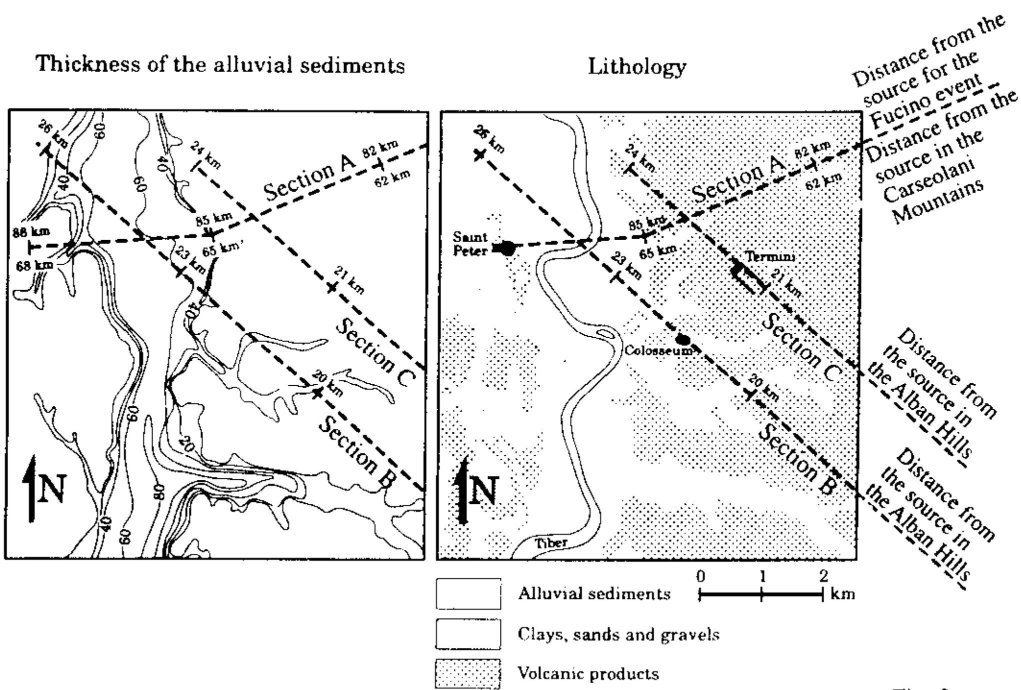

Thickness of the alluvial sediments
Lithology
Distance from the source for the Fucino event
Distance from the source in the Carseolani Mountains
Distance from the source in the Alban Hills
Distance from the source in the Alban Hills
Section A
Section B
Section C
Saint Peter
Termini
Colosseum
Tiber
N
Alluvial sediments
Clays, sands and gravels
Volcanic products
0
1
2
km

Fig. 2

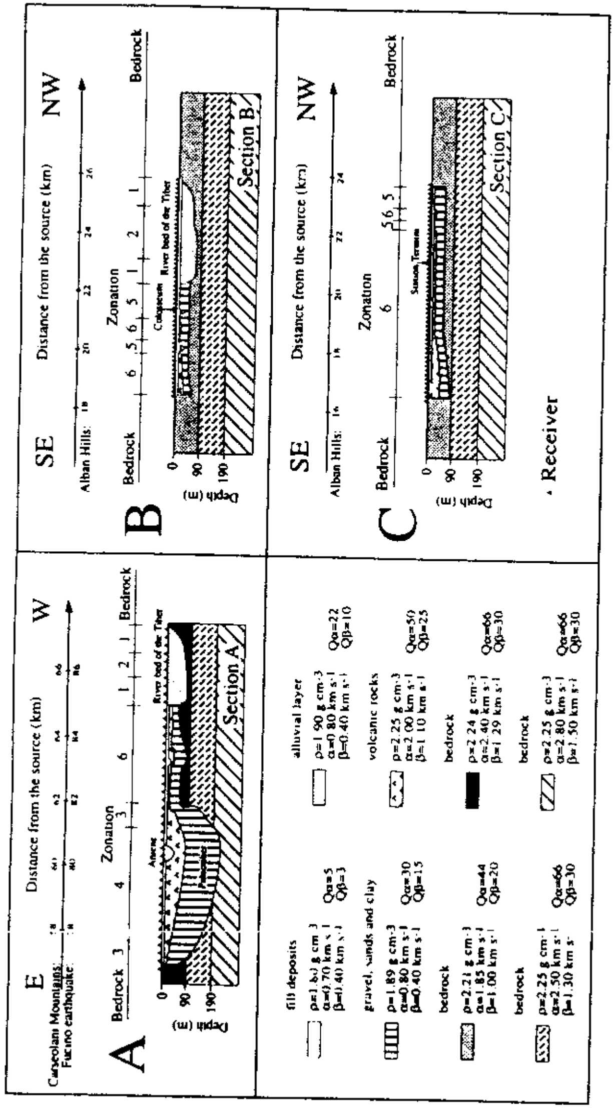
A
E
W
Distance from the source (km)
Carseolani Mountains:
Fucino earthquake:
Zonation
Bedrock
Depth (m)
River bed of the Tiber
Section A
B
SE
NW
Alban Hills:
Section B
C
Section C
fill deposits
gravel, sands and clay
bedrock
alluvial layer
volcanic rocks
Receiver

Fig. 3

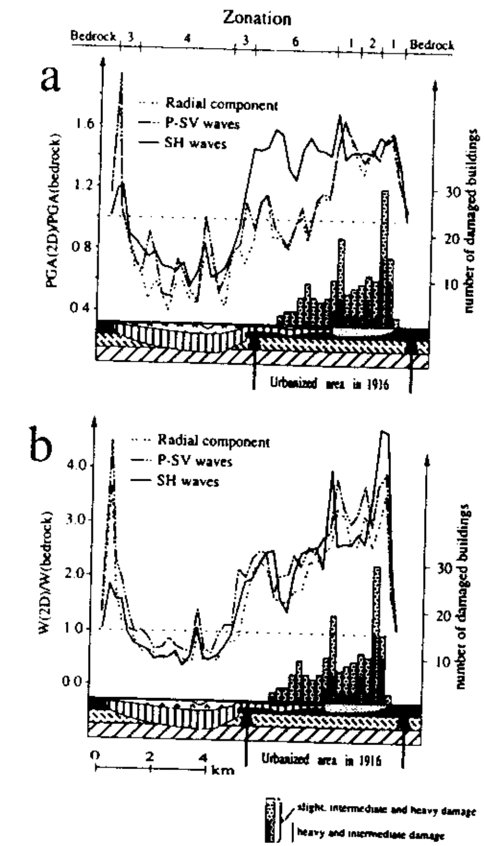
Zonation
Bedrock
a
Radial component
P-SV waves
SH waves
PGA(2D)/PGA(bedrock)
number of damaged buildings
Urbanized area in 1916
b
W(2D)/W(bedrock)
km
slight, intermediate and heavy damage
heavy and intermediate damage

Fig.4

40

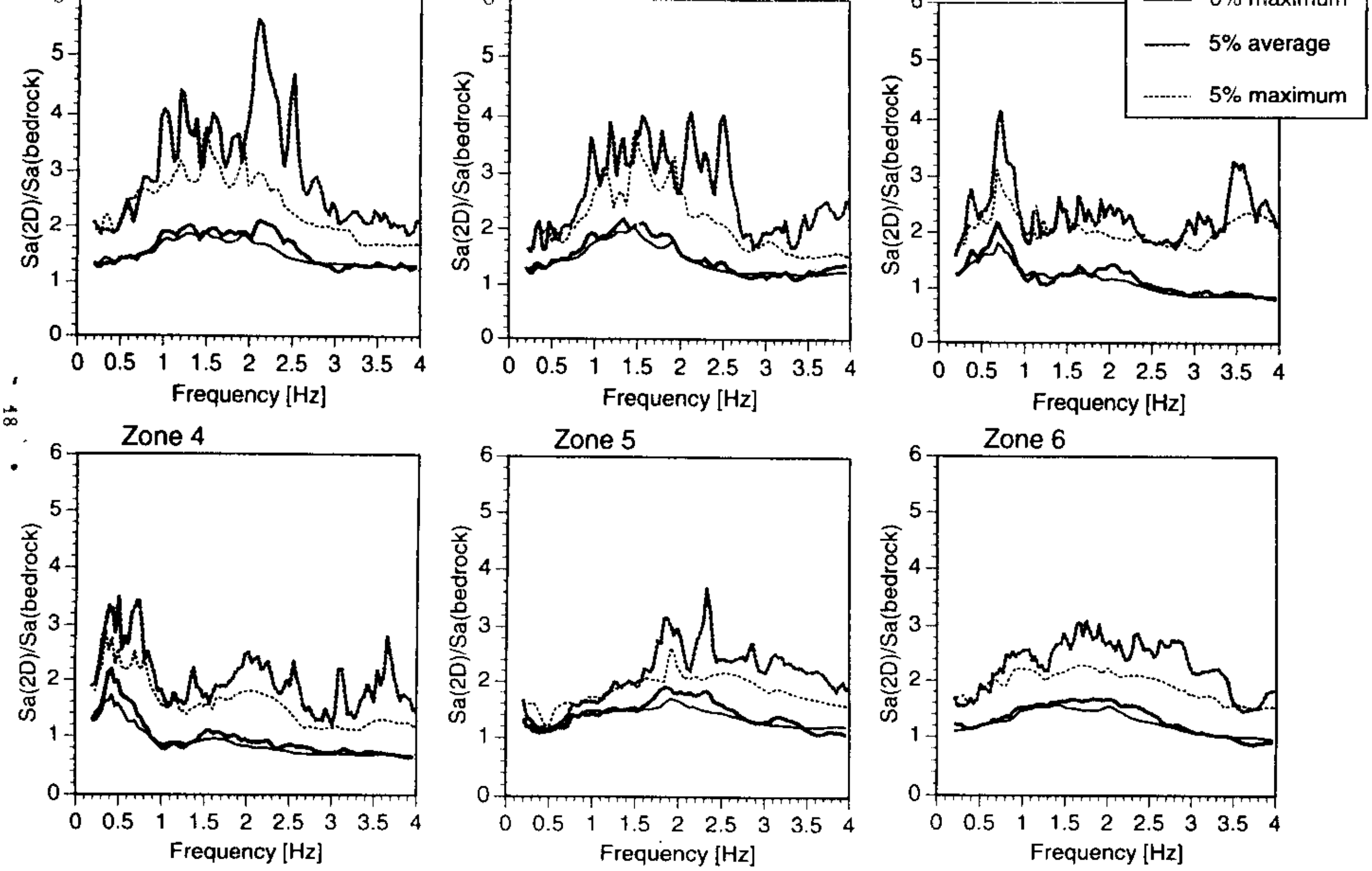
5% average
5% maximum
Zone 4
Zone 5
Zone 6
Sa(2D)/Sa(bedrock)
Frequency [Hz]

Fig.5

IC/94/49

INTERNATIONAL CENTRE FOR
THEORETICAL PHYSICS

REALISTIC MODELLING OF OBSERVED SEISMIC MOTION IN COMPLEX SEDIMENTARY BASINS

D. Fäh

and

G.F. Panza

INTERNATIONAL ATOMIC ENERGY AGENCY

UNITED NATIONS EDUCATIONAL, SCIENTIFIC AND CULTURAL ORGANIZATION

MIRAMARE-TRIESTE

43

IC/94/49

International Atomic Energy Agency
and
United Nations Educational Scientific and Cultural Organization
INTERNATIONAL CENTRE FOR THEORETICAL PHYSICS

REALISTIC MODELLING OF OBSERVED SEISMIC MOTION IN COMPLEX SEDIMENTARY BASINS

D. Fäh
Istituto di Geodesia e Geofisica, Università degli Studi di Trieste,
Trieste, Italy

and

G.F. Panza
International Centre for Theoretical Physics, Trieste, Italy
and
Istituto di Geodesia e Geofisica, Università degli Studi di Trieste,
Trieste, Italy.

MIRAMARE - TRIESTE
March 1994

ikk

Abstract

Three applications of a numerical technique are illustrated to model realistically the seismic ground motion for complex two-dimensional structures. First we consider a sedimentary basin in the Friuli region, and we model strong motion records from an aftershock of the 1976 earthquake. Then we simulate the ground motion caused in Rome by the 1915, Fucino (Italy) earthquake, and we compare our modelling with the damage distribution observed in the town. Finally we deal with the interpretation of ground motion recorded in Mexico City, as a consequence of earthquakes in the Mexican subduction zone. The synthetic signals explain the major characteristics (relative amplitudes, spectral amplification, frequency content) of the considered seismograms, and the space distribution of the available macroseismic data. For the sedimentary basin in the Friuli area, parametric studies demonstrate the relevant sensitivity of the computed ground motion to small changes in the subsurface topography of the sedimentary basin, and in the velocity and quality factor of the sediments. The total energy of ground motion, determined from our numerical simulation in Rome, is in very good agreement with the distribution of damage observed during the Fucino earthquake. For epicentral distances in the range 50km-100km, the source location and not only the local soil conditions control the local effects. For Mexico City, the observed ground motion can be explained as resonance effects and as excitation of local surface waves, and the theoretical and the observed maximum spectral amplifications are very similar. In general, our numerical simulations permit the estimate of the maximum and average spectral amplification for specific sites, i.e. are a very powerful tool for accurate micro-zonation.

Introduction

The presence of unconsolidated sediments with irregular geotechnical characteristics makes the sedimentary basins the zones which are most vulnerable to earthquakes. In fact, when the shear-wave velocity at the surface is low, quite large amplifications of the ground motion are observed, and localized amplification of the signals are often related to lateral irregularities in the subsurface topography (e.g. Jackson, 1971). Even smooth variations of the near-surface structure can cause large differential motion, and in relatively close points it is possible to observe signals with significantly different amplitude and duration.

It is well-known that incident plane waves are amplified when the seismic wave travels through an interface from a medium with high rigidity, into a medium with low rigidity. For vertically incident waves, the frequencies of the mechanical resonance which can occur in sedimentary basins, are given by $f_n=(2n+1)\beta/4h$, where β is the shear wave velocity in the basin and h is its thickness (Haskell, 1960; 1962). An irregular interface between bedrock and sediments can cause the focusing of waves (e.g. Aki and Larner, 1970; Boore et. al., 1971; Sánchez-Sesma et al., 1988), and can excite local surface waves (e.g. Trifunac, 1971; Bard and Bouchon, 1980a; 1980b). These local surface waves can be excited not only by body waves but also by the incidence of surface waves (Drake, 1980). Bard and Bouchon (1985) demonstrated that the occurrence of local surface waves is determined primarily by the depth of the basin and by the contrast between the shear-wave velocity of the basin and that of the bedrock. When the wavelength of the incident wave is comparable with the depth of the basin, the local surface waves can have larger amplitudes than the direct signal, and, if the contrast in the elastic parameters between the sediments and the underlying bedrock is high, they can be reflected at the edges of the basin, causing a long duration of the ground motion in the basin. This behavior does not change if a vertical stratification of the sediments, with a large vertical velocity gradient, is considered (Bard and Gariel, 1986).

For preparedness purposes, it is crucial to estimate the seismic ground motion, before an earthquake occurs, and to include these results in the assessment of seismic hazard or in (micro)-zonation studies. A powerful tool to estimate the amplification effects in complex structures are numerical simulations. One major problem which is encountered when doing such simulations is the large number of parameters which have to be specified as input. The choice of these parameters should be based on all available seismological, geological and geotechnical information for the area under consideration. At a specific site, the numerical simulation can predict the seismic response only if the properties of the seismic source and the mechanical (density, velocity, damping, etc.) and geometrical (such as thickness) parameters of the path from the source are reasonably well-known. In general this is not the case, and parametric studies are necessary to quantify the variability of the expected ground motion. Such simulations, whenever possible must be compared with observed ground motion.

The method we use for the modelling of the wave propagation in two-dimensional complex media, is the hybrid technique, which combines modal summation (Panza, 1985; Florsch et al., 1991) and the finite difference technique (Korn and Stöckl, 1982; Virieux, 1986), described by Fäh (1992), Fäh et al. (1993a; 1993b), and Fäh et al. (1994). The propagation of waves from the source to the sedimentary basin is treated with the mode summation method, applied to plane layered, anelastic structures which represent the average crustal properties along the source-basin path. In our modelling, this structure is used as the reference, bedrock model. The wavefield computed for this bedrock model is used as incident wavefield for the explicit finite difference schemes, which are used to simulate the propagation of seismic waves in the two-dimensional, anelastic model of the sedimentary basin. This hybrid method allows us to take into account the source and propagation effects, including local soil conditions, even when dealing with path lengths of a few hundred kilometers.

In the following, we illustrate a comparison between numerical simulations, and observed strong ground motion or the space distribution of the available macroseismic data. We will focus on the different effects of the source, the path and the local soil conditions. Special emphasis is given to understand the different features of ground motion in sedimentary basins, and the application of numerical simulations for seismic zonation. The three applications include sites close to the source (a sedimentary basin near to the epicenter of the September 11, 1976, Friuli aftershock at $16^h35^m04^s$), at an intermediate distance (Rome, about 80 km from the epicenter of the January 13, 1915, Fucino earthquake), and sites that are far from the source (Mexico City, about 400 km from the epicenter of the September 19, 1985, Michoacan earthquake).

The sedimentary basins in the Friuli area

The September 11, 1976 Friuli aftershock ($16^h35^m04^s$) has been recorded by a few accelerographic stations (CNEN-ENEL, 1977). Records from one of the nearest stations - the three-component records at station Buia (Figure 1)- are considered and compared with the theoretical computations. We focus on the variability of ground motion within the sedimentary basin, and on the sensitivity of the computed ground motion to small changes in the subsurface topography of the sedimentary basin, and in the velocity and quality factor of the sediments.

The bedrock model, describing the average mechanical properties of the path from the epicenter to the sedimentary basin, has been proposed by Fäh et al. (1993a), and its uppermost layers are shown in Figure 2. The source-depth used in the numerical modelling is 7.1 km, the angle between the strike of the fault and the epicenter-station line 19°, the dip 28°, the rake 115°, and the source duration is 0.6 s (Florsch et al., 1991).

The area where the station of Buia is located is characterized by terrigenous sediments (Flysch), widely outcropping at Monte Buia (Figure 1), which are covered locally by a thin quaternary layer, forming a sedimentary basin, and which overlap a carbonatic mesozoic sequence. The thickness of the quaternary sediments is well-known (Giorgetti and Stefanini, 1989) and locally can reach 100 m. The average model for the sedimentary basin is represented by the cross-section B, while the part of the basin with a thick sedimentary cover is well represented by the cross-section C, both shown in Figure 2.

The accelerograms obtained in correspondence of the cross-section B, with the shear-wave velocity of the unconsolidated sediments equal to 0.6 km/s and the quality factor Q_β equal to 20, are shown in Figure 3. At sites with a thick layer of low-velocity material near to the surface, the peak acceleration of the radial component is up to

two times larger than the vertical component, while, due to the source radiation pattern, the transverse component is of the same size of the radial component.

The heterogeneity, with size comparable to the wavelength of the incident wavefield, causes significant spatial variations in the ground motion (Figure 3). There are three major effects which are caused by the presence of the sedimentary cover: (1) the excitation of surface waves at the edge of the sedimentary basin, (2) the resonance in parts of the basin due to the subsurface topography of the bedrock, and (3) the excitation of very dispersed local surface waves, with peak energy at about 2 Hz, within the sedimentary basin for epicentral distances larger than 14 km.

Multiple reflections of SH-waves can generate local surface waves, (phase L_1) - forming the coda of the signals (Figure 3) - which are excited as soon as the fundamental Haskell's frequency of resonance (Haskell, 1960; 1962) for the sedimentary basin is reached. These local surface waves can be reflected inside the basin at places where the sediments become thin. One example is given by the phase L_{11} in Figure 3, which corresponds to the reflected local surface wave L_1. Also for P-SV-waves, a dipping layer at the edge of a sedimentary basin gives rise to multiple reflections of body waves and the excitation of local surface waves (phase R_2 in Figure 3), which are characterized by larger amplitudes on the radial than on the vertical component of motion, and can be the dominant part of the wavefield at the edge of the sedimentary basin. The reflections of the local Rayleigh waves inside the sedimentary basin (R_{22} in Figure 3) do not appear as clear as in the case of Love waves, since their amplitudes are small in comparison with the amplitudes of the primary waves.

Resonance occurs in those parts of the basins where the interface between the bedrock and the sediments is smoothly varrying, and originates from the superposition of forward propagating local surface waves with their reflections, within sub-basins of the sedimentary cover. Examples are seen for the two sub-basins in cross-section B, especially at 9.8 km and at 11.8 km from the source (Figure 3). The resonance is stronger for SH- than for P-SV-waves, and in general can give rise to very large duration and amplitude, as can be seen from the signal computed at 11.8 km from the source.

The excitation of strongly dispersed local surface waves by subsurface lateral heterogeneities can be observed in correspondence of the cross-section B at epicentral distances larger than 14 km, both for SH- and P-SV-waves.

The synthetic accelerograms, obtained from the numerical modelling, can be used to compute some ground motion related quantities. These quantities are (1) the peak ground acceleration PGA and (2) the so-called total energy of ground motion, W, given by:

$$W = \lim_{t \to \infty} \int_0^t [\ddot{x}(\tau)]^2 \, d\tau \quad ,$$

where x(t) is the time series describing the ground displacement. To discuss the site effects with respect to the bedrock model it is convenient to consider the quantities PGA(2D), and W(2D), i.e. PGA and W obtained from the accelerograms computed for the two-dimensional model, and PGA(bedrock) and W(bedrock), i.e. PGA and W obtained from the accelerograms computed for the model representing the average properties of the source-basin path. The ground motion computed for the different sites in the two-dimensional model is normalized with respect to the ground motion obtained for the same source-receiver distance considering the bedrock model.

The spatial distribution of the values of the relative PGA (PGA(2D)/PGA(bedrock)) and relative W (W(2D)/W(bedrock)) for the transverse component of motion, and for different shear-wave velocities and quality factors of the unconsolidated sediments are shown in Figure 4. The relative PGA increases only slightly when the shear-wave velocity of the sediments is reduced, whereas the relative W is very sensitive to small changes in the shear-wave velocity of the sediments. A low shear-wave velocity induces the largest amplitudes and dispersion of the local surface waves. These effects give the dominant contribution to the relative W at sites where resonance effects and excitation of local surface waves are important (for example at 11.8 km from the source). The relative PGA and W have been computed for three different quality factors Q_β of the sediments, by keeping the shear-wave velocity fixed at 0.6 km/s (right part of Figure 4). The attenuation of waves increases with decreasing quality factor. This causes the reduction of the duration of the signals at sites where resonance effects and excitation of local surface waves are important phenomena. The smaller the quality factor of the unconsolidated

sediments, the shorter is the duration of the resonance, and the smaller the propagation distance of the local surface waves. Consequently, low quality factors strongly reduce the relative W.

In Figure 5, we compare the synthetic signals computed for the two cross-sections B and C, shown in Figure 1, with the accelerograms recorded at station Buia. In correspondence of the recording station, which is at 15 km from the source, the thickness of the sedimentary cover is the same in the two cross-sections.

For the transverse component of motion, the local surface waves have amplitudes that are too large in comparison with the observation. In the choice of the geometry of the bedrock-sediment interface, we have restricted ourselves to that given by Giorgetti and Stefanini (1989). However, to reproduce the observed transverse component, the heterogeneity inside the sedimentary basins, responsible for the excitation of these local surface waves, would have to be different. The considered heterogeneity is either too close to station Buia or the bedrock-sediment interfaces are too close to the free surface. In the radial component the excitation of local surface waves is not very clear. When dealing with P-SV-waves, there are two sources of local surface waves: the edge of the sedimentary basin and the places where the bedrock-sediment interface approaches the free surface. From the signals computed for the two cross-sections, it can be concluded that the closer the sediment-bedrock interface is to the free surface, the greater are the amplitudes of the local Rayleigh waves. On the other hand, this lateral heterogeneity can cause the reflection of most of the local Rayleigh waves, generated at the sedimentary basins edge which is closer to the seismic source.

The comparison of the synthetic signals with the observed radial component shows good agreement between the observation and the signal obtained for cross-section C. Due to the small amplitudes of the coda in the observation, it can be concluded that the local surface waves have travelled through the deeper parts of the sedimentary basin, and that the lateral heterogeneity within the basin has reflected a relevant part the local surface waves, which is excited at the edge of the basin. To reproduce the observed signal, the lateral heterogeneity within the basin cannot be strong; a strong heterogeneity, in fact, would excite large-amplitude local surface waves inside the basin, and these are not observed experimentally.

The vertical component of the observed ground motion, especially at low-frequency (below 4 Hz), is quite similar to the synthetic signals, which do not change significantly from one cross-section to the other. The relatively small sensitivity of the vertical component of motion to the lateral variation of sedimentary basins has been observed also at different sites in Mexico City, and the results illustrated in this paper suggest to consider this fact a quite general property of sedimentary basin. The high-frequency component, not observed experimentally, but present in the synthetic signals for models B and C, is due to the resonance effects in the shallow part of the sedimentary cover. This difference between the computed and the observed signals indicates once again that, in the modelling, either the shallow parts of the sedimentary cover are too close to the observation point, or the bedrock-sediment interfaces are too close to the free surface.

The Rome area and the 1915 Fucino earthquake

The area of Rome, considered here, is characterized by several sedimentary basins of considerable thickness, which, in some parts, are covered by volcanic rocks. The area is very vulnerable to earthquakes, as indicated, for example, by the well documented damage distribution caused by the January 13, 1915, Fucino (Italy) earthquake (M_L=6.8) (Figure 6). Since no strong motion records are available for this event, we have applied the hybrid technique to explain the observed damage distribution (Fäh et al., 1993b). The source parameters, the bedrock model, describing the path from the source to Rome, and the two-dimensional model for the area of Rome are described in Fäh et al. (1993b).

To demonstrate that not only the local soil conditions are important to explain a local distribution of damage, but that there are also important regional effects due to the source location, we compare the results of two sets of computations, made by changing only the distance of the seismic source from the city of Rome (Figure 7). The epicenter of the Fucino event is about 85 km east of Rome, and the other hypothetical source, source 2 in Figure 7, is located at a distance of about 65 km, in the same direction.

The synthetic accelerograms are used to compute the total energy, W(2D), and the relative total energy, W(2D)/W(bedrock), of ground motion. The results for the

transverse component of motion, corresponding to the two source positions are shown in Figure 8. They are compared with the histogram of the damage distribution, which has been constructed by projecting each observation of damage, shown in Figure 6, on the cross-section used in the numerical modelling (Fäh et al., 1993b). Only those points of the distribution have been used which are located in an area where the geometry of the structure does not differ too much from the geometry of the two-dimensional cross section. This area is delimited in Figure 6 by the two dotted lines. Since neither the type of buildings nor the density of the urbanization can be known with great detail, the histogram shown in Figure 8 should be interpreted only in a qualitative manner.

The total energy, W, and the relative W, computed for the Fucino event are quite well correlated with the damage distribution, as is shown in Figure 8 (Fäh et al., 1993b). There are four relative peaks: two at the edges of the Tiber basin, one within the alluvial valley of the Aniene river, and a broad peak where the Sicilian low-velocity zone gets close to the surface. The largest values are observed at the margins of the Tiber bed. There the signals have the largest amplitudes and duration, due to the low impedance of the alluvial sediments, the excitation of local surface waves, and resonance effects. Minimum values can be observed for sites placed above the volcanic layer overlying the Paleotiber basin, which acts as a shield, and reflects part of the incoming energy: the thicker the volcanic layer, the smaller are the W values observed at the surface.

The results obtained considering source 2 are quite different. W, and relative W are similar in the area of the Paleotiber basin, whereas in the other areas the values obtained considering source 2 are considerably smaller, and the two peaks at the margin of the Tiber basin are significantly reduced. A comparison of W, determined from the two numerical experiments, shows that the total energy associated with the Fucino event is significantly larger than the one carried by source 2, even if the former event is 20 km farther from Rome than the latter.

These differences can be explained by the attenuation of PGA and W with distance. The example concerning the transverse component of motion, computed for the bedrock model, is shown in Figure 9. The PGA and W are not monotonically decreasing with distance. This behavior is due to the fact that for epicentral distances less than 50 km the PGA and W are essentially controlled by the crustal Sg phase, while at greater distances they are increasing owing to the contribution of several S-wave phases reflected mostly at the Moho (Suhadolc and Chiaruttini, 1985), which gradually become a part of the Lg waves and further increase PGA and W.

At distances of the order of 80 km (average distance of the Paleotiber from the Fucino event) and 60 km (average distance of the Paleotiber from the hypothetical source), the W values are about the same. This explains the similar values of W in the area of the Paleotiber (Figure 8) computed considering the two events. Similarly, it is possible to explain the values of W observed at distances in the range 61 km-67 km from source 2 (Figure 8), which are smaller than the ones corresponding to the Fucino event in the epicentral distance range 81 km-87 km. Finally from Figure 9, it is evident that, when dealing with earthquakes occurring in the Apennines, for epicentral distances between 50 and 100 km, the largest damage can be expected from an event as far as 90 km from Rome.

The Fourier-spectrum of the signal computed at 85km from the source, corresponding to the epicentral distance of the margin of the Tiber basin from the Fucino event, is quite large for frequencies below 2.5 Hz if compared with the spectrum of the signal obtained at 65 km from the source, which corresponds to the epicentral distance of the margin of the Tiber from source 2 (Figure 10). As we will see later, for frequencies below 2.5 Hz strong amplifications occur at the margins of the Tiber basin. Since the incident wavefield computed for source 2 contains relatively small energy at frequencies below 2.5Hz, resonance effects and excitation of local surface waves are not the dominant phenomena, and this justifies the absence of the peak at the margin of the Tiber basin in W computed for source 2. Thus, for epicentral distances in the range 50km-100km, the source location and not only the local soil conditions control the local site effects.

All the quantities used to measure strong ground motion like the maximum amplitude, the duration and the Fourier spectrum provide only a very limited description of the ground motion and certainly do not quantify its damage producing potential. A better quantity is the spectral acceleration Sa of the earthquake ground motion. A representation of the local soil effects is given by the spectral amplification Sa(2D)/Sa(bedrock) computed from the spectral accelerations obtained for the two-dimensional and the bedrock models. This procedure allows us to identify the frequency bands and sites at which amplification and attenuation effects occur. For SH-waves, the spectral amplification for zero damping are shown in Figure 11 for the two simulated events, as a function of frequency and of the spatial location along the

section. The darker an area, the stronger the amplifications due to the two-dimensional effects. The greatest amplification is observed for the Fucino event at the western edge of the sedimentary basin of the Tiber river (about 87 km from the source), for frequencies around 2 Hz. The maximum amplification is of the order of 5-6, and it is due to the combination of resonance effects and the excitation of local surface waves. This amplification effect is responsible for the relative peak in the total energy W at the margin of the Tiber basin (Figure 8).

The global distribution of the shaded areas can be related to the geometry of the structural model. The results are similar for the Fucino event and for source 2, except at the margins of the Tiber basin. An amplification over almost the entire frequency band is observed outside the Paleotiber basin (82-87 km from the source for the Fucino event, 62-67 km from source 2). Some amplification occurs in the Aniene basin, for frequencies above 2 Hz. For frequencies above 0.8 Hz, in the Paleotiber basin, the volcanic layer acts as a shield reflecting part of the incoming energy, and the values of the spectral amplification are smaller than 1. The underlying sedimentary complex (Sicilian) causes spectral amplification of the order of 2-3, due to resonances, which are most pronounced at frequencies around 0.4 Hz, where the fundamental resonance of this low-velocity zone is excited. In this part of the Paleotiber, in the frequency band 1.5-2.0 Hz, there is also evidence for the excitation of some higher modes of resonance. At distances of the order of 82-83 km from the Fucino event, and 62-63 km from source 2, between the Paleotiber and the Tiber basins, where the wave guide and overlying volcanic cover are thinning, focusing of seismic energy occurs and most of the trapped energy reaches the surface. This leads to amplifications, of the order of 2, over almost the entire frequency band considered. Therefore, the presence of a near-surface layer of rigid material is not sufficient to classify a site as a "hard-rock site". Reliable determinations of local soil effects, in addition to the knowledge of the frequency content and direction of the incoming signal, require the knowledge of both the thickness of the surficial layer and of the deeper parts of the structure, down to the real bedrock. This is especially important in volcanic areas, where pyroclastic material often covers alluvial basins.

Mexico City

Mexico City is an area of particular interest since extensive damage occurred in the lake-bed zone during the Michoacan earthquake of September 19, 1985. This can be attributed to the geotechnical and geometrical characteristics of the unconsolidated sediments in this zone. From the geotechnical point of view, the valley of Mexico City can be divided into the hill zone, the transition zone, and the lake-bed zone (Figure 12). The hill zone is formed by alluvial and glacial deposits, and by lava flows. The transition zone is mainly composed of sandy and silty layers of alluvial origin. The surficial layers in the lake-bed zone consist mainly of clays. These deposits are poorly consolidated, with high water content and very low rigidity. The thickness of this surficial layer varies between 10 m and 70 m, and increases regularly towards the east (Suarez et al., 1987). The clay layer is overlying the so-called "deep sediments" found below 10-70 m. These deeper deposits reach depths of the order of 700 m, with an uncertainty which may be as large as a few hundred meters (e.g. Bard et al., 1988). There are three outcrops of the basement: at Chapultepec, Peñon, and Cerro de la Estrella (Figure 12). In the last years, a strong motion network has been operating in the valley of Mexico City (e.g. Mena et al., 1986; Espinosa et al., 1990), and the positions of the stations used in this study are shown in Figure 12.

Today's research, to understand the extensive damage caused by the 1985 earthquake and the recorded ground motion in Mexico City, has shown the importance to consider source and propagation effects, including local soil conditions. This is dealt explicitly in the recent work by Fäh et al. (1994) in which the hybrid technique has been applied to study the ground motion in Mexico City. The model used by Fäh et al. (1994) explains the observed difference in amplitudes for receivers located inside and outside the lake bed zone. The ratio between the computed, horizontal peak ground displacements inside and outside the lake-bed zone reaches values ranging from 5 to 7, and about the same ratio is obtained for the observed ground motion. The validity of the modelling is further confirmed by the fact that the spectral ratios obtained for the horizontal components of the synthetic seismograms are very similar to comparable spectral ratios obtained from observations.

The structural model used in the numerical simulations for the 1985 Michoacan event, and a detailed parametric study of the effects of different soil

properties in Mexico City is given in Fäh et al. (1994). The flat-layered structure in Table 1 describes the path from the seismic source to the valley of Mexico City (Campillo et al., 1989). The structural model is rather simple, in agreement with the resolving power of the available data. The depth of the Moho is about 45 km, and the upper five kilometers are composed of low-velocity material. The two-dimensional structure for the Mexico City valley, modelling the Chapultepec-Peñon cross-section (solid line in Figure 12), is shown in Figure 13.

As in Fäh et al. (1994), to keep the source model as simple as possible and to avoid any, a priori, enhancement of resonance effects at the longer periods (above 2s), we consider first a constant, frequency independent, seismic moment rate spectrum. The focal mechanism is the one proposed by Campillo et al. (1989), based on the results of Houston and Kanamori (1986) and Riedesel et al. (1986). The distance from the source to the valley of Mexico City is 400 km, the angle between the strike of the fault and the epicenter-station line is 220°, the source depth is 10 km, the dip 15°, and the rake is 76°.

The use of an instantaneous time-function gives rise to synthetic signals that contain too much energy at high frequency (above 0.6Hz), and we can remove this drawback applying the ω^2 scaling law for the seismic moment rate spectrum, proposed by Kanamori et al. (1993) for the events occuring in the Mexican subduction zone:

$$\hat{M} = M_0 \omega_c^2 \,(\omega^2 + \omega_c^2)^{-1} \qquad (1)$$

where $\hat{M}$ is the seismic moment rate spectrum, M_0 is the seismic moment, and ω_c is the corner angular frequency. Following Kanamori et al. (1993), ω_c=0.196 s^{-1} and M_0=0.5 10^{21} N m. With these values we obtain a very good reproduction of the shape of the observed signals, over the entire frequency spectrum, but the absolute observed accelerations are underestimated by a factor ranging from 6 to 3. This last discrepancy can be reconciled considering the errors affecting the estimates of ω_c and M_0, and taking into account the subsequent rupture episodes of the Michoacan event, mainly the one occurring about 26s after the origin time. This kind of data fitting is, however, outside the purpose of the present paper, since it is unrelevant for the computation of the spectral amplification, and will be the subject of future investigations.

Spectral amplification at the site of interest computed with respect to a reference site gives a very good representation for micro-zoning purpose, especially from the engineering point of view (Fäh and Suhadolc, 1994). We compute the spectral amplification, i.e. the relative spectral accelerations Sa(2D)/Sa(Ref) and the relative spectral velocities Sv(2D)/Sv(Ref), for zero damping and 5% damping. Sa(2D) is the spectral acceleration and Sv(2D) is the spectral velocity obtained for the receivers in the two-dimensional structural model shown in Figure 13. Sa(Ref) and Sv(Ref) are the values obtained for the reference station shown in Figure 13. For all the receivers, we have computed the relative spectral accelerations and velocities for one hundred frequencies of the oscillator in the range 0.1-1.0 Hz. From these values we then computed the maximum spectral amplification (MSA) for the entire sedimentary basin. The MSA obtained from our numerical simulations are shown in Figure 14. The results for the relative spectral accelerations and the relative spectral velocities are similar, due to the approximate relation existing between them:

$Sa(\omega) \approx \omega \cdot Sv(\omega)$, where ω is the angular frequency of the oscillator.

In the following, we will, therefore, limit ourselves to the relative spectral velocities, which we will call spectral amplification.

In two-dimensional modelling, the SH-waves (transverse component of motion) and P-SV-waves (radial component of motion) are two independent wave fields. The direction of propagation of the local surface waves in the sedimentary basin is therefore well correlated with the source-receiver direction. In Mexico City, the local surface waves are excited at different locations of the interface between the bedrock and the sediments, and the direction of propagation of the local surface waves in the lake-bed zone does not correspond anymore to the source-receiver direction (F.J. Sánchez-Sesma, personal communication). Therefore, to justify the comparison between the observed ground motion and the synthetic signals, we have to compute the spectral amplification for the complete horizontal ground motion. For this purpose, we have applied the horizontal ground motion to an oscillator with two-degrees of freedom. The results for the synthetic signals are also given in Figure 14. Due to the larger amplitudes of the SH-waves, the MSA obtained for the horizontal ground motion are very similar to the result obtained for the transverse component. The maximum peaks in the MSA in Figure 14 can be attributed to sites where a strong interaction between the deep sediments and the surficial clay layer occurs. At such sites, the resonance frequencies of the two layers are almost the same.

The MSA obtained from the numerical simulation is rather independent from the shape of the seismic moment rate spectrum, as can be seen in Figure 15, where the results obtained with the seismic moment rate spectrum proposed by Kanamori et al. (1993) are compared with the results obtained for a frequency-independent spectrum.

The seismograms observed during the 1985 Michoacan earthquake, have been convolved with a high-pass Ormsby filter (Mena et al., 1986), and this filtering allows us an estimate of MSA only for frequencies above 0.1-0.2 Hz. The MSA, determined from the stations SC and CD using TY as reference, and shown in Figure 16, reaches lower values than those computed theoretically, as can be seen from a comparison with Figure 15. This is due to the fact that the site of station TY is not a hard rock site (e.g. Ordaz and Faccioli, 1993). Therefore, if any station in the transition zone or hill zone is taken as reference station, the MSA must be smaller than or equal to the theoretical values. For the Michoacan earthquake we have usable signals only from the stations CD, SC and TY, but we can test our theoretical results using observations from other events, such as the April 25, 1989 earthquake, since with our method, it is relatively easy to estimate the ground motion in a two-dimensional sedimentary basin if the ground motion is known at a reference point outside this basin (e.g. Luzon et al., 1994).

The epicenter of the 1989 event is located in the Guerrero gap, i.e. south of the epicenter of the 1985 Michoacan earthquake. Therefore, to justify a comparison between the numerical results based on the modelling of the 1985 event and the ground motion observed during the 1989 earthquake, we first have to compare the results obtained from the analysis of the records of the 1985 and 1989 earthquakes. The spectral amplification is shown in Figure 17, for station CD with respect to TY, both for the 1985 and for the 1989 earthquake. For the two events, the amplification effects at station CD occur in about the same frequency ranges. There is some difference in the maximum value, which is larger for the 1985 earthquake. The strong peaks in the spectral amplification observed at the station CD, during the 1985 earthquake, can be due to the fact that a relevant amount of energy of the incident wave field is present in the frequency band close to the resonance frequency of the clay layer at the site, and, therefore, local surface waves and resonance effects may dominate the horizontal components of motion. The two peaks in the MSA can be attributed to the deep sediments (peak at about 0.8 Hz) and the surficial clay layer (peak at about 0.25 Hz) (Fäh et al., 1994).

The observed MSA for the 1989 earthquake is shown in Figure 18. The MSA is determined for all the stations shown in Figure 12 using as reference station TY and station 78. The MSA obtained with the reference station TY (Figure 18a and 18c) has once again lower values than those computed theoretically (shown in Figure 15). This is due to the fact, mentioned before, that the station TY is not located on hard bedrock. The MSA obtained with the reference station 78 (Figure 18b and 18d), on the other hand, is very similar to the theoretical curves shown in Figure 15. The peaks, for zero damping of the oscillator, occur when the energy of the incident wave field is relevant in the frequency band close to the resonance frequency of the clay layer at the site of interest. This happens in different sites within the lake-bed zone, and therefore each peak in the MSA (Figure 18b) is obtained from a different receiver. The maximum values obtained theoretically and from the observations are about the same, and the greater complexity in the observed MSA for zero damping, with respect to the theoretical one, which has only two peaks around 0.27 Hz and 0.47 Hz (Fig. 15a and 15b), is not surprising since our numerical model is restricted to one cross section. Therefore, since in our model the maximum clay thickness is 65 m, the MSA shown in Figure 15 is valid only for sites in the lake-bed zone that are characterized by a clay layer with a thickness not exceeding this value.

For 5% damping, the theoretical (Figure 15c,d) and the observed MSA (Figure 18d) are very similar, both in shape and in maximum values, and the two-dimensional model under study can be considered representative for the general geological situation in Mexico City. This is a valuable contribution for micro-zoning purposes, and it permits for each site, where the stratigraphy is reasonably well-known, an estimate of the maximum and average spectral amplification with respect to a bedrock site. An example of the theoretical prediction, based on our results, appropriate for a site similar to the one of station CD (see Fig. 12), is shown in Figure 19a and 19c: the theoretical MSA values are quite satisfactorily compared with the observations made at the station CD in connection with the 1989 event (Figure 19b,d).

Conclusions

The hybrid technique presented in this study makes it possible (1) to study local effects even at large distances (hundreds of kilometers) from the source, (2) to include highly realistic modelling of the source, and (3) of the propagation path. This technique can assist in the interpretation and prediction of ground motion at a given site. It can be applied routinely in (micro-)zonation studies, and provides realistic estimates of ground motion for detailed two-dimensional, anelastic models. The resulting synthetic seismograms can be used to complete existing databases of recorded ground motion. Such databases can then serve to establish estimates of the maximum accelerations, total energies, and spectral amplification of ground motion to be expected at given sites.

The synthetic signals can explain the major characteristics of the observations, even when quite simple source models are assumed. The theoretical computations show that waveforms and frequency content of seismograms are sensitive to small changes in the subsurface topography of the sedimentary basin, the velocity and quality factor of the sediments. What remains constant for different, realistic structural models are the physical processes that occur within sedimentary basins, e.g., the excitation of local surface waves and resonance effects. The frequency content and dispersion characteristics of the waves induced by these processes are clearly related to the depth of the sediments, the steepness and irregularity of the sediment-bedrock interface and the seismic velocities.

To achieve a realistic simulation of seismic ground motion, it is necessary to include source, path and local soil effects, to study both SH and P-SV wave propagation, and to consider anelastic absorption. Following this approach, the reasons for the damage caused by the Michoacan earthquake and the Fucino event can be found not simply in the local site conditions, but also in the effects of the seismic source and of the long-distance propagation path in the crust. The spectral properties of the seismic source and the properties of wave propagation in the crust control the frequency content of the incident wavefield; if a relevant amount of energy is present in the frequency band close to the resonance frequency of the unconsolidated sediments, local surface waves and resonance effects may dominate the horizontal components of motion within the sedimentary basin.

One aspect which is not included in our discussion is the influence of surface topography on ground motion. This approximation can be justified for sites inside sedimentary basins, where topographic features are in general small. However, topography can become important at the edges of sedimentary basins and near outcrops, especially in mountainous regions. The inclusion of the treatment of surface topography is the subject of a forthcoming paper (Fäh and Suhadolc, 1994).

Acknowledgement

We would like to thank Peter Suhadolc and Claudio Iodice for their contribution to this research, ENEA for allowing us the use of the IBM3090E computer at the ENEA INFO BO Computer Center, and the Instituto de Ingenería of the University UNAM, the Centro de Instrumentación y Registro Sismico of the Fundación Javier Barros Sierra, and the Fundación del grupo Ingenieros Civiles Asosiados for the use of the strong motion data recorded in Mexico City. D.F. has been supported by the Swiss National Science Foundation under Grant Nr. 8220-037189. This study has been made possible by the CNR contracts 91.02692.CT15, 91.02550.PF54 and 92.02867.PF54, and EEC contract EPOC-CT91-0042. This research has been carried out in the framework of the ILP Task Group II.4 contributions to the IDNDR project "Physical Instability of Megacities".

53

References

AKI, K. and K.L. LARNER (1970): Surface motion of a layered medium having an irregular interface due to incident plane SH waves, *J. Geophys. Res.*, **75**, 933-954.

AMBROSINI, S., S. CASTENETTO, F. CEVOLANI, E. DI LORETO, R. FUNICIELLO, L. LIPERI and D. MOLIN (1986): Risposta sismica dell'area urbana di Roma in occasione del terremoto del Fucino del 13 gennaio 1915, Risultati preliminari. *Mem. Soc. Geol. It.*, **35**, 445-452.

BARD, P.-Y. and M. BOUCHON (1980a): The seismic response of sediment-filled valleys, Part 1: The case of incident SH waves, *Bull. Seism. Soc. Am.*, **70**, 1263-1286.

BARD, P.-Y. and M. BOUCHON (1980b): The seismic response of sediment-filled valleys, Part 2: The case of incident P and SV waves, *Bull. Seism. Soc. Am.*, **70**, 1921-1941.

BARD, P.-Y. and M. BOUCHON (1985): The two-dimensional resonance of sediment-filled valleys, *Bull. Seism. Soc. Am.*, **75**, 519-541.

BARD, P.-Y. and J.-C. GARIEL (1986): The seismic response of two-dimensional sedimentary deposits with large vertical velocity gradients, *Bull. Seism. Soc. Am.*, **76**, 343-366.

BARD, P.-Y., M. CAMPILLO, F.J. CHAVEZ-GARCIA and F.J. SÁNCHEZ-SESMA (1988): The Mexico earthquake of September 19, 1985 - A theoretical investigation of large- and small-scale amplification effects in the Mexico City valley, *Earthquake Spectra*, **4**, 609-633.

BOORE, D.M., K.L. LARNER and K. AKI (1971): Comparison of two independent methods for the solution of wave-scattering problems: Response of a sedimentary basin to vertically incident SH waves, *J. Geophys. Res.*, **76**, 558-569.

CAMPILLO, M., J.-C. GARIEL, K. AKI and F.J. SÁNCHEZ-SESMA (1989): Destructive strong ground motion in Mexico City: Source, path, and site effects during great 1985 Michaocan Earthquake, *Bull. Seism. Soc. Am.*, **79**, 1718-1735.

CNEN-ENEL (1977): Accelerograms from the Friuli, Italy, earthquake of May 6, 1976 and aftershocks: Part 3, uncorrected accelerograms, *Rome, Italy, November 1977.*

DRAKE, L.A. (1980): Love and Rayleigh waves in an irregular soil layer, *Bull. Seism. Soc. Am.*, **70**, 571-582.

ESPINOSA, J.M., G. IBARROLA, O.R. CONTRERAS, V.R. SILVA, L. CAMARILLO and C. PINEDA (1990): Sumario de acelerogramas colectados durante 1990, *Centro de instrumentación y registro sismico, a.c., fundación javier barros sierra, a.c.*

FÄH, D. (1992): A hybrid technique for the estimation of strong ground motion in sedimentary basins, *Ph.D. thesis Nr. 9767, Swiss Federal Institute of Technology, Zurich.*

FÄH, D., P. SUHADOLC and G.F. PANZA (1993a): Variability of seismic ground motion in complex media: the case of a sedimentary basin in the Friuli (Italy) area, *Journal of Applied Geophysics*, **30**, 131-148.

FÄH, D., C. IODICE, P. SUHADOLC and G.F. PANZA (1993b): A new method for the realistic estimation of seismic ground motion in megacities: the case of Rome, *Earthquake Spectra*, **9**, No.4, 643-668.

FÄH, D., P. SUHADOLC, P., ST. MUELLER and G.F. PANZA (1994): A hybrid method for the estimation of ground motion in sedimentary basins; quantitative modelling for Mexico City, *Bull. Seism. Soc. Am., **84**,* 000-000.

FÄH, D. and P. SUHADOLC (1994): Application of numerical wave-propagation techniques to study local soil effects: The case of Benevento (Italy), Submitted to *Pageoph.*

FEROCI, M., R. FUNICIELLO, F. MARRA and S. SALVI (1990): Evoluzione tettonica e paleogeografica plio-pleistocenica dell'area di Roma, *Il Quoternario*, **3**, 141-158.

FLORSCH, N., D. FÄH, P. SUHADOLC and G.F. PANZA (1991): Complete synthetic seismograms for high-frequency multimode SH-waves, *Pageoph*, 136, 529-560.

FUNICIELLO, R., G. LORIA and S. SALVI (1987): Ricostruzione delle superfici strutturali del sottosuolo della città di Roma, *Atti del 6° Convegno Gruppo Nazionale Geofisica della Terra Solida, CNR, Roma*, 395-415.

GIORGETTI, F. and S. STEFANINI (1989): Vulnerabilità degli acquiferi del campo di Osoppo-Gemona all' inquinamento (Provincia di Udine), *Istituto di Geologia e Paleontologia, Università degli Studi di Trieste*, Pubblicazione n.125.

HASKELL, N.A. (1960): Crustal reflection of plane SH waves, *J. Geophys. Res.*, **65**, 4147-4150.

HASKELL, N.A. (1962): Crustal reflection of plane P and SV waves, *J. Geophys. Res.*, **67**, 4751-4767.

HOUSTON, H. and H. KANAMORI (1986): Source characteristics of the 1985 Michoacan, Mexico earthquake at periods of 1 to 30 seconds, *Geophys. Res. Lett.*, **13**, 597-600.

JACKSON, P.S. (1971): The focusing of earthquakes, *Bull. Seism. Soc. Am.*, **61**, 685-695.

KANAMORI, H., P.C. JENNINGS, S.K. SINGH and L. ASTIZ (1993): Estimation of strong ground motions in Mexico City expected for large earthquakes in the Guerrero seismic gap, *Bull. Seism. Soc. Am.*, **83**, 811-829.

KORN, M. and H. STÖCKL (1982): Reflection and transmission of Love channel waves at coal seam discontinuities computed with a finite difference method, *J. Geophys.*, **50**, 171-176.

LUZON, F., S. AOI, D. FÄH and F.J. SÁNCHEZ-SESMA (1994): Simulation of the seismic response of a 2D sedimentary basin; a comparison between the indirect boundary element method and a hybrid technique. Submitted to *Bull. Seism. Soc. Am.*.

MENA, E., C. CARMONA, R. DELGADO, L. ALCÁNTARA and O. DOMINGUEZ (1986): Catálogo de acelerogramas procesados del sismo del 19 de septiembre de 1985, parte I: Ciudad de México, *Series del Instituto de Ingenieria No. 497, UNAM, México, D. F. México.*

54

ORDAZ, M. and E. FACCIOLI (1993): Site response analysis in the valley of Mexico: Selection of input motion and extent of nonlinear soil behaviour, *Earthq. Eng. Structural Dynamics*, in press.

PANZA, G.F. (1985): Synthetic seismograms: The Rayleigh waves modal summation, *J. Geophysics*, **58**, 125-145.

RIEDESEL, M.A., T.H. JORDAN, A.F. SHEEHAN and P.G. SILVER (1986): Moment-tensor spectra of the 19 Sept. 85 and 21 Sept. 85 Michaocan, Mexico, earthquakes, *Geophys. Res. Lett.*, **13**, 609-612.

SÁNCHEZ-SESMA, F.J., S. CHÁVEZ-PÉREZ, M. SUÁREZ, M.A. BRAVO and L.E. PÉREZ-ROCHA (1988): The Mexico earthquake of September 19, 1985 - On the seismic response of the Valley of Mexico, *Earthquake Spectra*, **4**, 569-589.

SUAREZ, M., F.J. SÁNCHEZ-SESMA, M.A. BRAVO and J. LERMO (1987): Caracteristicas de los depósitos superficiales del Valle de México, *Memorias VII Congreso Nacional de Ingenieria Sismica, Querétaro, México, November 19-21*, A61-A74.

SUHADOLC, P. and C. CHIARUTTINI (1985): A theoretical study of the dependence of the peak ground acceleration on source and structure parameters, in *strong ground motion seismology*, edited by M.Ö. ERDIK and M.N. TOKSÖZ, *Proceedings of the NATO ASI on Strong Ground Motion Seismology, Ankara, Turkey, 1985*, 143-183.

TRIFUNAC, M.D. (1971): Surface motion of a semi-cylindrical alluvial valley for incident plane SH waves, *Bull. Seism. Soc. Am.*, **61**, 1755-1770.

VENTRIGLIA, U. (1971): La geologia della città di Roma, *Amm. Prov. di Roma, Roma.*

VIRIEUX, J. (1986): P-SV wave propagation in heterogeneous media: Velocity-stress finite-difference method, *Geophysics*, **51**, 889-901.

Layer	Thickness (km)	ρ (g/cm^3)	α (km/s)	β (km/s)	Q_α	Q_β
1	5.0	2.67	4.30	2.53	800	500
2	10.0	2.77	5.70	3.30	800	500
3	15.0	3.09	6.80	4.03	800	500
4	15.0	3.09	7.00	4.10	800	500
5	∞	3.30	8.20	4.82	800	500

Table 1. Numerical parameters for the schematic crustal model describing the path from the source in the Michoacan subduction zone, to Mexico City (Campillo et al., 1989).

FIGURE CAPTIONS

Figure 1. Overview of the Friuli seismic region, showing the presence of the quaternary basin, the ISC epicenter determination of the September 11, Friuli 1976 aftershock ($16^h35^m04^s$), and the position of station Buia. The solid lines indicate the position of the two cross-sections for which 2D modelling has been performed.

Figure 2. Surficial layers of the one-dimensional model, describing the propagation of waves from the source position to the sedimentary basin (Fäh et al., 1993a), and of the 2D models corresponding to cross-sections B and C in Figure 1. Only the part near to the surface is shown, where the 2D models are different from the one-dimensional model.

Figure 3. Acceleration time series for SH and P-SV waves at an array of receivers, for cross-section B shown in Figure 2 (β=0.6 km/s and Q_β=20 for the unconsolidated sediments). All amplitudes are related to a source with a seismic moment of 10^{-7} N m. The signals are normalized to the peak acceleration given in units of cm s^{-2}. The distance to the source for each seismogram is given in units of km. The time scale is shifted by 2 seconds from the origin time (0 s in the figure is really 2 s from the origin time).

Figure 4. Relative peak ground acceleration PGA(2D)/PGA(bedrock) and relative total energy W(2D)/W(bedrock) obtained for cross-section B. The values are shown for four different shear-wave velocities of the sediments (0.5 km/s, 0.6 km/s, 0.7 km/s and 0.8 km/s) and for three different quality factors of the sediments (Q_β=5, Q_β=10, and Q_β=20).

Figure 5. Comparison between (A) the recorded transverse, radial and vertical components of acceleration, and synthetic signals, computed for (B) the cross-section B and (C) the cross-section C. The time-scale is shifted by 2 s from the origin time. The recorded seismograms are aligned to agree with the synthetic signals. All amplitudes of the synthetic signals correspond to a source with a seismic moment of 10^{-7} N m. The synthetic signals are normalized to the same peak acceleration which is given in units of cm s^{-2}.

Figure 6. Damage distribution in Rome caused by the January 13, 1915 Fucino earthquake (after Ambrosini et al., 1986), and thickness of the alluvial sediments (given in meters) (Ventriglia, 1971; Funiciello et al., 1987; Feroci et al., 1990). Three types of damage are distinguished: slight damage (cracking of plaster, the downfall of small pieces of mouldings), intermediate damage (between slight and heavy damage), and heavy damage (deep and diffuse damage of indoor and outdoor walls, downfall of large parts of mouldings and of chimneys). The dashed line indicates the position of the cross section, for which numerical modelling has been performed. The distribution of damage within the area limited by the two dotted lines has been projected on the cross section to construct the histograms, shown in Figure 8.

Figure 7. Approximate epicenter location of the January 13, 1915 earthquake in the Fucino valley (1), and of a hypothetical event (2) located at about 65 km from Rome. The dashed line indicates the cross section along which the numerical modelling has been performed. The source depth is 8 km, the angle between the strike of the fault and the epicenter-station line is 38°, the fault dip 39°, and the rake with respect to the strike 172°. The seismic moment is 10^{19} N m (Fäh et al. 1993b).

Figure 8. A) Total energy W(2D) obtained for the two-dimensional model and the two source positions given in Figure 7, and B) corresponding relative total energy W(2D)/W(bedrock). The results are compared with the histogram of the damage distribution caused by the January 13, 1915 Fucino earthquake. The part of the structure near to the surface, where the 2D model deviates from the 1D bedrock model, is given at the bottom of both parts of the figure.

Figure 9. A) Attenuation of PGA(bedrock), and B) attenuation of W(bedrock) with distance from the seismic source for the one-dimensional layered model (bedrock model).

Figure 10. Fourier-spectra of the signals obtained at 65 km and 85 km from the source for the one-dimensional layered model. The distances correspond to the distance of the eastern margin of the Tiber basin from source 2 and from the Fucino earthquake.

Figure 11. Spectral amplification for the transverse component of motion over the entire cross section, A) for the Fucino event and B) for the hypothetical earthquake. The reference signals are the one obtained for the one-dimensional layered model. At

56

the bottom of the figure, the geometry of the two-dimensional cross-section is given, while its mechanical parameters are given in Figure 8.

Figure 12. Map of the area of Mexico City showing the locations of strong motion accelerometric stations. The stations represented by large triangles were operating during the 1985 Michoacan event, while the small gray triangles represent the stations which recorded the April 25, 1989 event. The solid line indicates the position of the cross-section, for which the 2D modelling has been performed.

Figure 13. Two-dimensional model of the Chapultepec-Peñon cross-section. Only the part of the structure near to the surface is shown, where the 2D model deviates from the plane-layered structural model (Table 1).

Figure 14. Maximum relative spectral accelerations Sa(2D)/Sa(Ref) (a,c) and velocities Sv(2D)/Sv(Ref) (b,d), for zero damping (a,b) and 5% damping (c,d), obtained with synthetic signals. The results are shown for a single-degree of freedom oscillator for the transverse and the radial component of motion, and for an oscillator with two degrees of freedom for the horizontal ground motion. The synthetic signals are scaled assuming the seismic moment rate spectrum proposed by Kanamori et al. (1993).

Figure 15. Maximum relative spectral velocities Sv(2D)/Sv(Ref), for zero damping (a,b) and 5% damping (c,d), obtained with the synthetic signals, which are scaled by assuming the seismic moment rate spectrum proposed by Kanamori et al. (1993) (a and c), and by assuming a constant, frequency independent, spectrum (b and d).

Figure 16 Observed maximum relative spectral velocities Sv/Sv(TY) for the 1985 Michoacan earthquake, for (a) zero damping and (b) 5% damping. They are determined from the stations SC and CD using TY as reference.

Figure 17. Relative spectral velocities Sv(CD)/Sv(TY), for zero damping (a,b) and 5% damping (c,d). They are determined from the stations CD using TY as reference. Results are shown for the 1985 Michoacan earthquake (a,c) and the April 25, 1989 event (b,d).

Figure 18. Maximum relative spectral velocities Sv/Sv(TY) and Sv/Sv(78) observed during the 1989 event, for zero damping (a,b) and 5% damping (c,d), obtained for all stations shown in Figure 12, using as reference station TY (a,c) and station 78 (b,d), respectively.

Figure 19. Average and maximum relative spectral velocities for zero damping (a), and 5% damping (c), computed with the synthetic signals obtained for the receivers at distances between 408.5 and 410 km from the source. They are compared with the observed relative spectral velocities Sv(CD)/Sv(78) for the 1989 earthquake, for zero damping (b), and 5% damping (d), determined from the station CD using station 78 as reference.

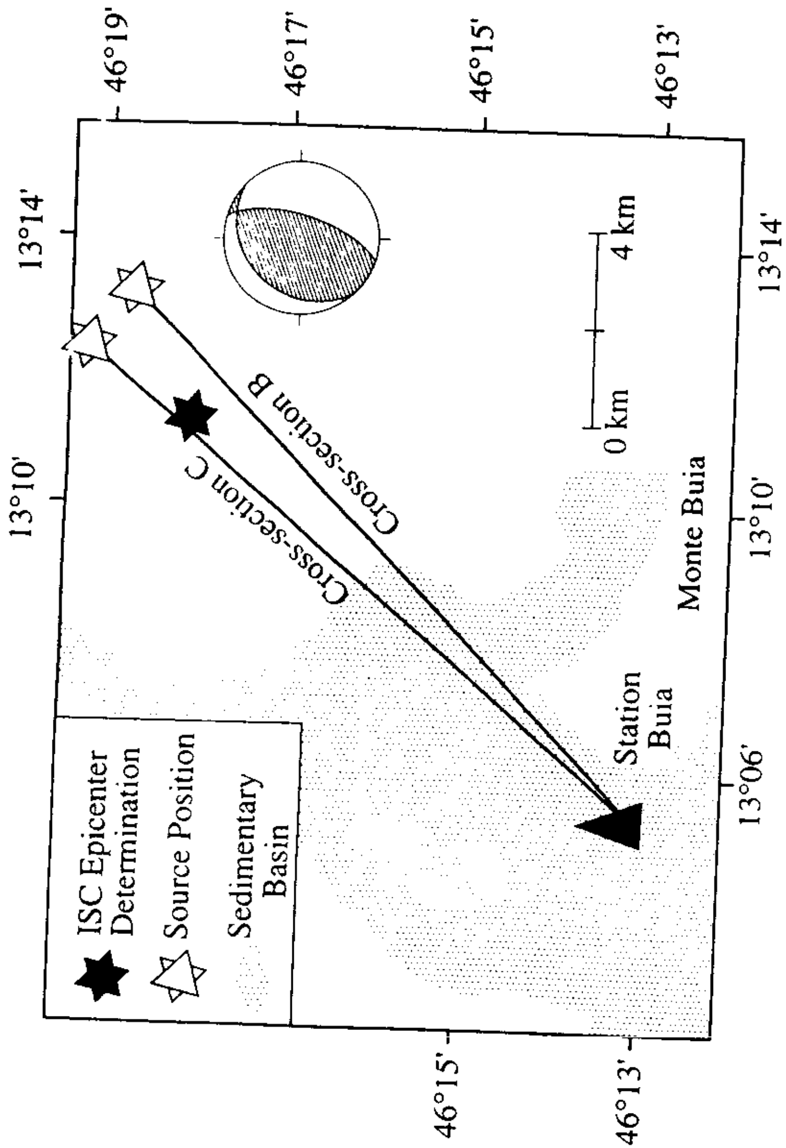
46°19'
46°17'
46°15'
46°13'
13°14'
13°10'
13°06'
ISC Epicenter
Determination
Source Position
Sedimentary
Basin
Cross-section B
Cross-section C
0 km
4 km
Station
Buia
Monte Buia

Fig.1

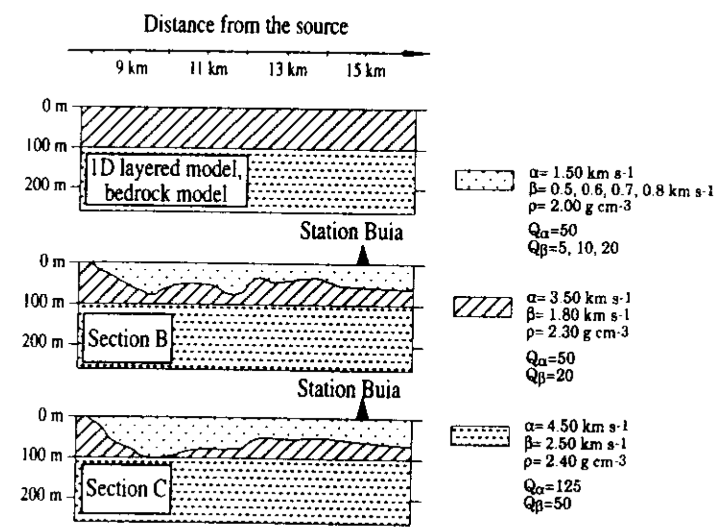
Distance from the source
9 km
11 km
13 km
15 km
0 m
100 m
200 m
1D layered model,
bedrock model
Station Buia
Section B
Section C
α= 1.50 km s-1
β= 0.5, 0.6, 0.7, 0.8 km s-1
ρ= 2.00 g cm-3
Qα=50
Qβ=5, 10, 20
α= 3.50 km s-1
β= 1.80 km s-1
ρ= 2.30 g cm-3
Qα=50
Qβ=20
α= 4.50 km s-1
β= 2.50 km s-1
ρ= 2.40 g cm-3
Qα=125
Qβ=50

Fig.2

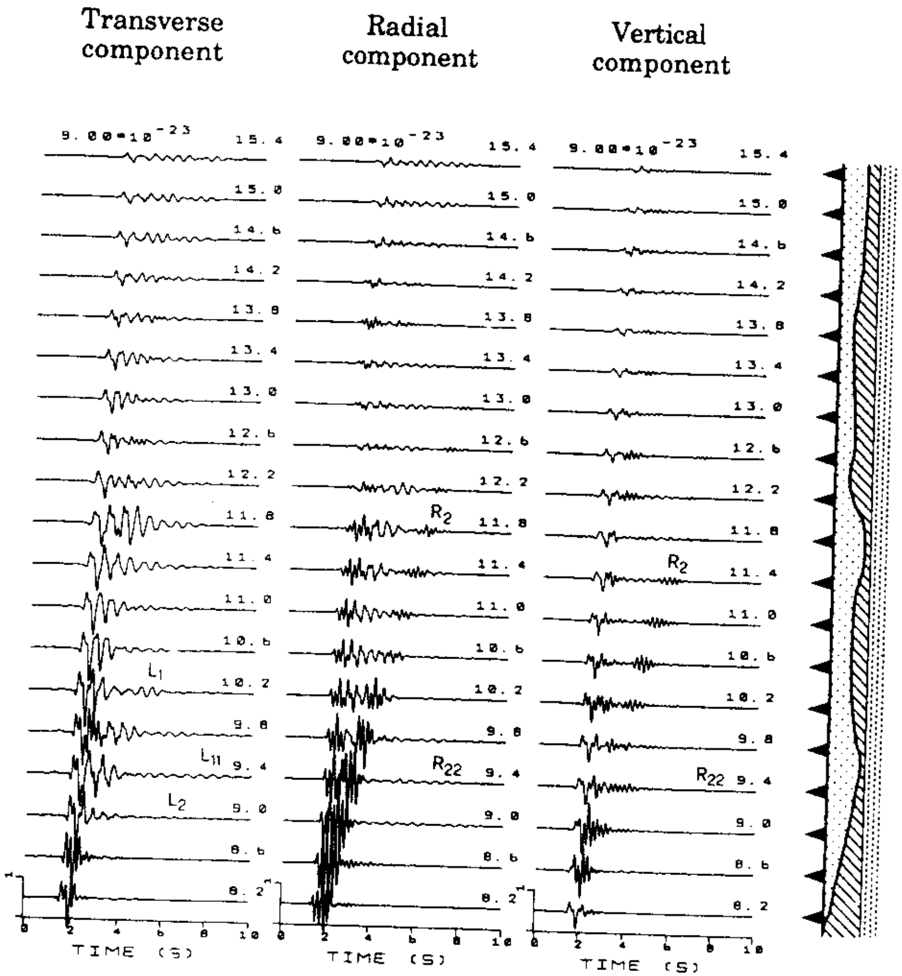

Fig.3

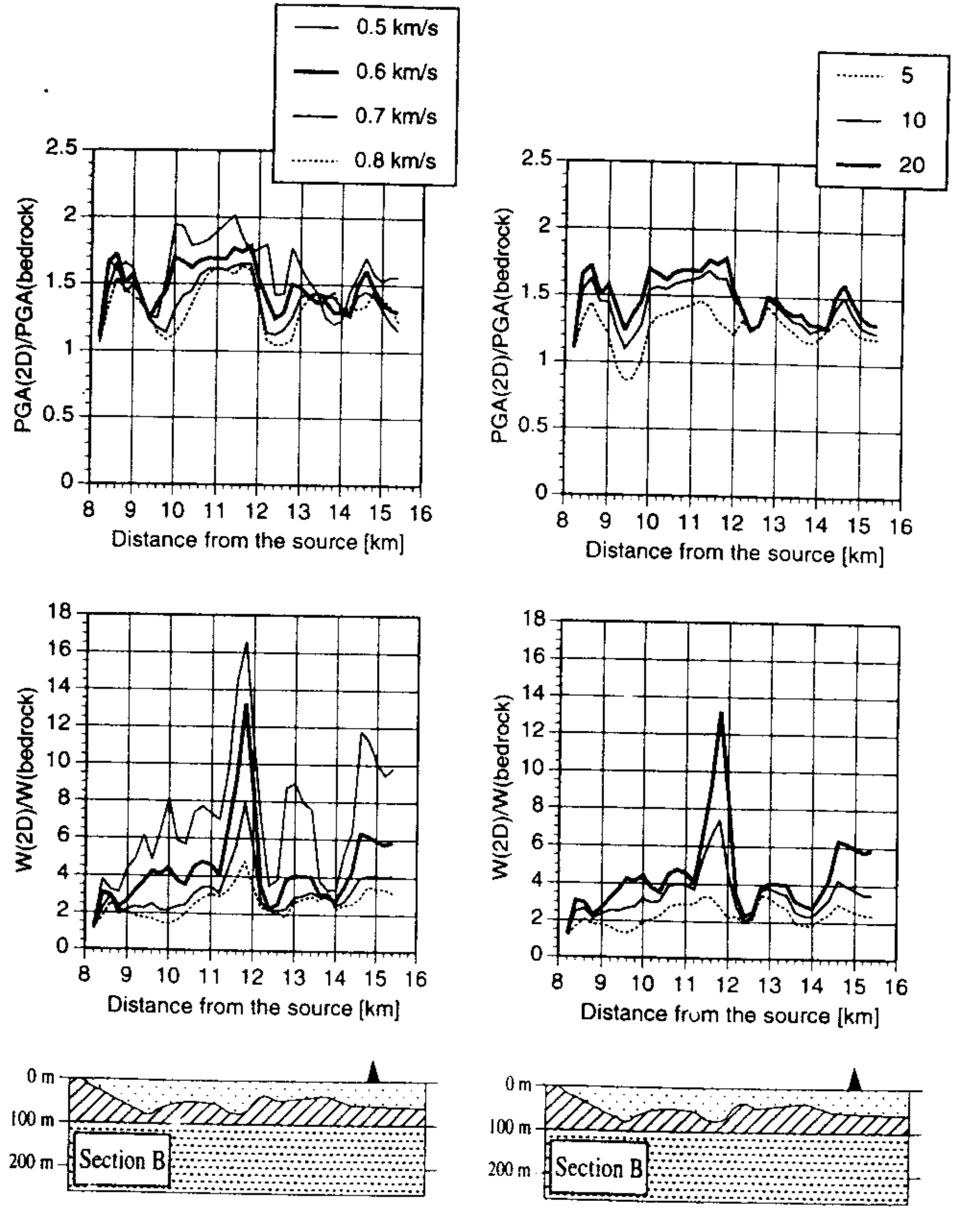

Fig.14

JP

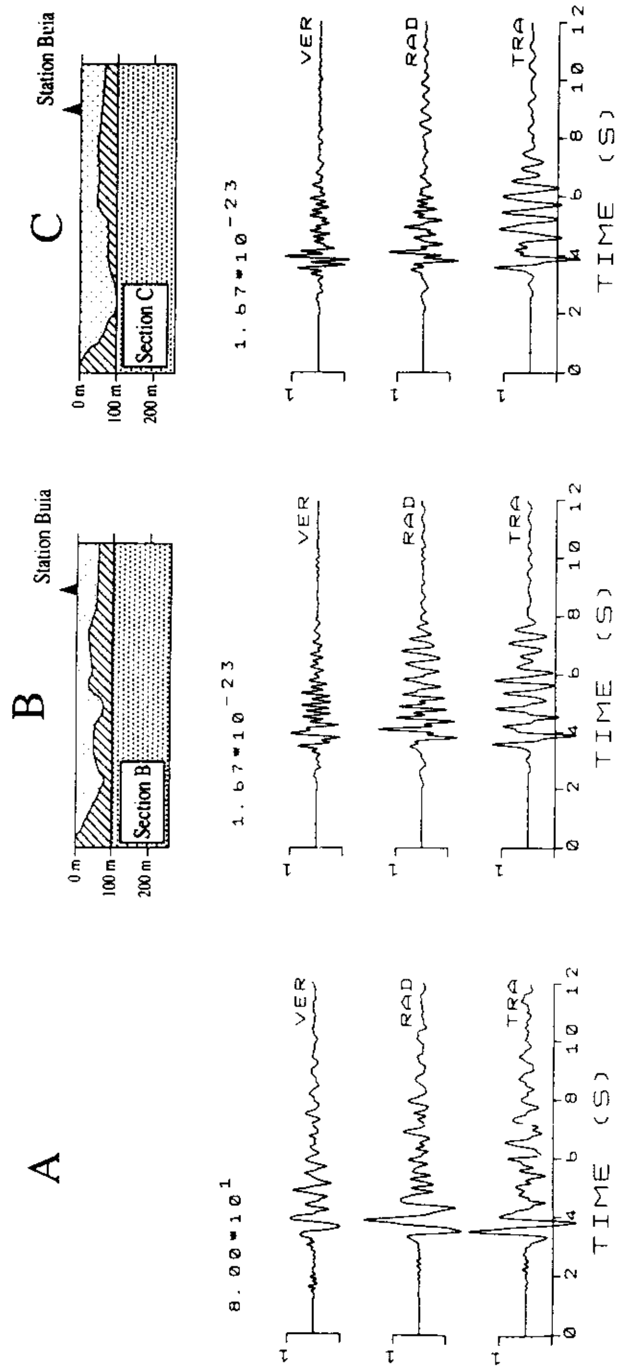

Fig.5

Figure-6 22/2/94 12:08 PM

Thickness of the alluvial sediments
and damage distribution

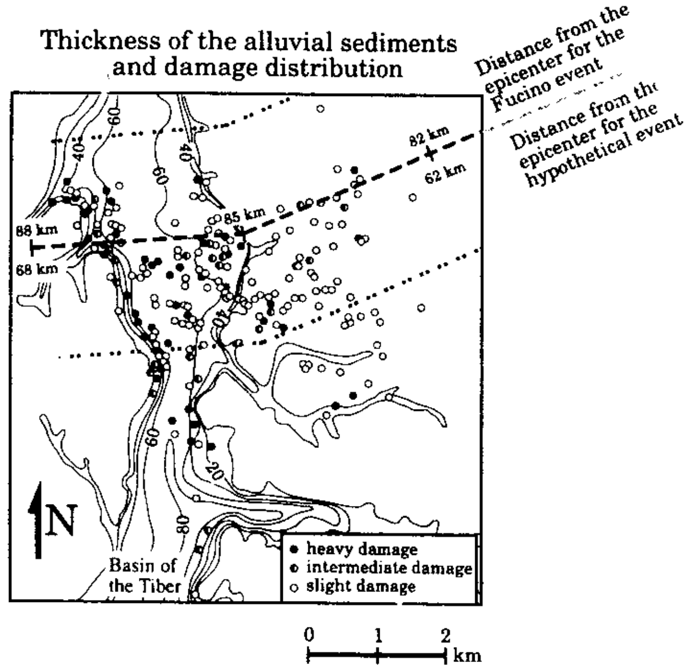

Fig.6

60

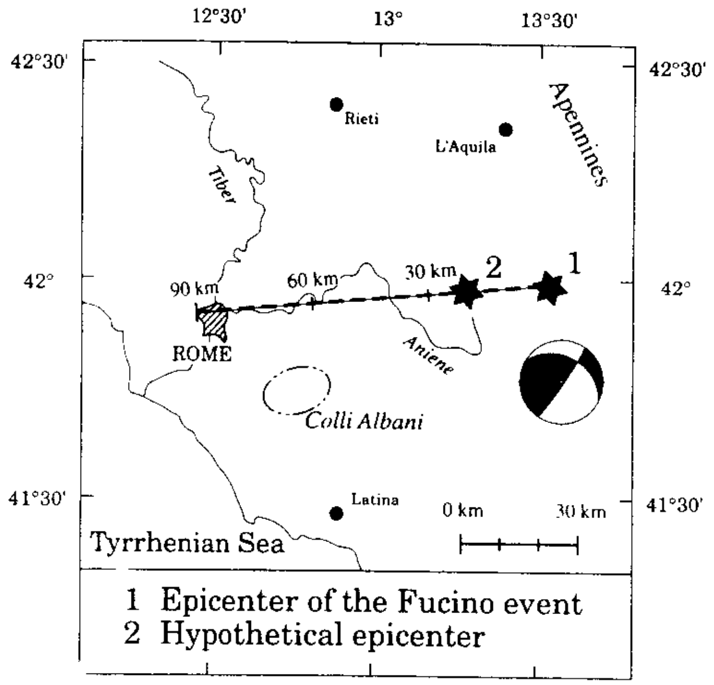
12°30'
13°
13°30'
42°30'
42°
41°30'
Rieti
L'Aquila
Apennines
Tiber
90 km
60 km
30 km
2
1
ROME
Aniene
Colli Albani
Latina
0 km
30 km
Tyrrhenian Sea
1 Epicenter of the Fucino event
2 Hypothetical epicenter

Fig.7

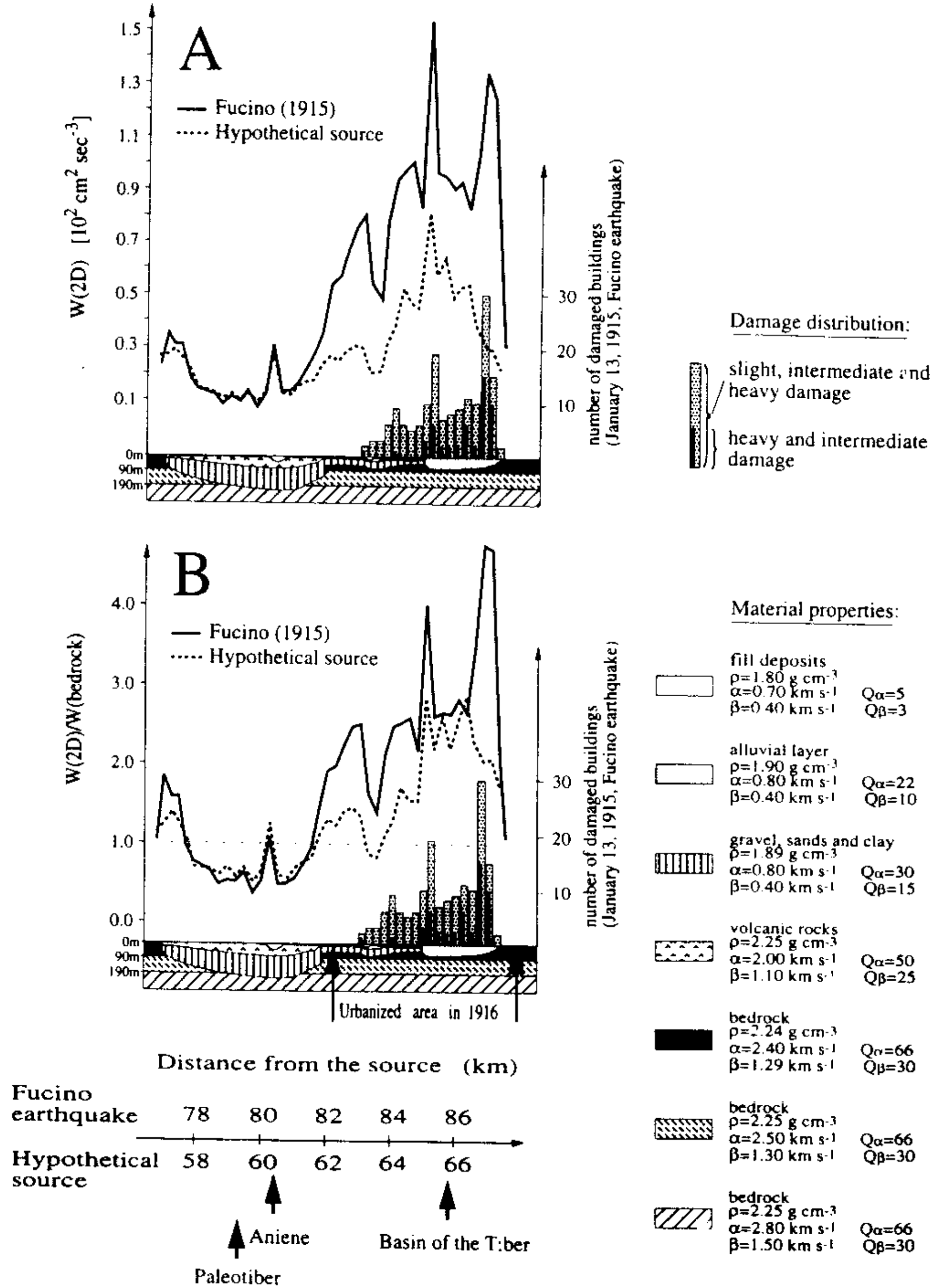
A
— Fucino (1915)
···· Hypothetical source
W(2D) [10^2 cm^2 sec^{-3}]
number of damaged buildings
(January 13, 1915, Fucino earthquake)
B
— Fucino (1915)
···· Hypothetical source
W(2D)/W(bedrock)
Urbanized area in 1916
Distance from the source (km)
Fucino earthquake 78 80 82 84 86
Hypothetical source 58 60 62 64 66
Aniene
Paleotiber
Basin of the Tiber
Damage distribution:
slight, intermediate and heavy damage
heavy and intermediate damage
Material properties:
fill deposits ρ=1.80 g cm-3 α=0.70 km s-1 β=0.40 km s-1 Qα=5 Qβ=3
alluvial layer ρ=1.90 g cm-3 α=0.80 km s-1 β=0.40 km s-1 Qα=22 Qβ=10
gravel, sands and clay ρ=1.89 g cm-3 α=0.80 km s-1 β=0.40 km s-1 Qα=30 Qβ=15
volcanic rocks ρ=2.25 g cm-3 α=2.00 km s-1 β=1.10 km s-1 Qα=50 Qβ=25
bedrock ρ=2.24 g cm-3 α=2.40 km s-1 β=1.29 km s-1 Qα=66 Qβ=30
bedrock ρ=2.25 g cm-3 α=2.50 km s-1 β=1.30 km s-1 Qα=66 Qβ=30
bedrock ρ=2.25 g cm-3 α=2.80 km s-1 β=1.50 km s-1 Qα=66 Qβ=30

Fig.8

61

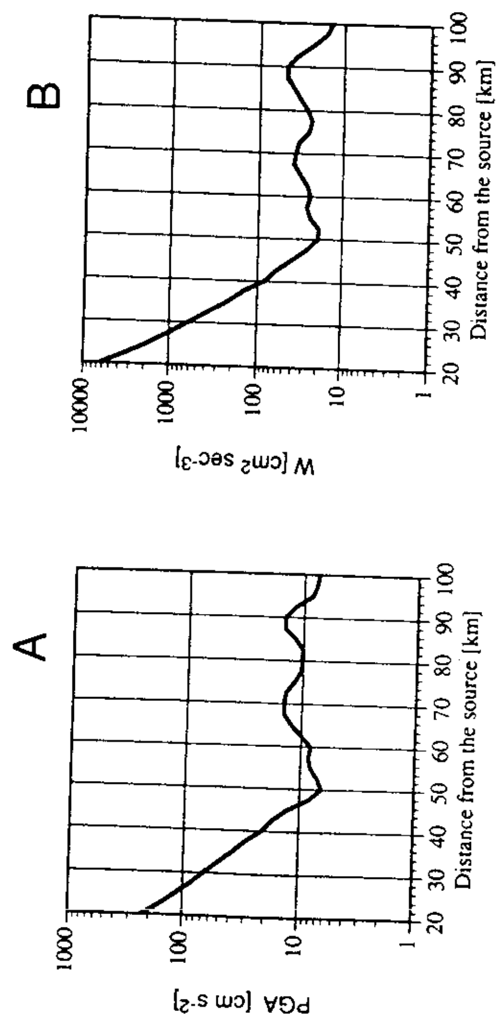
A
PGA [cm s-2]
Distance from the source [km]
B
W [cm2 sec-3]
Distance from the source [km]

Fig.9

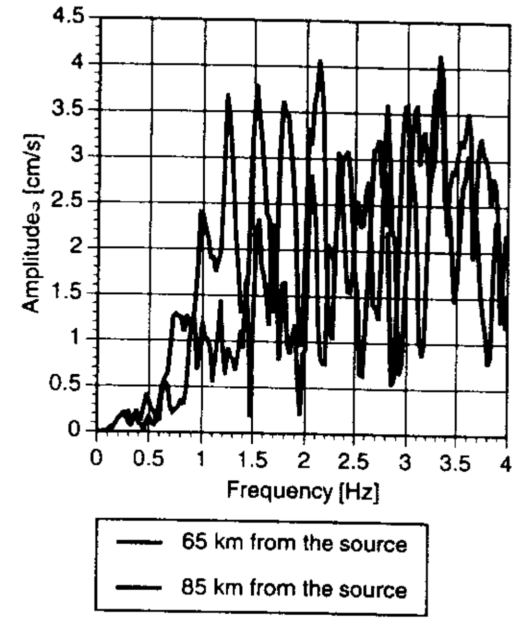
Amplitudes [cm/s]
Frequency [Hz]
65 km from the source
85 km from the source

Fig.10

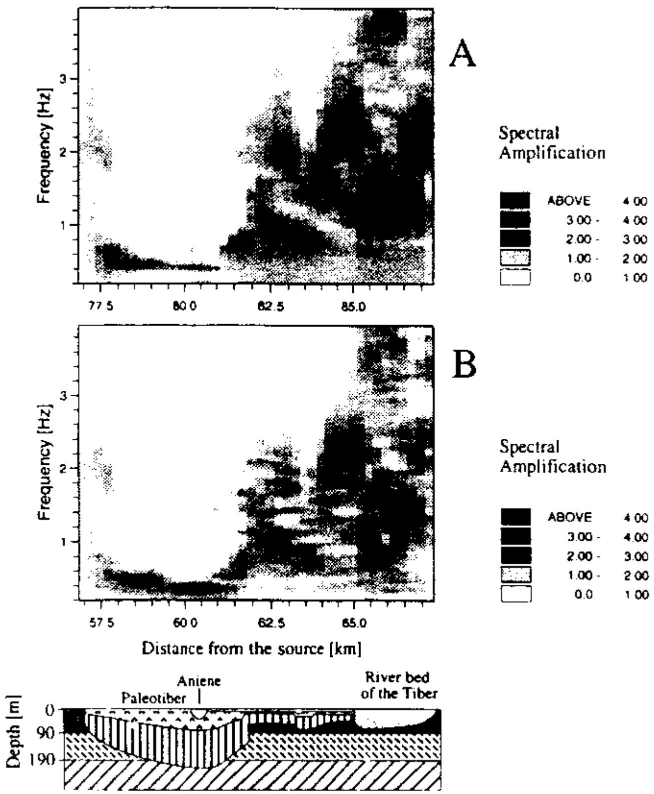

Fig.11

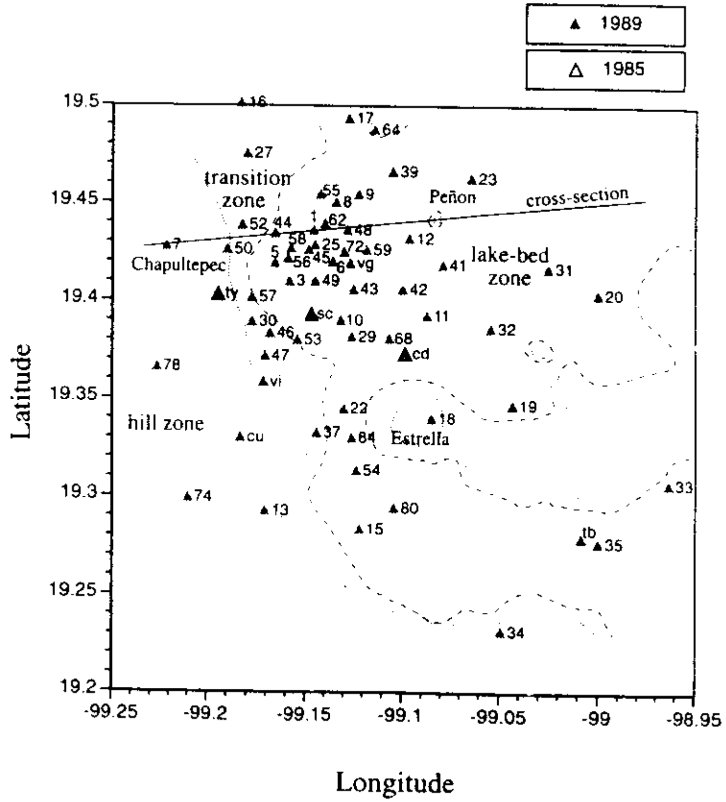

Fig.12

63

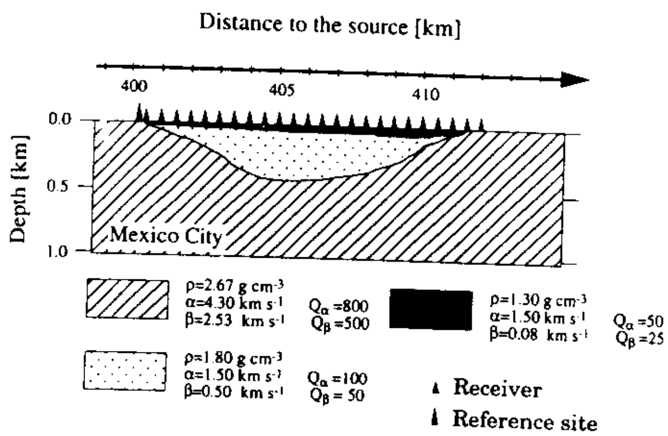

Fig.13

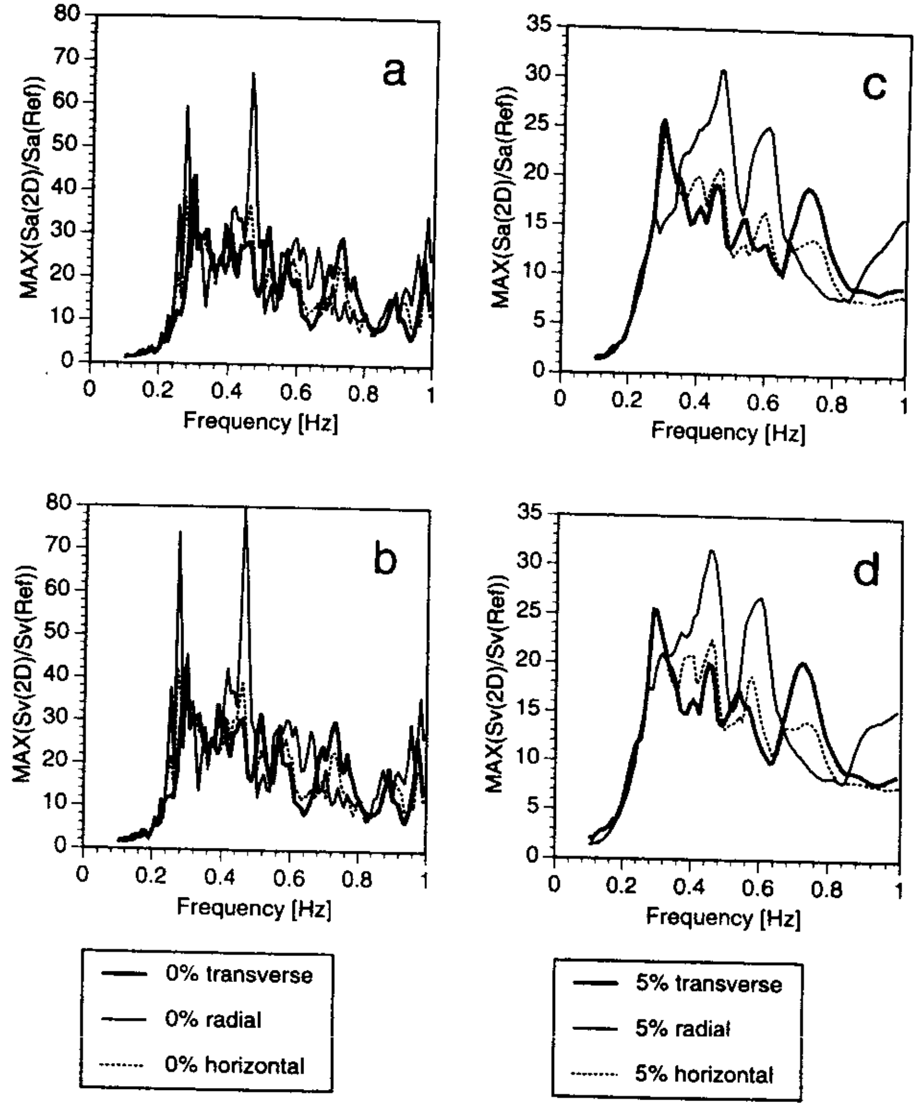

Fig.14

64

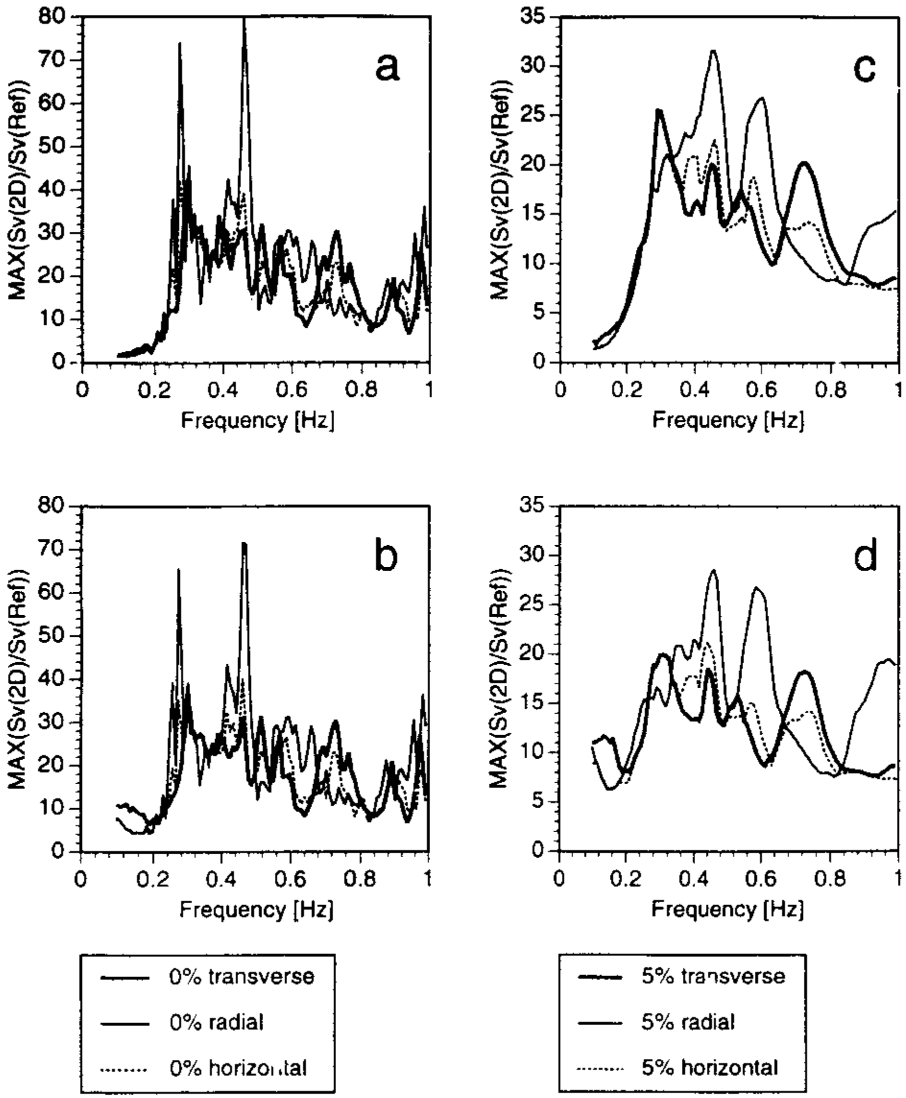

Fig.15

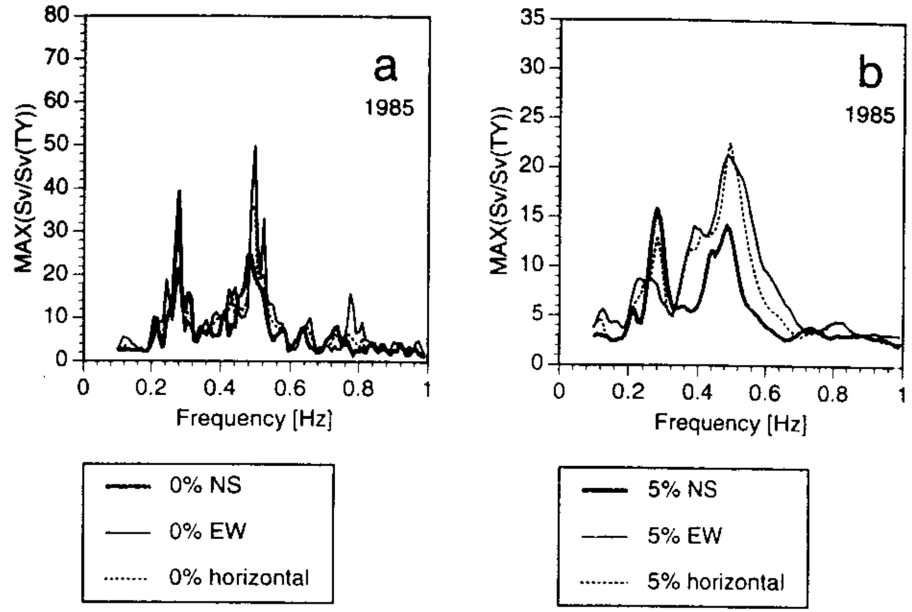

Fig.16

6)

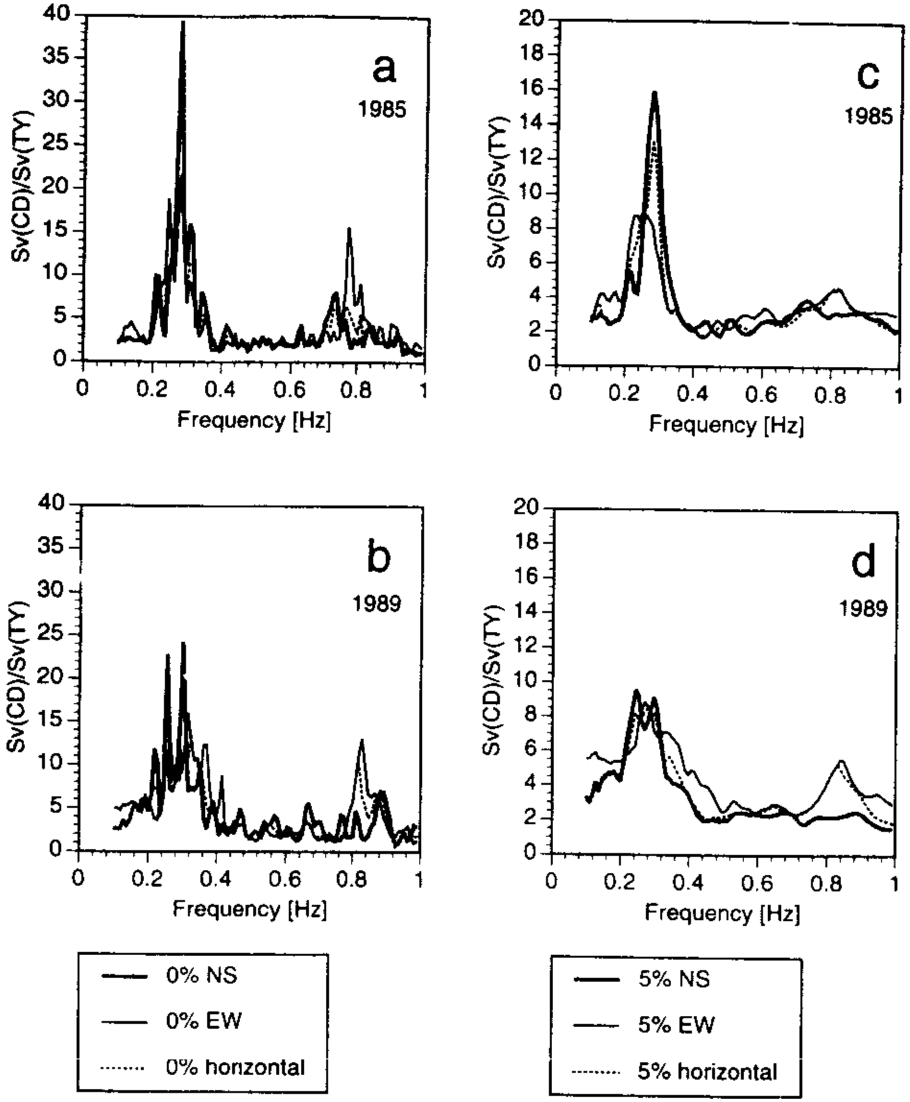

Fig.17

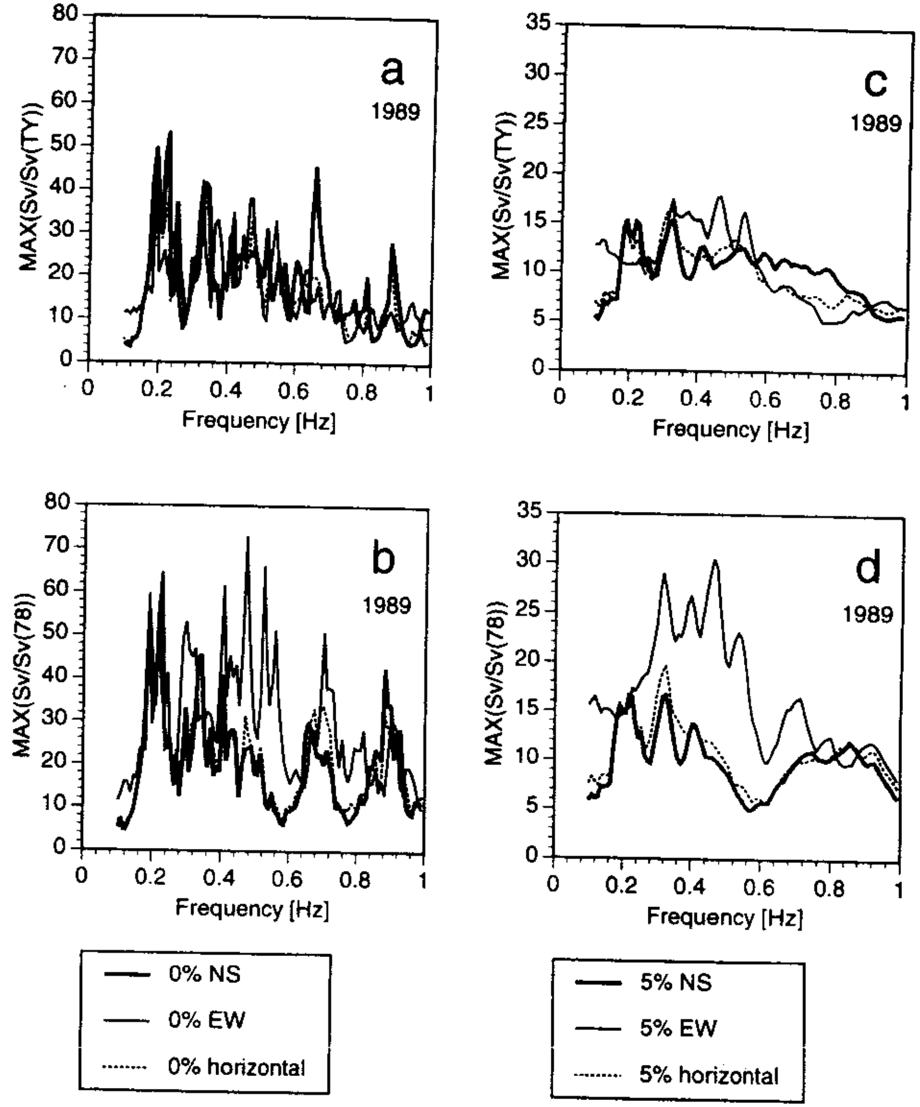

Fig.18

66

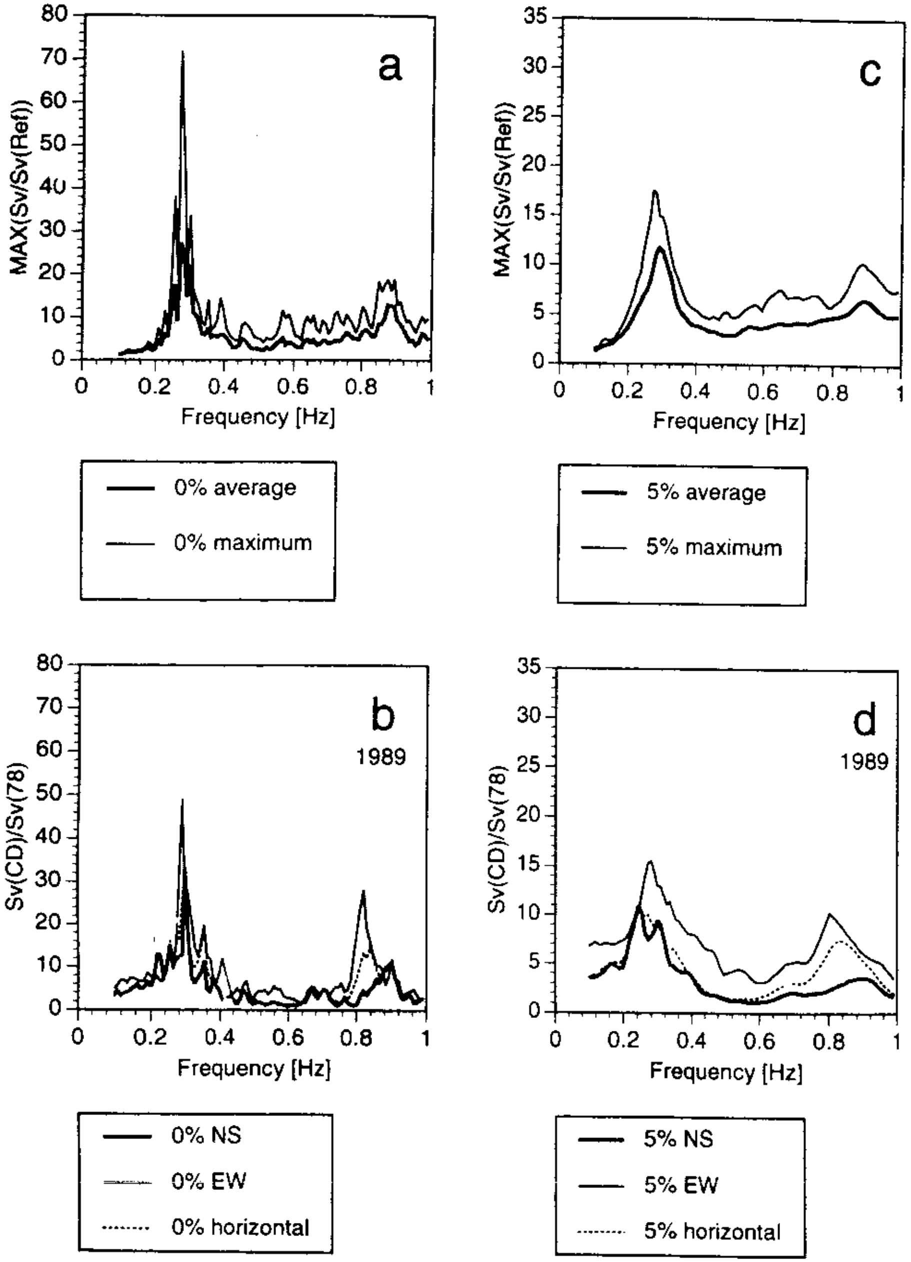
a
MAX(Sv/Sv(Ref))
Frequency [Hz]
0% average
0% maximum
c
5% average
5% maximum
b
1989
Sv(CD)/Sv(78)
0% NS
0% EW
0% horizontal
d
1989
5% NS
5% EW
5% horizontal

Fig.19

67